
UNIVERSITÄT ZU LÜBECK
INSTITUT FÜR ROBOTIK
UND KOGNITIVE SYSTEME

# Ventricular Tachycardia Target Registration and Cardiac Motion Estimation for Stereotactic Arrhythmia Radioablation

Jingyang Xie

Dissertation

University of Lübeck
Institute of Robotics and Cognitive Systems

UNIVERSITÄT ZU LÜBECK

**From the Institute of Robotics and Cognitive Systems**
**of the University of Lübeck**
**Director: Prof. Dr. rer. nat. habil. Floris Ernst**

# Ventricular Tachycardia Target Registration and Cardiac Motion Estimation for Stereotactic Arrhythmia Radioablation

Dissertation
for Fulfillment of
Requirements
for the Doctoral Degree
of the University of Lübeck

from the Department of Computer Sciences and Engineering

Submitted by

Jingyang Xie
from Chengdu, China

Lübeck 2025

First referee: Prof. Dr.-Ing. Achim Schweikard

Second referee: Prof. Dr. phil. Mattias Heinrich

Date of oral examination: August 29th, 2025

Approved for printing. Lübeck, September 2nd, 2025

# Abstract

Ventricular tachycardia (VT) is a severe life-threatening arrhythmia originating in the ventricles, potentially causing sudden cardiac death. Stereotactic arrhythmia radioablation (STAR) is a novel and non-invasive bailout treatment option for refractory VT. The paramount goal of STAR is to precisely deliver focused high-dose radiation beams to treat the VT targets in the heart ventricles while minimizing exposure to the surrounding organs at risk. As a novel therapeutic approach, STAR presents several challenges including VT target transfer from the electroanatomical mapping (EAM) system to the radiation treatment planning system (TPS), as well as cardiac motion estimation of the cardiac clinical target volume (CTV) and American Heart Association (AHA) 17 segments of the left ventricle (LV) for motion management.

On the one hand, unlike typical radiotherapy tumors that are easily identifiable in computed tomography (CT) scans, the VT substrate is primarily characterized by its electrophysiological properties which are typically determined through an electrophysiological study using a three-dimensional (3D) EAM procedure. Studies show that freehand delineation of the VT target region on the treatment planning CT, as defined on the EAM surface, has poor inter-observer consistency, even among experienced electrophysiologists and radiation oncologists. Additionally, clinically relevant errors have been reported with such freehand VT target registration method. Therefore, practical VT target registration methods are crucial for accurately transferring the VT target from the EAM system to treatment planning imaging data. On the other hand, as a moving organ, the heart contains respiratory and cardiac motion. During STAR treatments, respiratory motion can be effectively managed with gating, deep inspiration breath-hold or robotic tracking techniques. However, cardiac motion, particularly the movement of the cardiac CTV and the 17 LV segments, poses a significant challenge in the precise definition of cardiac internal target volume (ITV). This movement can lead to misalignments, which may reduce STAR treatment effectiveness

and increase the risk of harm to nearby organs at risk via dose wash-out. Estimating cardiac motion is essential for defining an appropriate cardiac ITV margin, thereby enhancing the effectiveness of STAR and patient outcomes.

The aim of this dissertation is to investigate four main aspects in the field of STAR: (1) practical methods for VT target registration, (2) validation of these methods using real-world VT patient data, (3) accuracy assessment of target registration methods in the absence of ground truth, and (4) a patient- and segment-specific cardiac motion estimation method.

To address (1), a software was developed, which includes three practical semi-automatic VT target registration methods, namely the AHA 17-segment model registration, 3D-3D registration and 2D-3D registration. The AHA 17-segment model registration method divides the LV myocardium structure contoured from cardiac CT into 17 segments according to the AHA 17-segment model, enabling the assessment of targeted LV segment(s) and follow-up studies. The 3D-3D registration method reads vendor-specific EAM raw data and transfers the 3D VT ablation points to the 3D LV contours with respect to the treatment planning imaging data. The 2D-3D registration method is a versatile approach that supports any EAM system and enables the transfer of the VT target region marked on the 2D EAM screenshots in standard anatomical views to the 3D LV contours with respect to the treatment planning imaging data. These three registration methods are semi-automatic rather than fully automatic due to strict accuracy requirements in clinical applications. Automatic registration methods may not be sufficiently reliable, as the LV and aorta structures are derived from different modalities, which can introduce inaccuracies and data incompleteness, making them unsuitable for clinical use. In contrast, the proposed semi-automatic registration methods have demonstrated practical feasibility on real-world STAR datasets. They provide the necessary flexibility, allowing clinicians to refine the registration process based on their expertise and the specific characteristics of each STAR case, ensuring both accuracy and clinical applicability.

For aspect (2), the software was successfully validated as a quality assurance tool in the STAR treatment planning procedure for 5 VT cases within the German RAVENTA trial. Particularly, the 2D-3D registration method eliminates the need for interpreting proprietary formats exported from different EAM systems. The semi-automated VT target registration methods enable quality assurance of the manually transferred cardiac CTV, reducing clinician-dependent inconsistencies and enhancing the safety and robustness of the VT target registration. Additionally, retrospective findings of incorrectly transferred VT target could potentially

help explain VT recurrences.

In a cross-validation study addressing (3), the proposed 2D-3D registration method and the 3D-3D registration method from the 3D Slicer extension EAMapReader outputted nearly identical cardiac CTV structures. This result indicates that both methods are suitable for quality assurance and VT target transfer to avoid mistargeting and provide standardized workflows.

Finally, regarding aspect (4), this dissertation presents an electrocardiogram-gated cardiac CT-based patient- and segment-specific cardiac motion estimation method using the intensity-based non-rigid automatic image registration in STAR for VT. The method was utilized on case data from 10 STAR-treated VT patients, and the estimated cardiac motion demonstrated considerable individual variability in cardiac CTVs and 17 LV segments across different VT patients, highlighting the need for individualized cardiac ITV margins and motion management strategies to enhance accuracy and effectiveness in STAR. Additionally, this analysis provides reference data on cardiac motion for STAR treatment planning in VT patients. This method has been integrated into the proposed software as a module.

In summary, three practical semi-automatic VT target registration methods were developed and validated, and a patient- and segment-specific cardiac motion estimation method was proposed. These methods bridge the gap between EAM systems and radiation TPS, enhancing STAR performance and improving VT patient outcomes, with potential for future clinical applications.

# Zusammenfassung

Ventrikuläre Tachykardie ist eine schwerwiegende, potenziell letale Arrhythmie, die von den Herzkammern ausgeht und einen plötzlichen Herztod bedingen kann. Die stereotaktische Radioablation von Herzrhythmusstörungen stellt eine neuartige, nicht-invasive Behandlungsoption für refraktäre ventrikuläre Tachykardien dar. Das Hauptziel der stereotaktischen Radioablation von Herzrhythmusstörungen besteht in der präzisen Abgabe fokussierter, hochdosierter Strahlen zur Behandlung der ventrikulären Tachykardieziele in den Herzkammern bei gleichzeitiger Minimierung der Exposition der umliegenden Risikoorgane. Die stereotaktische Radioablation von Herzrhythmusstörungen stellt einen neuartigen therapeutischen Ansatz dar, der eine Reihe von Herausforderungen mit sich bringt. Hierzu zählen die Übertragung des Ziels für ventrikuläre Tachykardien vom elektroanatomischen Kartierungssystem auf das Planungssystem für die Bestrahlung sowie die Schätzung der Herzbewegungen des klinischen Zielvolumens und der 17 Segmente des linken Ventrikels der American Heart Association (AHA) für das Bewegungsmanagement.

Einerseits ist das Kammertachykardiesubstrat im Gegensatz zu typischen Strahlentumoren, die in Computertomographien leicht identifizierbar sind, in erster Linie durch seine elektrophysiologischen Eigenschaften charakterisiert, die in der Regel durch eine elektrophysiologische Studie mit einem elektroanatomischen 3D-Kartierungsverfahren bestimmt werden. Studien zeigen, dass die freihändige Abgrenzung des Zielgebiets der ventrikulären Tachykardie auf der Computertomographie zur Behandlungsplanung, wie sie auf der elektroanatomischen Kartierungsfläche definiert ist, selbst bei erfahrenen Elektrophysiologen und Radioonkologen eine schlechte Konsistenz zwischen den Beobachtern aufweist. Darüber hinaus wurde über klinisch relevante Fehler bei der freihändigen Registrierung von ventrikulären Tachykardien berichtet. Daher sind praktische Methoden zur Registrierung des ventrikulären Tachykardie-Ziels von entscheidender Bedeutung für die genaue Übertragung des ventrikulären

Tachykardie-Ziels vom elektroanatomischen Kartierungssystem auf die Bilddaten der Behandlungsplanung. Andererseits ist das Herz als ein sich bewegendes Organ mit Atem- und Herzbewegungen verbunden. Bei der stereotaktischen Radioablation von Herzrhythmusstörungen kann die Atembewegung durch Gating, Atemanhalten bei tiefer Inspiration oder robotergestützte Tracking-Techniken wirksam gesteuert werden. Die Bewegung des Herzens, insbesondere die Bewegung des klinischen Zielvolumens des Herzens und der 17 Segmente des linken Ventrikels, stellt jedoch eine große Herausforderung für die präzise Definition des internen Zielvolumens des Herzens dar. Diese Bewegung kann zu Fehlausrichtungen führen, die die Wirksamkeit der stereotaktischen Radioablation bei Herzrhythmusstörungen beeinträchtigen und das Risiko einer Schädigung benachbarter Risikoorgane durch Dosisauswaschung erhöhen können. Die Schätzung der Herzbewegung ist für die Festlegung eines angemessenen kardialen Zielvolumens unerlässlich, um die Wirksamkeit der stereotaktischen Arrhythmie-Radioablation und die Ergebnisse für den Patienten zu verbessern.

Ziel dieser Dissertation ist es, vier Hauptaspekte im Bereich der stereotaktischen Radioablation von Arrhythmien zu untersuchen: (1) praktische Methoden für die Zielregistrierung von ventrikulären Tachykardien, (2) Validierung dieser Methoden anhand von realen Patientendaten mit ventrikulären Tachykardien, (3) Bewertung der Genauigkeit von Zielregistrierungsmethoden in Abwesenheit von Ground Truth und (4) eine patienten- und segmentspezifische Methode zur Schätzung von Herzbewegungen.

Zur Lösung von (1) wurde eine Software entwickelt, die drei praktische halbautomatische Methoden zur Registrierung ventrikulärer Tachykardien umfasst, nämlich die AHA-17-Segment-Modellregistrierung, die 3D-3D-Registrierung und die 2D-3D-Registrierung. Die AHA 17-Segment-Modellregistrierungsmethode teilt die aus der kardialen Computertomographie konturierte Myokardstruktur des linken Ventrikels in 17 Segmente gemäß dem AHA 17-Segment-Modell auf und ermöglicht so die Beurteilung der anvisierten Segmente des linken Ventrikels und Folgeuntersuchungen. Die 3D-3D-Registrierungsmethode liest herstellerspezifische elektroanatomische Mapping-Rohdaten und überträgt die 3D-Punkte für die Ablation ventrikulärer Tachykardien auf die 3D-Konturen des linken Ventrikels in Bezug auf die Bilddaten der Behandlungsplanung. Die 2D-3D-Registrierungsmethode ist ein vielseitiger Ansatz, der jedes elektroanatomische Mapping-System unterstützt und

die Übertragung der auf den 2D-Screenshots des elektroanatomischen Mappings in anatomischen Standardansichten markierten ventrikulären Tachykardie-Zielregion auf die 3D-Konturen des linken Ventrikels in Bezug auf die Bilddaten der Behandlungsplanung ermöglicht. Diese drei Registrierungsmethoden sind aufgrund der strengen Genauigkeitsanforderungen bei klinischen Anwendungen eher halbautomatisch als vollautomatisch. Automatische Registrierungsmethoden sind unter Umständen nicht ausreichend zuverlässig, da die Strukturen des linken Herzens und der Aorta aus verschiedenen Modalitäten abgeleitet werden, was zu Ungenauigkeiten und unvollständigen Daten führen kann, so dass sie für den klinischen Einsatz ungeeignet sind. Im Gegensatz dazu haben die vorgeschlagenen halbautomatischen Registrierungsmethoden ihre praktische Durchführbarkeit bei realen stereotaktischen Radioablationssätzen für Herzrhythmusstörungen bewiesen. Sie bieten die nötige Flexibilität, so dass Kliniker den Registrierungsprozess auf der Grundlage ihres Fachwissens und der spezifischen Merkmale jedes einzelnen stereotaktischen Arrhythmie-Radioablationsfalls verfeinern können, was sowohl Genauigkeit als auch klinische Anwendbarkeit gewährleistet.

Für den Aspekt (2) wurde die Software erfolgreich als Qualitätssicherungsinstrument in der stereotaktischen Radioablation von Herzrhythmusstörungen im Rahmen der deutschen RAVENTA-Studie für 5 Fälle von ventrikulärer Tachykardie validiert. Insbesondere die 2D-3D-Registrierungsmethode macht die Interpretation von proprietären Formaten, die von verschiedenen elektroanatomischen Mapping-Systemen exportiert werden, überflüssig. Die halbautomatischen Methoden der ventrikulären Tachykardie-Zielregistrierung ermöglichen eine Qualitätssicherung des manuell übertragenen kardialen klinischen Zielvolumens, wodurch klinikerabhängige Inkonsistenzen reduziert und die Sicherheit und Robustheit der ventrikulären Tachykardie-Zielregistrierung erhöht werden. Darüber hinaus könnten retrospektive Erkenntnisse über falsch übertragene ventrikuläre Tachykardie-Targets möglicherweise dazu beitragen, ventrikuläre Tachykardie-Rezidive zu erklären.

In einer Kreuzvalidierungsstudie (3) ergaben die vorgeschlagene 2D-3D-Registrierungsmethode und die 3D-3D-Registrierungsmethode der 3D-Slicer-Erweiterung EAMapReader nahezu identische kardiale klinische Zielvolumenstrukturen. Dieses Ergebnis deutet darauf hin, dass beide Methoden für die Qualitätssicherung und die Übertragung von Targets für ventrikuläre Tachykardien geeignet sind, um Fehltargeting zu vermeiden und standardisierte Arbeitsabläufe zu ermöglichen.

Was schließlich den Aspekt (4) betrifft, so wird in dieser Dissertation eine elektrokardiogrammgestützte, auf kardialer Computertomographie basierende Methode zur patienten- und segmentspezifischen Schätzung der Herzbewegung unter Verwendung der intensitätsbasierten, nicht-starren automatischen Bildregistrierung bei der stereotaktischen Arrhythmieradioablation bei ventrikulären Tachykardien vorgestellt. Die Methode wurde an Falldaten von 10 mit stereotaktischer Arrhythmie-Radioablation behandelten Kammertachykardie-Patienten angewandt. Die geschätzte Herzbewegung zeigte eine beträchtliche individuelle Variabilität der klinischen Zielvolumina des Herzens und der 17 Segmente des linken Ventrikels bei verschiedenen Kammertachykardie-Patienten, was die Notwendigkeit individualisierter kardialer interner Zielvolumensgrenzen und Bewegungsmanagement-Strategien zur Verbesserung der Genauigkeit und Effektivität der stereotaktischen Arrhythmie-Radioablation unterstreicht. Darüber hinaus liefert diese Analyse Referenzdaten zur Herzbewegung für die Planung der stereotaktischen Radioablation bei Patienten mit ventrikulären Tachykardien. Diese Methode wurde als Modul in die vorgeschlagene Software integriert.

Zusammenfassend wurden drei praktische halbautomatische Methoden zur Zielregistrierung bei ventrikulärer Tachykardie entwickelt und validiert, und es wurde eine patienten- und segmentspezifische Methode zur Schätzung der Herzbewegung vorgeschlagen. Diese Methoden überbrücken die Lücke zwischen elektroanatomischen Mapping-Systemen und Strahlenbehandlungsplanungssystemen, verbessern die stereotaktische Arrhythmie-Radioablation und die Ergebnisse für Patienten mit ventrikulärer Tachykardie, mit Potenzial für zukünftige klinische Anwendungen.

# Contents

**Abstract** **vii**

**Zusammenfassung** **xi**

**Contents** **xv**

**List of Abbreviations** **xix**

**1 Introduction** **1**
- 1.1 Research Questions . . . 2
- 1.2 Structure of this Dissertation . . . 4
- 1.3 Notes on Terminology . . . 4
- 1.4 Ethics Approval . . . 4

**2 Medical Background** **7**
- 2.1 Ventricular Tachycardia . . . 7
- 2.2 Electroanatomical Mapping . . . 8
- 2.3 Stereotactic Arrhythmia Radioablation . . . 9

**3 Treatment Planning in Stereotactic Arrhythmia Radioablation** **13**
- 3.1 Ventricular Tachycardia Target Registration . . . 13
- 3.2 Validation of Target Registration . . . 18
- 3.3 Cardiac Motion Estimation for Motion Management . . . 21

**4 CARDIO-RT Target Registration Methods** **23**
- 4.1 Scientific Contributions . . . 23
- 4.2 AHA 17-Segment Model Registration . . . 24
  - 4.2.1 Registration Workflow . . . 24
  - 4.2.2 Visualization of the Registered 17 Segments . . . 29
- 4.3 3D-3D Registration . . . 32
  - 4.3.1 Registration Workflow . . . 32
  - 4.3.2 Visualization of the Registered Target . . . 43

4.4 2D-3D Registration . . . 45
4.4.1 Registration Workflow . . . 45
4.4.2 Visualization of the Registered Target . . . 54
4.5 Significance of Aorta Mapping . . . 56
4.5.1 Inter- and Intra-Observer Variability Analysis . . . 56
4.5.2 Results . . . 56
4.6 Additional Functions . . . 57
4.6.1 Visualize Cardiac Target Volume and Dose Calculation . . . 57
4.6.2 Register Cardiac CT with Planning CT . . . 59
4.6.3 Generate Transmural Target . . . 60
4.7 Discussion . . . 62
4.8 Chapter Summary . . . 66

**5 Validations of Target Registration Methods 69**
5.1 Scientific Contributions . . . 69
5.2 Validation for Quality Assurance . . . 70
5.2.1 Data Acquisition and Patient Characteristics . . . 70
5.2.2 Target Registration . . . 73
5.2.3 Structure Analysis . . . 74
5.2.4 Validation Results . . . 74
5.2.5 Discussion . . . 82
5.3 Cross-Validation . . . 85
5.3.1 Data Acquisition and Patient Characteristics . . . 86
5.3.2 Independent Target Registration . . . 88
5.3.3 Structure Analysis . . . 92
5.3.4 Cross-Validation Results . . . 92
5.3.5 Discussion . . . 96
5.4 Chapter Summary . . . 99

**6 Patient- and Segment-Specific Cardiac Motion Estimation 101**
6.1 Scientific Contributions . . . 101
6.2 Data Preparation . . . 102
6.3 Intensity-Based Non-Rigid Automatic Image Registration . . . 104
6.4 Estimation of Cardiac Motion . . . 108
6.5 Statistical Analysis . . . 108
6.6 Motion Estimation Results . . . 109
6.6.1 Evaluation of Image Registration Performance . . . 109

6.6.2 Cardiac Motion Estimation of CTV and 17 Segments . . . . 109
6.6.3 ICD Lead Tip Motion Estimation and Its Accordance with Cardiac Motion . . . . . 111
6.7 Discussion . . . . . 113
6.8 Chapter Summary . . . . . 116

**7 Conclusion** **119**
7.1 Summary . . . . . 119
7.2 Conclusion on the Research Questions . . . . . 121
7.3 Future Work . . . . . 123

**A Ethics Approval** **125**

**B Case Histories** **131**

**Bibliography** **135**

**List of Figures** **159**

**List of Tables** **169**

**Acknowledgements** **171**

**Curriculum Vitae** **173**

# List of Abbreviations

| | |
|---|---|
| 2D | Two-Dimensional |
| 3D | Three-Dimensional |
| 4D | Four-Dimensional |
| AF | Atrial Fibrillation |
| AHA | American Heart Association |
| AP | Anterior-Posterior |
| BMI | Body Mass Index |
| CAU | Caudal |
| CE | Conformité Européenne |
| CoM | Center of Mass |
| CR | Cardiac Radioablation |
| CRA | Cranial |
| CRS | Cardiac Radiosurgery |
| CSBRT | Cardiac Stereotactic Body Radiotherapy |
| CSV | Comma-Separated Values |
| CT | Computed Tomography |
| CTV | Clinical Target Volume |
| DIBH | Deep Inspiration Breath-Hold |
| DICOM | Digital Imaging and Communications in Medicine |
| DSC | Dice-Sørensen Coefficient |
| EAM | Electroanatomical Mapping |
| ECG | Electrocardiogram |
| ECGI | Electrocardiographic Imaging |
| FDA | Food and Drug Administration |
| GTV | Gross Target Volume |
| GUI | Graphical User Interface |
| HD | Hausdorff Distance |
| HU | Hounsfield Unit |
| ICD | Implantable Cardioverter-Defibrillator |
| ICP | Iterative Closest Point |

| | |
|---|---|
| IDE | Interactive Development Environment |
| INF | Inferior |
| ITV | Internal Target Volume |
| JPG/JPEG | Joint Photographic Experts Group |
| LAO | Left Anterior Oblique |
| LL | Left Lateral |
| LV | Left Ventricle |
| LVEF | Left Ventricular Ejection Fraction |
| MRI | Magnetic Resonance Imaging |
| MSE | Mean Squared Error |
| OAR | Organs at Risk |
| PA | Posterior-Anterior |
| PCA | Principal Component Analysis |
| PCC | Pearson Correlation Coefficient |
| PNG | Portable Network Graphics |
| PVC | Premature Ventricular Contraction |
| PTV | Planning Target Volume |
| RA | Radioablation |
| RAO | Right Anterior Oblique |
| RAVENTA | RAdiosurgery for VENtricular TAchycardia |
| RL (except in Chapter 6) | Right Lateral |
| RL (used in Chapter 6 only) | Right-Left |
| ROI | Region of Interest |
| RTSS | Radiotherapy Structure Set |
| RV | Right Ventricle |
| SABR | Stereotactic Ablative Radiotherapy |
| SBRT | Stereotactic Body Radiation Therapy |
| SI | Superior-Inferior |
| SRS | Stereotactic Radiosurgery |
| STAR | Stereotactic Arrhythmia Radioablation |
| STOPSTORM | Standardized Treatment and Outcome Platform for Stereotactic Therapy Of Re-entrant tachycardia by a Multidisciplinary |
| SUP | Superior |
| TPS | Treatment Planning System |
| VT | Ventricular Tachycardia |

# Chapter 1

# Introduction

In the field of stereotactic body radiation therapy (SBRT), the paramount goal is to deliver precisely focused high-dose radiation beams to treat specific targets in the body while minimizing exposure to the surrounding organs at risk (OAR). In recent years, SBRT has been applied to treat refractory ventricular tachycardia (VT) patients without other interventional options in clinical cases [1]–[6], to ablate the arrhythmogenic substrate with an adequate dose and minimal safety margins using steep dose gradients to avoid cardiac radiation toxicity [7], and this approach is called stereotactic arrhythmia radioablation (STAR). STAR has emerged as a novel and non-invasive treatment modality, gaining acceptance in the cardiology community [8]. The accuracy of STAR depends on the precise delineation of the cardiac clinical target volume (CTV) and the information on dynamic behavior of the heart, which is influenced by both cardiac and respiratory motion.

Unlike typical radiotherapy tumors that are easily identifiable in computed tomography (CT) scans, VT substrates are primarily characterized by the electrophysiological properties which are typically determined through an electrophysiological study using a three-dimensional (3D) electroanatomical mapping (EAM) procedure [9]–[11]. Conventionally, the cardiac CTV is freehand delineated on the treatment planning CT slices directly within the radiation treatment planning system (TPS) by visually side-by-side comparing the EAM data with the 3D contoured left ventricle (LV) structure [12]–[14], and thus is highly observer-dependent [15], [16]. Therefore, it is crucial to explore practical VT target registration methods that can assist in transferring the VT target region defined in the EAM system to the treatment planning imaging data as a reference for cardiac CTV delineation in the radiation TPS. In this way, the uncertainties in the VT target delineation can be reduced [17], diminishing the risk of VT recurrence and radiation toxicity [5], [18], [19].

Once the cardiac CTV structure is defined in the radiation TPS, the cardiac

internal target volume (ITV) margin, representing the CTV with an additional margin to compensate for a known or estimated range of internal motion during the STAR treatment, needs to be defined [20]–[22]. This process requires detailed information on the dynamic behavior of the heart due to respiratory motion and cardiac motion. Respiratory motion can be accurately managed with gating, deep inspiration breath-hold (DIBH) techniques or robotic tracking [23], [24]. However, cardiac motion, particularly the movement of the cardiac CTV and the American Heart Association (AHA) 17 segments of the LV [25], presents a significant challenge in the precise definition of cardiac ITV margin. This motion can lead to marginal misses, reducing the efficacy of the treatment and potentially causing damage to the surrounding OAR via dose wash-out [26]. Additionally, active motion management strategies have been under investigation in recent years [27], [28], and the estimates of cardiac motion could help to identify VT patients with larger cardiac motion who would particularly benefit from them. Therefore, estimating the cardiac motion of the CTV and 17 LV segments is essential tor enhance the performance of STAR and patient outcomes.

## 1.1 Research Questions

Overall, the dissertation is intended to address the following research questions:

- Q1: What are the practical methods for registering VT target structure from the EAM system to radiation TPS for STAR? Is there a versatile VT target registration method applicable to all EAM systems?
- Q2: Is it possible to employ the VT target registration methods in the quality assurance process for STAR?
- Q3: Is it possible to assess the accuracy of the VT target registration methods used for STAR in the absence of ground truth?
- Q4: Is it possible to estimate the cardiac motion of the cardiac CTV and substructures based on electrocardiogram (ECG)-gated contrast-enhanced breath-hold CT?

These research questions are consecutive, and the key idea of each research question is elaborated in detail below:

**Q1: What are the practical methods for registering a VT target structure from the EAM system to radiation TPS for STAR? Is there a versatile VT target registration method applicable to all EAM systems?**
This question investigates practical methods for registering the defined VT target region, marked by the cardiac electrophysiologist in the EAM system, to the radiation treatment planning CT for the cardiac CTV delineation process in STAR treatment. Additionally, due to the inconsistency in the export formats of EAM raw data across different EAM systems or versions of the same system, this study also explores whether there is a versatile registration method that can be applied to any EAM systems.

**Q2: Is it possible to employ the VT target registration methods in the quality assurance process for STAR?**
Based on the newly developed practical VT target registration methods from the research question Q1, and given the current absence of a commercial product or clinically validated method with Conformité Européenne (CE) or Food and Drug Administration (FDA) certification for dedicated and semi-automated VT target transfer from EAM data to the radiation TPS, it is important to assess these methods in the quality assurance process in clinical STAR centers on real-world VT patients as a clinical feasibility validation.

**Q3: Is it possible to assess the accuracy of the VT target registration methods used for STAR in the absence of ground truth?**
Currently, due to the absence of ground truth for the registered VT target structure in STAR, evaluating the accuracy and performance of the VT target registration methods proposed in the research question Q1 is essential. Cross-validating two different VT target registration methods is necessary to evaluate their reliability in the STAR quality assurance process.

**Q4: Is it possible to estimate the cardiac motion of the cardiac CTV and substructures based on ECG-gated contrast-enhanced breath-hold CT?**
The output of the VT target registration methods in the research question Q1 can serve as a reference for cardiac CTV delineation in the STAR treatment planning process. Furthermore, it is crucial to define an appropriate and individualized cardiac ITV margin based on cardiac motion when adequate respiratory motion management strategies (e.g., gating, DIBH or robotic tracking) are applied. Estimates of cardiac motion for the cardiac CTV and 17 LV segments could also help

identify VT patients with large cardiac motion who would particularly benefit from active motion management strategies. Therefore, this research question investigates whether patient- and segment-specific cardiac motion can be estimated using ECG-gated contrast-enhanced breath-hold cardiac CT.

## 1.2 Structure of this Dissertation

The structure of this dissertation is organized around the aforementioned four research questions. First, an overview of the related medical background is provided in Chapter 2. Then, in Chapter 3, the current status and challenges of treatment planning for STAR are presented in three aspects. In Chapter 4, the CARDIO-RT software including three practical VT target registration methods with three main additional functions is introduced. Next, Chapter 5 demonstrates the validations of the proposed VT target registration methods by employing them in the treatment planning process for STAR, and by cross-validating the proposed 2D-3D registration and the 3D-3D registration in the 3D Slicer extension EAMapReader. Afterwards, based on ECG-gated contrast-enhanced breath-hold CT, the patient- and segment-specific cardiac motion of the cardiac CTV and AHA 17 LV segments is estimated using an intensity-based non-rigid automatic image registration method. Finally, a conclusion chapter summarizes the work and related research questions, and suggests potential future directions in the field of STAR.

## 1.3 Notes on Terminology

The terms used for the concept of applying SBRT to ablate the substrate of cardiac arrhythmias are inconsistent across different publications, including cardiac radioablation (CR), cardiac radiosurgery (CRS), cardiac stereotactic body radiotherapy (CSBRT), radioablation (RA), stereotactic ablative radiotherapy (SABR) and stereotactic arrhythmia radioablation (STAR). The term STAR is used throughout this dissertation.

## 1.4 Ethics Approval

For the patient data used in this dissertation, pseudonymized data were collected from the treating centers based on the RAdiosurgery for VENtricular TAchycardia (RAVENTA) trial protocol (NCT03867747) [4], [29], either directly within the

RAVENTA study in Germany [29] or within a harmonized trial in Israel (national trial number: 202225964) [30] and/or within the Standardized Treatment and Outcome Platform for Stereotactic Therapy Of Re-entrant tachycardia by a Multidisciplinary (STOPSTORM) registry [5]. Ethics approval was obtained for the coordinating center (reference number D555/18, see Appendix A) and each local site and/or for the STAR benchmark studies (D476/19 and D483/21).

# Chapter 2

# Medical Background

In this chapter, a brief medical background of this dissertation is presented. After introducing the heart arrhythmia VT and its traditional treatment options, an overview of the relevant diagnostic technique EAM and a novel non-invasive bailout treatment option STAR is provided.

## 2.1 Ventricular Tachycardia

VT is a type of life-threatening cardiac arrhythmia originating from the ventricles, the lower chambers of the heart [31], [32]. A healthy heart beats about 60-100 times per minute at rest, while VT patients often have a rapid heart rate exceeding 100 beats per minute due to abnormal electrical signals in the ventricles. This condition can severely impair the heart's ability to pump blood effectively, leading to reduced cardiac output and, in some cases, sudden cardiac death. VT is often associated with structural heart disease, such as myocardial infarction, cardiomyopathy or scarring from prior cardiac injuries [33], [34]. VT is closely linked to coronary artery disease, with approximately 15% of individuals diagnosed with coronary artery disease also exhibiting VT [35].

The primary steps in VT management include risk assessment for sudden death, evaluating the extent of underlying heart disease, and determining the most appropriate therapeutic options [29]. VT therapeutic options include medication, device-based interventions and catheter ablation [36]. Antiarrhythmic drugs (e.g., amiodarone and beta-blockers) and implantable cardioverter-defibrillator (ICD) are typically the first line of treatments for VT patients [37], [38]. However, the efficacy of these antiarrhythmic drugs is often limited, and they can cause substantial side effects [39]. The ICDs are essential to prevent

fatal arrhythmias by antitachycardia pacing or shock when VT episodes are detected [4]. However, ICDs do not prevent arrhythmia recurrence and may negatively impact patients' quality of life due to frequent shocks and related complications [40]. When antiarrhythmic drugs fail to control VT episodes, catheter ablation of the VT substrate, commonly located in areas of myocardial scar, becomes the standard treatment option [29], [31], [32], [41]. Catheter ablation aims to modify the electrical pathways that sustain VT, and it has shown improved outcomes for selected patients [42]–[46]. Despite its potential benefits, catheter ablation faces significant limitations, as up to 50% of patients experience VT recurrence within 6 months of an initially successful catheter ablation procedure [47]. Additionally, catheter ablation carries side effects such as vascular complications, cardiac complications, neurologic complications and even death [48]–[52]. Comparatively, escalating antiarrhythmic drug doses is associated with more adverse events than catheter ablation, indicating the limitations of pharmacological therapy as a sole treatment option for VT [47], [53]. These side effects, combined with the VT recurrence rates, highlight the pressing need for more effective and less invasive treatment alternative options for VT patients, especially for those who are not suitable candidates for catheter ablation due to complications or inaccessible anatomical location of VT substrates.

## 2.2 Electroanatomical Mapping

3D EAM systems were first introduced in the 1990s and have become essential in the management of VT, especially for identifying the arrhythmogenic substrates for catheter ablation [54]. EAM is a technique used to generate a 3D representation of the targeted cardiac chambers, integrating both anatomical and electrical information [55]. This combination allows for accurate identification of abnormal conduction pathways in the heart chambers. 3D EAM systems can display catheter positions in real-time on a computer screen, and reconstruct the detailed 3D surface anatomy of specific cardiac chambers. The reconstructed surfaces of the heart's inner (endocardial) or outer (epicardial) layers form a shell in the virtual 3D space of the system. This shell is annotated with local electrophysiological data, including activation time, which represents the timing of local electrical activity. They also measure the voltage amplitude, either unipolar or bipolar, to indicate the presence of normal or scar tissue.

Currently, three major EAM systems are commonly used in clinical practice: RHYTHMIA HDx (Boston Scientific, St. Paul, Minnesota, USA), CARTO

3 (Biosense Webster, Diamond Bar, California, USA) and EnSite (Abbott Laboratories, Chicago, Illinois, USA) systems. The RHYTHMIA HDx mapping system uses both magnetic- and impedance-based methods for catheter tracking (see Figure 2.1) [56]. It is the first 3D mapping platform to enable automated high-density mapping using a specialized steerable 64-electrode mini-basket catheter [57]–[59]. The CARTO 3 mapping system makes use of magnetic field emitting coils for accurate localization of proprietary mapping and ablation catheters [54], [60]. The EnSite system uses impedance measurements to localize diagnostic and ablation catheters [61].

FIGURE 2.1: RHYTHMIA HDx electroanatomical mapping system. *Image provided courtesy of Boston Scientific. ©2025 Boston Scientific Corporation or its affiliates. All rights reserved.*

## 2.3 Stereotactic Arrhythmia Radioablation

The first intracranial stereotactic radiosurgery (SRS) technique was introduced in the 1950s, a head frame was fixed to the skull and provided an external 3D reference system to accurately localize the intracranial target and direct high doses of radiation therapy in a single session [62]. SBRT is an extension of this well-established technique that encompasses all sites below the cranium, which provides precise targeting and dose delivery, allowing for potent ablative doses to be delivered with acceptable toxicity in appropriately selected patients. Over the

past few decades, SBRT has emerged as a standard treatment modality for extracranial malignancies, facilitated by advancements in image guidance and motion management, which enable precise targeting despite respiratory and organ motion. SBRT has shown remarkable success in treating lung, liver, pancreas, prostate, kidney cancers [63]–[66]. SBRT is also utilized for treating oligometastases in various locations, including the lung, liver, bone and abdominal regions [67]–[69].

In 2003, the concept of using SBRT for non-invasive cardiac arrhythmia treatment was filed as the first patent in this field [70]. It delivers highly focused radiation beams to target and ablate arrhythmogenic tissue within the heart with a single fraction radiotherapy dose of 25 Gy [5], [29]. For VT, the primary aim of STAR is to ablate the arrhythmogenic substrate with a sufficient dose while minimizing safety margins and employing steep dose gradients to reduce the risk of cardiac radiation toxicity [7]. This concept eventually led to preclinical studies [71], [72], as well as the first-in-human treatments for VT and atrial fibrillation (AF) in 2012 and 2015, respectively [1], [73]. For patients with refractory VT who lack other interventional options, cardiac SBRT, also known as STAR, has emerged as a promising non-invasive bailout treatment option [2], [3], [5], [6], [74]–[80], and has gained acceptance in the cardiology community [8]. The feasibility of STAR has already been confirmed by several early-phase prospective trials, and their results have been recently summarized in a systematic review and a meta-analysis on behalf of the STOPSTORM.eu consortium [5], [6]. Figure 2.2 shows two commonly used radiotherapy systems in clinical practice: TrueBeam (Varian Medical Systems, Palo Alto, California, USA) and Cyberknife M6 (Accuray, Inc., Sunnyvale, California, USA).

Varian TrueBeam system

Accuray CyberKnife M6 system

FIGURE 2.2: Commonly used radiotherapy systems in clinical practice. Left: Varian TrueBeam. *Image courtesy of Varian Medical Systems, Inc. All rights reserved.*; right: Cyberknife M6. *Images used with permission from Accuray Incorporated. All rights reserved.*

In STAR treatment planning process, the CTV, ITV and planning target volume (PTV) need to be determined. The CTV defines the 3D VT substrate, determined by the treatment team using all available electrophysiologic and imaging data [11]. The size of the CTV should be reasonably small to avoid toxicity [81]. Since the CTV moves during STAR treatment, an ITV is generated by expanding the CTV [20]–[22] to account for cardiac and respiratory motion. A PTV is then created by further expanding the ITV to account for residual uncertainties such as setup and registration errors, as well as patient positioning and movement [20], [22], [29], [82]–[84]. Figure 2.3 illustrates the definitions of these cardiac target volumes.

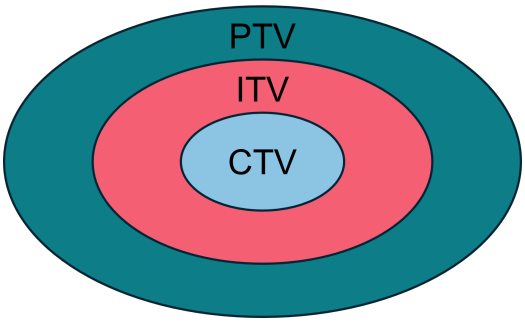


FIGURE 2.3: Definitions of cardiac volumes in stereotactic arrhythmia radioablation. See main text for details. Abbreviations: CTV = clinical target volume; ITV = internal target volume; PTV = planning target volume.

# Chapter 3

# Treatment Planning in Stereotactic Arrhythmia Radioablation

In this chapter, the current status and challenges of treatment planning process for STAR are discussed in three aspects: VT target registration methods between EAM systems and radiation TPS, validation of VT target registration methods, as well as cardiac motion estimation for STAR motion management.

## 3.1 Ventricular Tachycardia Target Registration

The accurate definition and localization of the cardiac CTV structure on treatment planning CT is essential for STAR treatment success and better patient outcomes, and it is an interdisciplinary task that involves electrophysiologists, cardiac radiologists, radiation oncologists and medical physicists.

The usual radiotherapy targets are readily identifiable in CT images due to the abnormal Hounsfield Unit (HU) values of the CT pixels, whereas the VT substrate is primarily defined by its electrophysiological properties which are mostly established through an electrophysiological study using 3D EAM procedure [9]. Freehand delineation of the target region as defined on EAM LV surface in the radiation TPS on treatment planning CT shows poor inter-observer consistency even when performed by experienced electrophysiologists or radiation oncologists [15], [16]. Furthermore, clinically relevant errors have been reported with such freehand delineation methods [18], and studies showed that the size of the cardiac CTV should be limited [81]. The implementation of a (semi-)automatic registration tool which can transfer the VT target defined on the LV surface in the

EAM system to the radiation TPS would greatly enhance the accuracy and reproducibility of cardiac CTV definition, and thereby improve the STAR performance and patient outcomes. Currently, the EAM data cannot directly be integrated into the radiation TPS. Indirect integration of the EAM data into the radiation TPS is possible through in-house script-based transformations of the EAM-derived data into a Radiotherapy Structure Set (RTSS) file based on different algorithms.

In this section, the state-of-the-art VT target registration approaches are discussed, including traditional manual freehand target registration, AHA 17-segment model registration and 3D-3D registration.

**Manual Freehand Target Registration**

During the initial STAR development, the cardiac CTV was freehand delineated on the treatment planning CT slices directly within the radiation TPS by visually side-by-side comparing the EAM data with the 3D contoured LV structure [12]–[14]. As expected, such manual cardiac CTV delineation method is significantly operator-dependent and lead to low inter-observer variability [15], [16]. In the benchmark study conducted by Boda-Heggemann *et al.* [15], the absolute distance of center of mass (CoM) was up to 43.9 mm with a lowest Dice-Sørensen coefficient (DSC) value of 0.02, while van der Ree *et al.* [16] reported a DSC value of $0.31 \pm 0.21$.

As a result, several studies have shown that manual delineation is prone to errors and can result in STAR treatment failure with recurring VT from regions directly neighboring the previously irradiated PTV with a necessity of repeat catheter ablation or STAR [12], [16], [18], [85].

**AHA 17-Segment Model Registration**

In 2002, the AHA recommended dividing the LV into 17 segments for regional analysis of ventricular function or myocardial perfusion based on autopsy data [25]. Figure 3.1 illustrates the location and the recommended names for the 17 LV myocardial segments on a bull's-eye map. The LV is divided into three circular sections, namely basal, mid-cavity and apical segments, perpendicular to the long axis. The relative contribution of the basal, mid-cavity and apical segments are 35% (6/17), 35% (6/17) and 30% (5/17), respectively. The basal section is subdivided into six $60^\circ$ segments: basal anterior, anteroseptal, inferoseptal, inferior, inferolateral and anterolateral, with the right ventricular wall attachment serving as a landmark for septal identification. In addition, the aortic valve root is placed at the center of LV segment 2. Similarly, the mid-cavity section is divided

into six 60° segments: mid anterior, anteroseptal, inferoseptal, inferior, inferolateral and anterolateral. Due to myocardial tapering, the apical section contains four 90° segments: apical anterior, septal, inferior and lateral. At the extreme tip of the left ventricle, the apical cap, composed solely of muscle without a cavity, represents the apex.

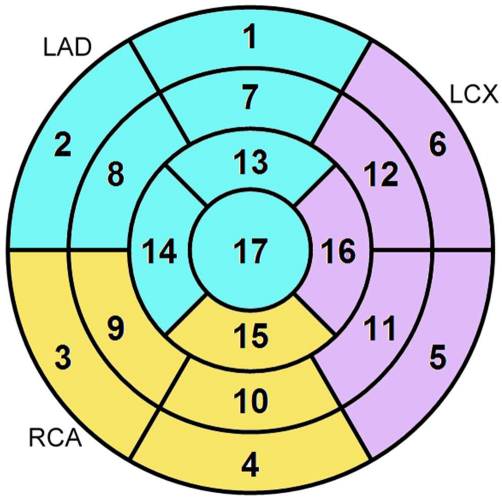


| Basal Segments | Mid-cavity segments | Apical segments |
|---|---|---|
| 1. Basal anterior | 7. Mid anterior | 13. Apical anterior |
| 2. Basal anteroseptal | 8. Mid anteroseptal | 14. Apical septal |
| 3. Basal inferior | 9. Mid inferoseptal | 15. Apical inferior |
| 4. Basal inferior | 10. Mid inferior | 16. Apical lateral |
| 5. Basal inferolateral | 11. Mid inferolateral | 17. Apex |
| 6. Basal anterolateral | 12. Mid anterolateral | |

FIGURE 3.1: American Heart Association (AHA) 17 myocardial segments with recommended nomenclature for the left ventricle tomographic imaging displayed on a bull's-eye map (circumferential polar plot). The AHA guidelines highlight the significant variability in the coronary artery blood supply to different myocardial segments. With the recognition of the anatomic variability the individual segments may be assigned to specific coronary artery territories: left anterior descending (LAD, cyan), right coronary artery (RCA, yellow) and left circumflex (LCX, magenta).

In a previous study conducted by Brownstein *et al.*, a step-by-step guide was proposed to rotate the heart from standard orthogonal views captured during radiation simulation to the cardiac-specific orientation required for visualizing the AHA 17-segment model [86]. Without an appropriate (semi-)automated segmentation tool, the manual segmentation of the LV structure based on the AHA

17 segments showed considerable inter-observer variability with DSC values of 0.31 ± 0.21 [16]. This study highlighted the need for a (semi-)automated tool to segment the LV structure in a more accurate and efficient approach.

In another study, a set of semi-automated angulation and segmentation tools were developed in C++ with the use of Digital Imaging and Communications in Medicine (DICOM) ToolKit library, to obtain the standardized AHA 17 segments of the LV for STAR. With assistance of this tool, the inter-observer variability is reduced and result in a DSC of 0.8 (interquartile range: 0.70-0.87) and a median of the mean Hausdorff distance (HD) of 0.9 mm (interquartile range: 0.5-1.7 mm) [87]. Another semi-automated tool named ASSET was developed within the MATLAB programming environment based on the mathematical method principal component analysis (PCA) [88]. The ASSET tool could accomplish the LV segmenting procedure in less than 5 minutes while the manual segmentation took more than 2 hours per patient, which is significantly time-saving for STAR treatment. In a prospective trial on patients with VT or cardiomyopathy related to premature ventricular contraction (PVC), the AHA 17-segment model was used to compare and determine the final target for STAR based on the combination of electrical information and the anatomic scar information [77]. As a result, for the evaluable patients, VT episodes or PVC burden were reduced in 17/18 patients (94%), with a concurrent reduction in antiarrhythmic medication. Similarly, in another prospective trial, with the help of the main efficacy measure of $\geq$ 50% reduction in treated VT episodes was achieved in four evaluable patients at the 12 months follow-up.

However, as discussed in a STAR case report, most likely, the cardiac CTV created by AHA 17-segment model approach will be larger than the expected CTV [89]. This is because usually the VT target is only partially but not exactly located in one or several LV segments. Therefore, the 17-segment model registration approach is not expected to accurately localize the cardiac CTV in the treatment planning CT. On the other hand, the AHA 17-segment model is designated for the LV structure that cannot be applied to cases where the VT substrate locates on the right ventricle (RV) structure.

**3D-3D Registration**

In commonly used commercial EAM systems in clinical practice (i.e., RHYTHMIA HDx, CARTO 3 and EnSite), the mapped cardiac structures data and the catheter ablation points can be exported in vendor-specific formats during typical catheterization procedure as 3D EAM raw data. The exported EAM raw data

can then be registered to the 3D CT contours with respect to the planning imaging data. This VT target registration concept can be classified as 3D-3D registration.

EAMapReader [90] written in Python programming language is an extension within the open-source 3D Slicer software [91]. It can define the cardiac CTV on the radiation treatment planning CT in a 3D-3D registration manner. It is able to import the raw data exported from the EAM systems in the corresponding vendor-specific data format. The significant parts of the EAM raw data are then extracted for reverse engineering, to recreate the map as a triangulated mesh with overlaid scalar information of voltage and local activation time. For VT target registration, a contrast-enhanced cardiac CT and the corresponding RTSS file including the LV and aorta structures are loaded into the 3D Slicer software with its extension SlicerRT [92]. A manual alignment was initially performed, followed by an automatic registration using iterative closest point (ICP) algorithm for fine-tuning. Afterwards, a cardiac CTV can be created on the cardiac CT based on the aligned map. Eventually, the cardiac CTV structure can be exported in an RTSS file which can be read by the radiation TPS.

In recent years, based on this 3D-3D registration concept, some research groups have developed different VT target registration tools: register the 3D mesh of the mapped cardiac substructures (e.g., LV and aorta) from the EAM output data to the CT contours of the LV structure with respect to the radiation treatment planning CT, and define the VT target on the EAM mesh based on the arrhythmogenic substrate from the EAM data in order to finalize the cardiac CTV [18], [93]–[98]. In addition, some commercial products have been developed. Mimics Innovation Suite (Materialise, Leuven, Belgium) can fuse imaging data (in DICOM format) and EAM data [78]. ADAS 3D (Galgo Medical S.L., Barcelona, Spain) is capable of performing landmark-based 3D-3D VT target registration [89], [99].

Despite the increased accuracy of the 3D-3D registration method compared with the traditional manual delineation and semi-automated AHA 17-segment model registration, one drawback of the 3D-3D registration is that the EAM raw data is highly vendor- and version-specific. Therefore, designated scripts are prerequisite for different models of EAM systems, or even for different versions of a same model. To overcome this and make the VT target registration tool more versatile, it is of interest to investigate if the EAM data can be utilized in another form such as its screenshots in commonly used image formats Portable Network Graphics (PNG) and Joint Photographic Experts Group (JPG/JPEG).

## 3.2 Validation of Target Registration

**Implementation for Quality Assurance**

Despite high initial success rates of STAR treatments for VT patients, VT target definition and methods of data transfer from the electrophysiology to the radiation TPS is a research hotspot. Harmonizing these processes is particularly challenging within multi-center, multi-platform clinical studies such as the RAVENTA trial (NCT03867747) [29], [100], which involves various EAM systems and radiation platforms [80], [100], [101]. A recent RAVENTA benchmark on VT target definition and contouring highlighted significant clinician-to-clinician deviations in cardiac CTV delineation for STAR [15]. This variability partly comes from differing approaches to VT catheter ablation [102], but current manual methods for transferring VT targets from EAM to radiotherapy planning imaging data further introduces uncertainty and variation.

Quality assurance of the VT target transfer from the EAM data to the radiation TPS conducted as a pre-treatment verification during treatment planning is crucial for ensuring treatment performance and patients' outcomes in STAR [2], [4], [6], [17], [29], [101], [103]. In several prospective studies investigating the use of STAR for the treatment of VT, different quality assurance tools of VT target definition in the radiation TPS have been employed [6].

In the Electrophysiology-Guided Noninvasive Cardiac Radioablation for Ventricular Tachycardia (ENCORE-VT) trial (NCT02919618), the AHA 17-segment model of the LV was used for VT target volume transfer from the electrocardiographic imaging (ECGI) to the radiation TPS [77] for 19 patients (17 with VT and 2 with PVC cardiomyopathy). In another prospective study (NCT02661048) published in 2020, 5 patients were treated with STAR for refractory scar-related VT [12].The anatomical cardiac CTV for STAR was defined based on study-specific preprocedural imaging with cardiac CT and delineated using a cardiac-specific radiotherapy planning software called CardioPlan (CyberHeart, Portola Valley, California, USA). However, the quality assurance approach used for VT target transfer was not specified in that publication.

Later, the preliminary results of the STereotactic RadioAblation by Multimodal Imaging for Ventricular Tachycardia (STRA-MI-VT) study (NCT04066517) including 7 patients were reported in 2021 [104]. A consensus on the VT target structure was identified by an interdisciplinary team (including an electrophysiologist, a clinical cardiologist, a cardio-radiologist, a biomedical engineer, a radiation oncologist and a medical physicist) based on cardiac CT, EAM analysis, as

well as all additional ECG and ECGI information. The details of the quality assurance tool used for verifying the defined VT target was not given in that study.

In a study published in 2022 including 6 VT patients, the quality assurance tool for EAM-TPS transfer was also not specified [105]. In the same year, a single-center case series (HeartSABR, KCT0004302) involving 6 patients with intractable VT or PVC-induced cardiomyopathy was published, but the target transfer quality assurance tool remained unspecified [106].

The results of the Stereotactic management of arrhythmia - radiosurgery in treatment of ventricular tachycardia (SMART-VT) trial (NCT04642963), which included 11 patients and was published in 2023, stated that the quality assurance tools used for VT target registration were the 3D Slicer extension named EAMapReader (primarily) [90] and the AHA 17-segment model, with the CARDIO-RT software used for retrospective data analysis [107]. Additionally, the AHA 17-segment model was employed as a quality assurance tool for VT target transfer in the StereoTactic Arrhythmia Radiotherapy in the Netherlands no.1 (STARNL-1) trial (Netherlands Trial Register: NL7510) [108] and the Stereotactic Radioregulation Antiarrhythmic Therapy (SRAT) trial (ID: jRCTs032190041) [109], which included 6 and 3 VT patients, respectively. In another prospective study, 14 VT patients were treated with STAR, but again, the quality assurance tool for target transfer was not specified.

The ventricular wall thinning and perfusion information provided by the in-HEART online platform [110] was also mentioned for quality assurance in a retrospective analysis [111]. Similarly, in the initial experience with the STAR study in an Australia cohort of 12 drug-refractory VT patients, the ADAS 3D software (wall thickness derived from CT data) and the AHA 17-segment model were utilized for quality assurance [112]. The ADAS 3D software was also used in two case reports to fuse the EAM data and CT contours of the cardiac substructures (e.g., LV, aorta, etc.) [89], [99].

Within the STOPSTORM.eu consortium, to enable harmonization, standardization and optimization of STAR treatment, a comprehensive quality assurance programme including mandatory benchmark studies with target definition, treatment planning and a dedicated STAR case review software for secondary quality assurance has been established [5].

**Cross-Validation for Target Registration Methods**

Freehand delineation of the VT target region, defined on the mapped EAM LV

surface, in the radiation TPS on treatment planning CT demonstrates low inter-observer consistency, even performed by experienced electrophysiologists and radiation oncologists [15], [16]. Moreover, clinically significant errors have been reported with these freehand "eyeballing" approaches [18].

In 2021, a 3D-3D VT target registration workflow implementing the 3D Slicer software was published, and this workflow was reported to be robust and compatible with another cardiac magnetic resonance imaging (MRI) based STAR treatment planning system ADAS-3D (Galgo Medical S.L., Barcelona, Spain) [93]. However, the intra-/inter-observer variability or the associated reproducibility rate was not demonstrated. In the same year, a research group conducted an inter-observer variability study of a 3D-3D VT target registration workflow, using an in-house program written in Python for CARTO EAM raw data conversion [18] and the 3D Slicer software for a manual EAM-CT registration [113]. The cardiac gross target volume (GTV)s were created by two observers independently using case data for 9 VT patients who underwent STAR, and the percentage of the overlapping and non-overlapping GTV in relation to the total volume was calculated. Created GTVs were significantly different (8 vs 19 $cm^3$) with lowest GTV overlap of 35% for lateral wall target areas. Later in 2024, this research group published another work to analyze the intra- and inter-observer variability of their refined 3D-3D VT target registration workflow which enables automatic EAM-CT registration [97]. Cardiac CTVs were created by two observers independently for datasets of 10 VT patients who underwent STAR. For the inter-observer variability, the DSC and mean HD was 0.81 ± 0.11 and 0.87 ± 0.45 mm, respectively. Regarding the intra-observer variability, the DSC and mean HD was 0.82 ± 0.06 and 0.71 ± 0.22 mm, respectively. The high inter-observer similarity of delineated cardiac CTVs confirmed the robustness of the VT target registration workflow.

However, these studies were focused on the intra- and inter-observer variability of a specific VT target registration tool, but not the conformity between different VT registration approaches.Although several novel semi-automatic VT target registration tools have been developed, there is still a lack of studies to evaluate the conformity of the cardiac CTVs generated by different novel semi-automated VT target transfer approaches. Such studies would be significantly beneficial to confirm the accuracy and effectiveness of these different tools for STAR.

## 3.3 Cardiac Motion Estimation for Motion Management

During STAR treatments, although respiratory motion can be accurately managed by e.g., gating, DIBH techniques or tracking using robotic based techniques [23], [24], [114], radiotherapy systems are not equipped to account for cardiac motion during STAR treatment, which is rarely a concern in traditional radiation oncology [115]. Cardiac motion, particularly the movement of the CTV and the AHA 17 LV segments [25], presents a significant challenge in the precise definition of cardiac ITV margin. This motion can lead to marginal misses, reducing the efficacy of the treatment and potentially causing damage to the surrounding OAR via dose wash-out [26]. Additionally, active motion management strategies have been under investigation in recent years [27], [28], and cardiac motion estimation could help identify VT patients with larger cardiac motion who would particularly benefit from them. Moreover, a previous review conducted by the STOPSTORM.eu consortium has demonstrated that the cardiorespiratory motion is patient-specific, suggesting the need for personalized motion management in STAR for VT [26]. Therefore, estimating the cardiac motion of the CTV and 17 LV segments is essential for defining an appropriate individualized cardiac ITV margin, thereby enhancing the performance of STAR.

In recent years, several studies focusing on cardiac motion analysis for STAR have been published. In 2020, a research team investigated the motion of the LV (CoM), RV, ascending aorta, ostia of the right coronary artery, left coronary artery and left anterior descending artery using breath-hold cardiac gated CT of 10 patients who underwent transcatheter aortic valve replacement, and reported that more than 90% of the motion was less than 5 mm [116]. Then in 2024, a study was conducted to analyze the geometric centroid of the target arrhythmogenic substrate of 12 patients with refractory arrhythmia treated by STAR, using four-dimensional (4D) cardiac CT and 4D CT with a deformation vector field [117]. The mean maximum displacement of the target arrhythmogenic substrate in 3D due to cardiac pulsation was 5.2 mm (range: 2.6-8.0 mm) in that study. In the same year, an analysis on cardiorespiratory motion including 44 patient datasets with catheter ablation geometrical data recorded during EAM procedures was performed. It was reported that the average cardiac and respiratory motion was 1.6 ± 1.2 mm and 12.1 ± 4.1 mm, respectively [118]. Additionally, the average ratio of respiratory to cardiac motion was approximately 11:1. Recently, a research team used breath-hold cardiac magnetic resonance cine images to quantify AHA 17 LV segments motion during the cardiac cycle, and provided an estimate of

epicardial and endocardial displacement for the AHA 17 LV segments for patients with normal and impaired LV function [119]. Moreover, they demonstrated that cardiac cycle motion is an important component of overall target motion and varies depending on the anatomic cardiac segment [120]. Wu *et al.* measured the displacement of transvenous right atrial appendage, RV ICD, coronary sinus lead tips and prosthetic cardiac devices across the cardiac cycle from breath-hold 4D cardiac CT in 31 patients who underwent catheter ablation procedure for atrial or ventricular arrhythmias [121]. In that study, there was considerable variation in cardiac contractile motion among the patients, ranging from 1 to 15 mm, and the RV ICD lead tip motion was 8.6 ± 3.5 mm.

However, current studies focusing on patient- and segment-specific cardiac motion analysis of the cardiac CTV (especially at the voxel-wise level), as well as the correlation between ICD lead tip motion and the motion of both the CTV and the 17 LV segments in VT patients who underwent STAR, remain limited.

# Chapter 4

# CARDIO-RT Target Registration Methods

In this chapter, practical methods of registering the VT target determined by the treatment team using all available EAM data are explored, resulting in a software named CARDIO-RT including three semi-automatic target registration methods. This chapter provides the answer to the research question Q1 addressed in section 1.1.

This chapter begins with a short summary of the scientific contributions in section 4.1. This is followed by the demonstrations of three practical VT target registration methods, namely the AHA 17-segment model registration (section 4.2), 3D-3D registration (section 4.3) and 2D-3D registration (section 4.4). Next, section 4.5 addresses the significance of aorta mapping in EAM systems for the 2D-3D registration method. In section 4.6, three main additional functions of the registration software are introduced. Finally, the chapter ends with a discussion in section 4.7 and a summary in section 4.8.

## 4.1 Scientific Contributions

In this chapter, a stand-alone software named CARDIO-RT including three practical semi-automatic VT target registration methods between the EAM system and the radiation TPS for STAR is demonstrated. This software has an intuitive graphical user interface (GUI) and has been developed and maintained within the MATLAB App Designer development environment (version R2024b, The MathWorks Inc., Natick, Massachusetts, USA) [122]. The CARDIO-RT software is compatible with Windows, Linux, and Mac operating systems. This software includes three VT target registration methods: the AHA 17-segment model registration,

3D-3D registration and 2D-3D registration. The AHA 17-segment model registration is able to divide the LV myocardium structure contoured from the cardiac CT into 17 segments according to the 17-segment model published by the AHA [25]. The 3D-3D registration method can read the raw data including the LV, aorta and catheter ablation points exported from the EAM system in corresponding vendor-specific data formats, and then register the catheter ablation points to the radiation treatment planning imaging data. It currently supports three EAM systems: RHYTHMIA HDx, CARTO 3, and EnSite. For the 2D-3D registration, it transfers the VT target marked on the EAM screenshots (in PNG or JPG/JPEG format) in standard anatomical views to the radiation treatment planning imaging data.

The practical VT target registration software proposed in this chapter has been employed as a quality assurance tool within the German RAVENTA trial (NCT03867747) [4], [29], a harmonized trial in Israel (national trial number: 202225964) [30], as well as the SMART-VT trial (NCT04642963) [6], [107]. As of the writing of this dissertation, at least 39 prospective STAR cases for VT have been performed with assistance of the CARDIO-RT software as a quality assurance tool for VT target registration. Some clinical trials and studies that employed the software have already been published [4], [30], [123]–[132].

## 4.2 AHA 17-Segment Model Registration

### 4.2.1 Registration Workflow

**Data Preparation and Import**

The AHA 17-segment model registration is a versatile method that supports all EAM systems. Figure 4.1 illustrates the workflow of the CARDIO-RT AHA 17-segment model registration.

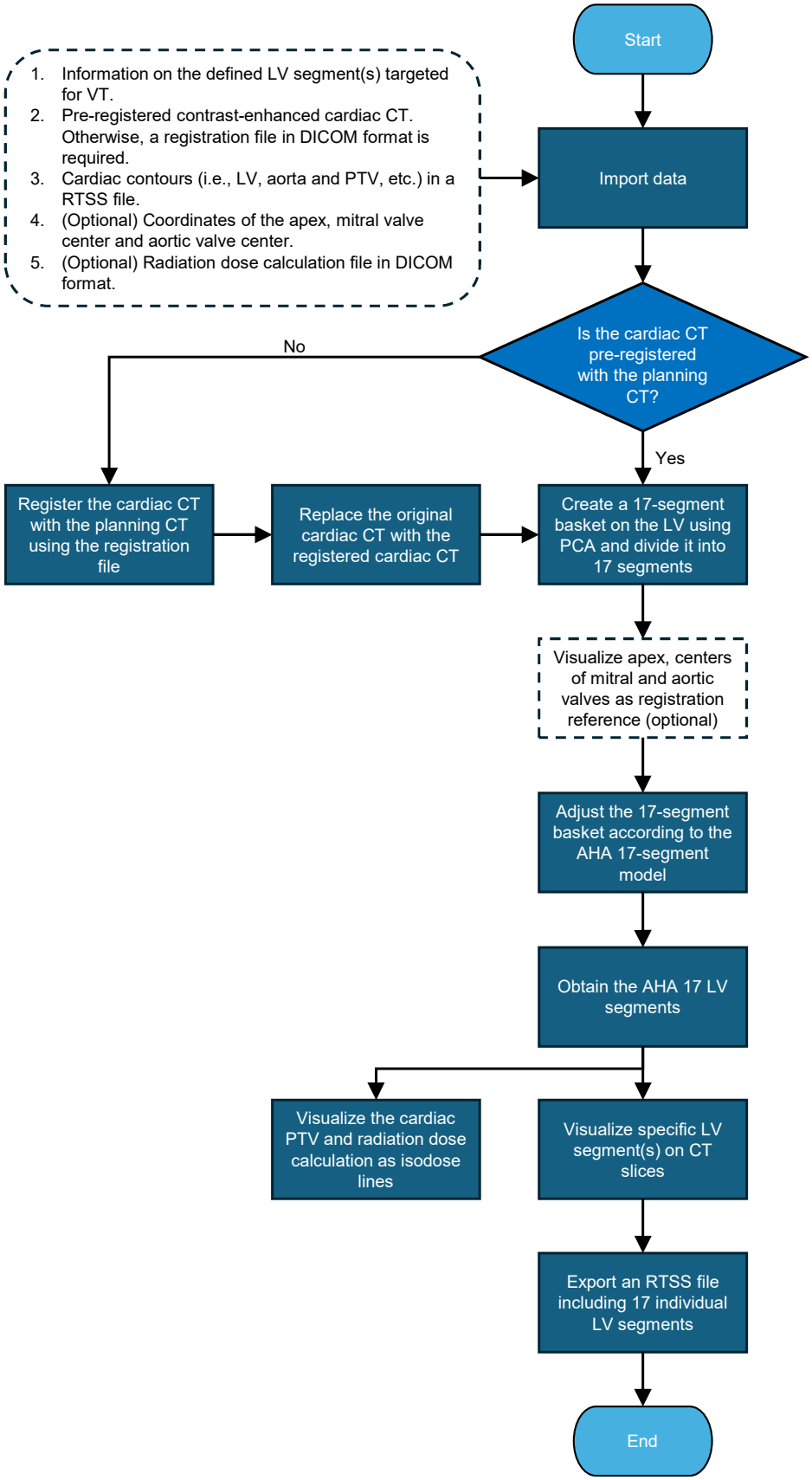


FIGURE 4.1: CARDIO-RT American Heart Association (AHA) 17-segment model registration. See main text for details. Abbreviations: LV = left ventricle; VT = ventricular tachycardia; CT = computed tomography; DICOM = Digital Imaging and Communications in Medicine; PTV = planning target volume; RTSS = radiotherapy structure set; PCA = principal component analysis.

The RTSS file including the cardiac substructures (i.e., LV myocardium, aorta, etc.) is imported, and the LV myocardium and aorta (if available) contours are imported as individual point clouds. The inclusion of aorta structure could improve the accuracy of 17-segment model registration by serving as a reference for registration.

For the LV structure extracted from the RTSS file, the contour points on some slices may be sparse. On the most superior and inferior slices, the points are only located along the LV boundary (see Figure 4.2). Therefore, very limited LV points can be defined as VT target points. To address this issue, the density of LV points can be increased using the following procedure. For each contour of the LV structure, the $x$-, $y$- and $z$-coordinates of LV points are extracted from the DICOM metadata of the corresponding RTSS file in order to generate a binary mask. For all binary masks except the most superior and inferior ones, only the perimeter pixels of the binary map are kept. Next, based on these pixels, a set of rasterized points is generated for each contour. Eventually, an LV point cloud with higher density is obtained (see Figure 4.2).

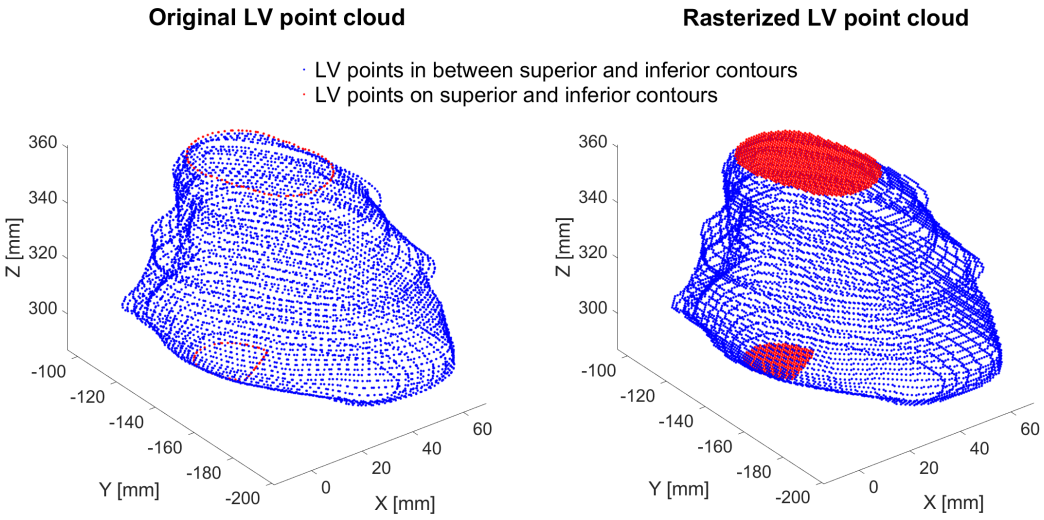


FIGURE 4.2: Original and rasterized left ventricle (LV) point clouds.

For CT scans, either the planning CT, the cardiac CT, or both should be imported. The CT slices are exported in DICOM format from the radiation TPS and then imported as a volume into the CARDIO-RT software.

After importing all required and optional data, if both the planning CT and cardiac CT datasets are imported, it will be checked whether the cardiac CT is already registered to the planning CT. If not, the cardiac CT can be registered to the planning CT (see section 4.6.2).

**Divide Left Ventricle Myocardium into 17 Segments**

Initially, the CoM $(\bar{x}, \bar{y}, \bar{z})$ of the original point cloud $\mathbf{P}^0_{\text{LV}}$ of the LV myocardium is calculated. A translation matrix $\mathbf{M}_1$ is then defined based on this CoM. This translation matrix is applied to the point cloud $\mathbf{P}^0_{\text{LV}}$ to obtain the transformed point cloud $\mathbf{P}^1_{\text{LV}}$, ensuring that its CoM is aligned with the origin:

$$\mathbf{P}^1_{\text{LV}} = \mathbf{M}_1 \cdot \mathbf{P}^0_{\text{LV}}. \tag{4.1}$$

Afterwards, PCA will be performed on the point cloud $\mathbf{P}^1_{\text{LV}}$ to determine the principal component coefficient matrix $\mathbf{R}_{\text{PCA}}$:

$$\mathbf{R}_{\text{PCA}} = \begin{pmatrix} \mathbf{v}_1 & \mathbf{v}_2 & \mathbf{v}_3 & \mathbf{0} \\ 0 & 0 & 0 & 1 \end{pmatrix}, \tag{4.2}$$

where each of $\mathbf{v}_1$, $\mathbf{v}_2$ and $\mathbf{v}_3$ contains the coefficients for one principal component. The point cloud $\mathbf{P}^1_{\text{LV}}$ is then rotated accordingly, to be aligned with its principal axes:

$$\mathbf{P}^2_{\text{LV}} = \mathbf{R}_{\text{PCA}} \cdot \mathbf{P}^1_{\text{LV}}. \tag{4.3}$$

In the GUI, for each principal axis, the additional rotations $\mathbf{R}(x, \theta_1)$, $\mathbf{R}(y, \theta_2)$ and $\mathbf{R}(z, \theta_3)$ about the three component axes can be defined. A new point cloud $\mathbf{P}^3_{\text{LV}}$ is then obtained by applying the composite rotation matrices:

$$\mathbf{P}^3_{\text{LV}} = \mathbf{R}(x, \theta_1) \cdot \mathbf{R}(y, \theta_2) \cdot \mathbf{R}(z, \theta_3) \cdot \mathbf{P}^2_{\text{LV}}. \tag{4.4}$$

In the next step, the point cloud $\mathbf{P}^3_{\text{LV}}$ will be translated according to the matrix $\mathbf{M}_2$ to align the apex with the origin:

$$\mathbf{M}_2 = \begin{pmatrix} 1 & 0 & 0 & -x_{\text{apex}} \\ 0 & 1 & 0 & 0 \\ 0 & 0 & 1 & 0 \\ 0 & 0 & 0 & 1 \end{pmatrix}, \tag{4.5}$$

where $x_{\text{apex}} = \min(x)$ from the transformed points $\mathbf{P}^3_{\text{LV}}$. Since the size of the LV structure varies among VT patients, the LV myocardium point cloud is normalized according to the length between the apex and mitral valve $l_{\text{LV}}$:

$$l_{\text{LV}} = x_{\text{mitral valve}} - x_{\text{apex}}, \tag{4.6}$$

and

$$\mathbf{M}_3 = \begin{pmatrix} \frac{1}{l_{\mathrm{LV}}} & 0 & 0 & 0 \\ 0 & \frac{1}{l_{\mathrm{LV}}} & 0 & 0 \\ 0 & 0 & \frac{1}{l_{\mathrm{LV}}} & 0 \\ 0 & 0 & 0 & 1 \end{pmatrix}, \tag{4.7}$$

where $x_{\text{mitral valve}} = \max(x)$ from the points $\mathbf{P}^3_{\mathrm{LV}}$. The final normalized LV myocardium points $\mathbf{P}^f_{\mathrm{LV}}$ can then be obtained:

$$\mathbf{P}^f_{\mathrm{LV}} = \mathbf{M}_3 \cdot \mathbf{M}_2 \cdot \mathbf{P}^3_{\mathrm{LV}}. \tag{4.8}$$

For each point in the point cloud $\mathbf{P}^f_{\mathrm{LV}}$, it is categorized based on the definition of the AHA 17-segment model of the LV. Points in the basal region are those with a distance greater than 65%, and this region is further divided into six segments (1-6), with each segment spanning 60 degrees of the circular bullseye. Similarly, the mid-cavity region corresponds to points with distances between 30% and 65%. This region is also divided into six segments (7-12), with identical angular divisions as the basal region. The apical region consists of points with distances less than 30% of the radius and includes four segments (13-16), with each spanning 90 degrees. Points close to the origin are assigned to the apex section (segment 17).

The LV myocardium structures before and after the AHA 17-segment model registration process are shown in Figure 4.3. A black line basket consists of radial lines and concentric circular segments with corresponding segment numbers is generated on the LV myocardium point cloud, to assist in dividing the LV myocardium point cloud (see Figure 4.3A). Optionally, as shown in Figure 4.3, the $x$-, $y$- and $z$-coordinates of the apex, mitral valve center and aortic valve center can be input, and these three points will then be visualized as three spheres on the LV 17-segment model and serve as a registration reference. This option is highly recommended in case the aorta structure is not available or the adjacent part of the aorta with the LV is incomplete in the RTSS file. Due to the absence of aorta structure, the aortic valve center can serve as a registration reference instead. During the 17-segment model registration, the segmented LV points are visualized in real time in the GUI.

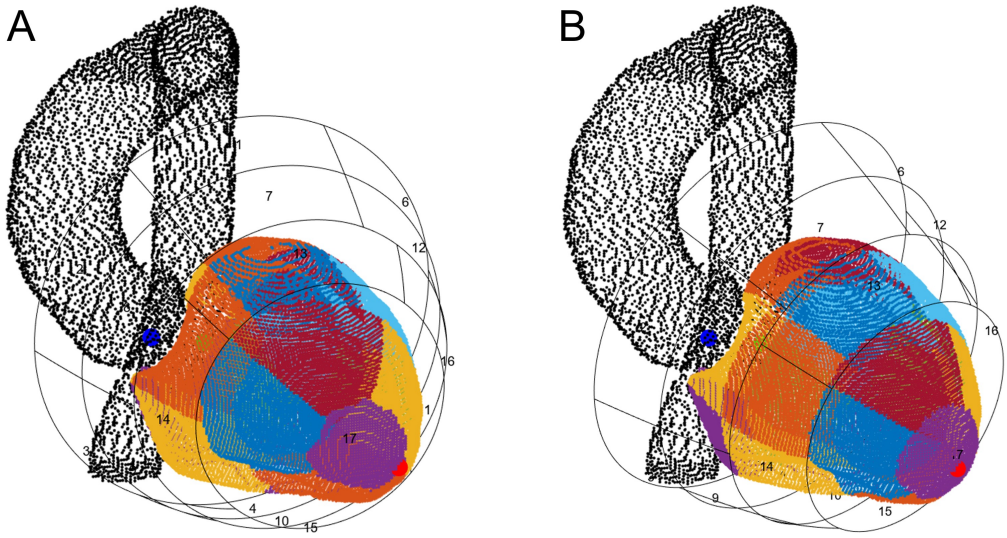


FIGURE 4.3: Representative case for the American Heart Association 17-segment model registration with the spheres of apex (red), mitral valve center (green) and aortic valve center (blue) as registration references. The left ventricle (LV) segments are shown in different colors, and the basket of the 17-segment model is shown as black concentric circles and radial lines. (A) The LV myocardium structure before the 17-segment model registration. (B) The LV myocardium structure after the 17-segment model registration.

**Data Output**

The $x$-, $y$- and $z$-coordinates of individual points from the registered VT targets cannot be directly added to the original RTSS file because the radiation TPS cannot interpret structures with the DICOM attribute ContourGeometricType set to POINT. Therefore, for each point in each LV segment structure, three additional points are defined to form a square with a side length of 1 mm. Afterwards, the $x$-, $y$- and $z$-coordinates of these four points are then saved in the DICOM metadata under the ROIContourSequence attribute, with ContourGeometricType set to CLOSED_PLANAR. The point clouds of all 17 LV segments are added to the original RTSS file as 17 individual structures, and exported as a new RTSS file.

It has been verified that the DICOM attributes of the saved structures have to be meticulously assigned. Otherwise, some radiation TPS may not be able to import the CARDIO-RT exported structures saved in the RTSS file correctly.

### 4.2.2 Visualization of the Registered 17 Segments

The registered LV segment(s) of interest can be selected and visualized on the imported CT slices in coronal, axial and sagittal views. If both cardiac CT and planning CT datasets are imported, the type of current visualized CT can be selected.

Additionally, the registered VT target, LV and aorta structures are visualized in the 3D view (see Figure 4.4). The visualized CT slices in the three anatomical views (i.e., coronal, axial and sagittal) can be adjusted. If needed, the CT slices in three anatomical views can be reset to the initial position. The slice position and the corresponding world position (unit: mm) for the current anatomical views are also shown in the GUI. The window width and level values for visualized medical images can be adjusted as needed. Additionally, the coronal, axial and sagittal views of the images can be displayed individually in the 3D view. The registered 17 LV segments are shown in Figure 4.5.

A

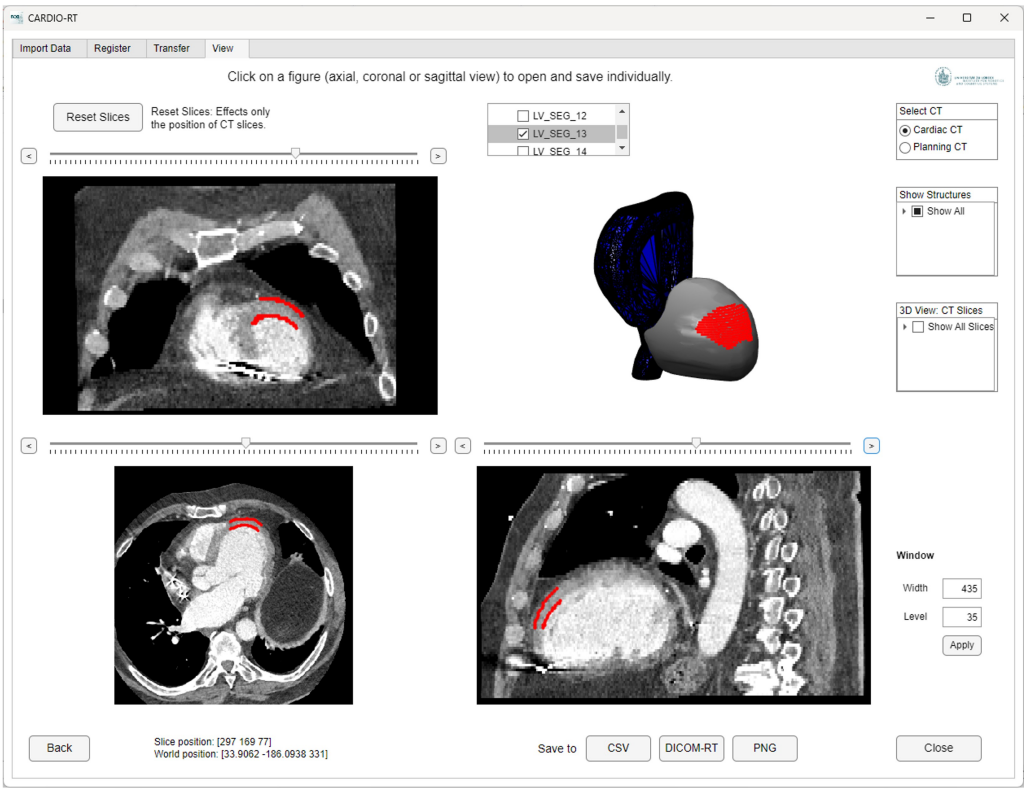


B

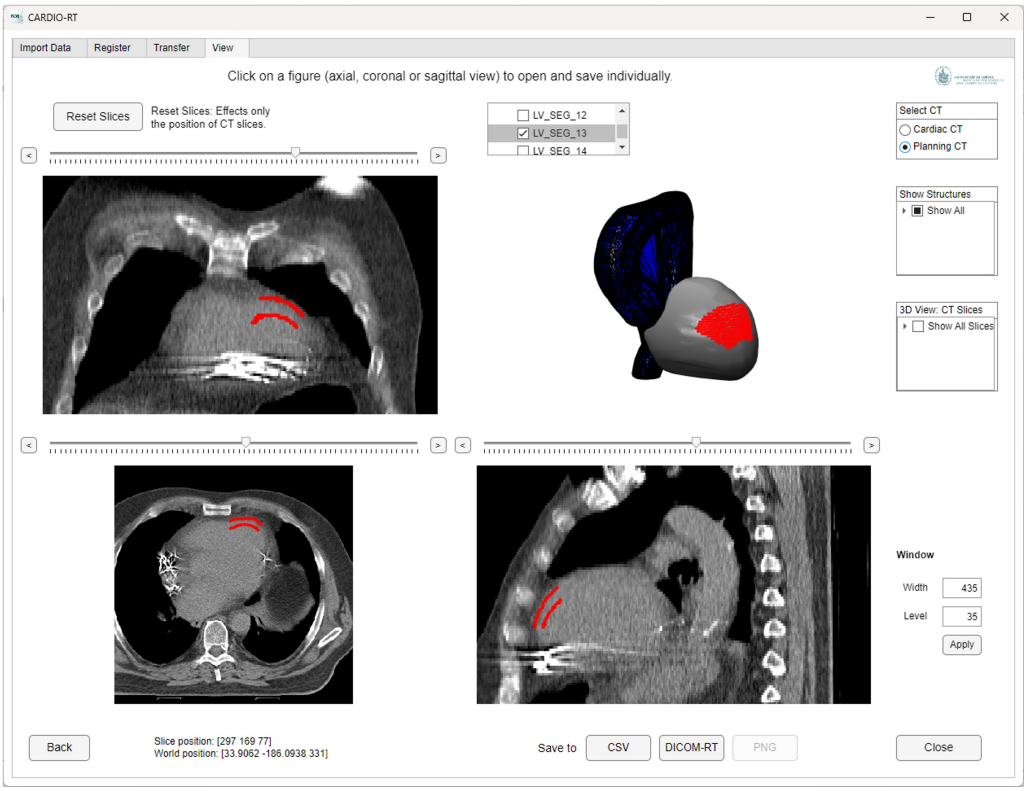


FIGURE 4.4: Representative case: Visualization of the registered left ventricle segment 13 (red) on the cardiac computed tomography (CT) (A) and planning CT (B) in the CARDIO-RT software.

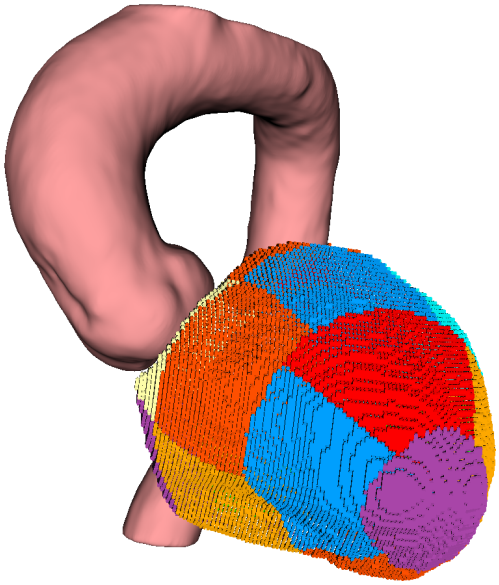

FIGURE 4.5: Representative case: Visualization of the registered American Heart Association left ventricle 17 segments (in different colors) and aorta (pink).

## 4.3 3D-3D Registration

### 4.3.1 Registration Workflow

**Data Preparation and Import**

Currently, the 3D-3D registration method supports the following three EAM systems:

- RHYTHMIA HDx
- CARTO 3
- EnSite

In the EAM system, during typical catheter procedures, the LV and aorta (optional) are mapped, and the VT catheter ablation points are defined and saved. These structures are exported as EAM raw data in vendor-specific formats. Data export processes vary across EAM systems, with limited documentation on export files.

For RHYTHMIA HDx system, cardiac substructures (i.e., LV, aorta, etc.) and catheter ablation points are exported in a single MATLAB .m file. In the CARTO 3 system, cardiac substructures are exported separately as individual files with the .mesh extension, while the catheter ablation points are saved in a file with

the _car.txt extension. For the EnSite system, cardiac substructures and catheter ablation points are exported in a single file with the .xml extension.

Exported and archived data files from the EAM systems were analyzed. Significant portions of the undocumented export and archive file formats were deciphered through manual inspection of binary raw data and comparisons of file structures. Custom MATLAB scripts were developed for the three EAM systems individually to ensure proper import of EAM data, including the LV, aorta (optional) and VT ablation points.

For CT scans, either the planning CT, the cardiac CT, or both should be imported. The CT scans are exported in DICOM format from the radiation TPS and then imported as a volume into the CARDIO-RT software.

Typically, cardiac substructures (i.e., LV, aorta, etc.) are contoured in the radiation TPS, and are exported as an RTSS file. In the DICOM metadata of the RTSS file, the segmentations are stored in individual structure arrays under the DICOM attribute ROIContourSequence. The point cloud of a specific segmentation is organized, sorted and stored based on the $z$-coordinates of the individual points in the point cloud. Points with the same $z$-coordinate are stored in a single field within the DICOM attribute ContourData inside the corresponding ContourSequence. LV contours are essential, while the aorta contours are optional and serve as a registration reference. Importing aorta contours enhances the accuracy of 3D-3D registration.

After importing all required and optional data, if both the planning CT and cardiac CT datasets are imported, it is checked whether the cardiac CT is already registered to the planning CT. If not, the cardiac CT can be registered to the planning CT (see section 4.6.2).

**EAM-CT Left Ventricle Registration**

Figure 4.16 illustrates the workflow of the 3D-3D registration.

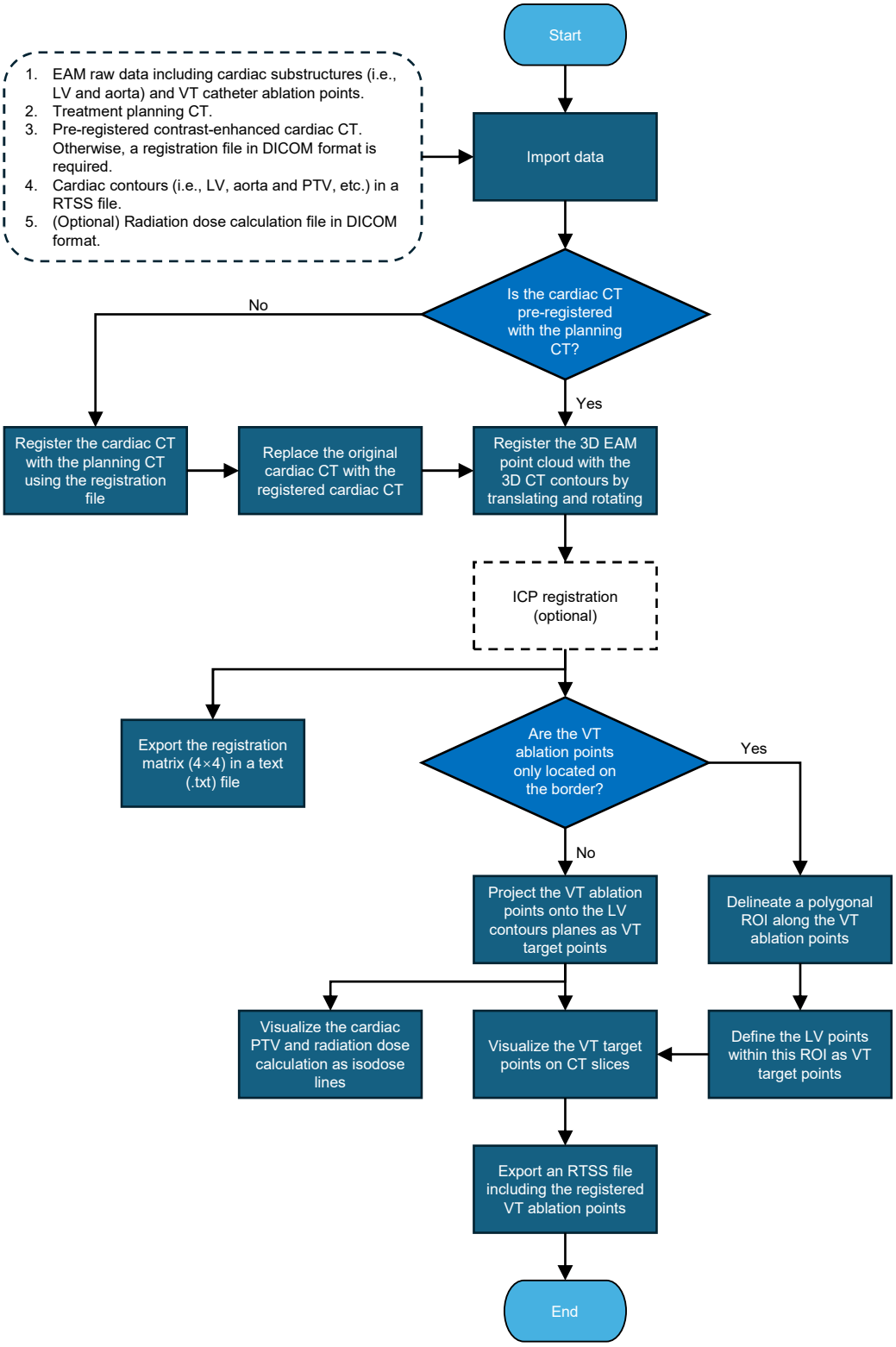


FIGURE 4.6: 3D-3D registration workflow. See main text for details. Abbreviations: EAM= electroanatomical mapping; LV = left ventricle; VT = ventricular tachycardia; CT = computed tomography; DICOM = Digital Imaging and Communications in Medicine; PTV = planning target volume; RTSS = radiotherapy structure set; ICP = iterative closest point; ROI = region of interest.

The orientation of the patient in the coordinate system across different EAM systems (i.e., CARTO 3, RHYTHMIA HDx and EnSite) is different. Therefore, after importing the EAM point cloud and CT contours, a rotation matrix $\mathbf{R}_{\text{ini}}$ is applied to the EAM point cloud to diminish this variation of orientations initially. The values of the Euler angles depend on the EAM system used. For RHYTHMIA HDx EAM data, the initial rotation angles are set as $\alpha_{\text{ini}} = \pi/2$, $\beta_{\text{ini}} = \pi$ and $\gamma_{\text{ini}} = 0$. For CARTO 3 EAM data, the initial rotation angles are set as $\alpha_{\text{ini}} = \pi/2$, $\beta_{\text{ini}} = 0$ and $\gamma_{\text{ini}} = 0$. For EnSite EAM data, the initial rotation angles are set as $\alpha_{\text{ini}} = 0$, $\beta_{\text{ini}} = 0$ and $\gamma_{\text{ini}} = -\pi/4$. The initial rotation matrix $\mathbf{R}_{\text{ini}}$ is then defined as:

$$\mathbf{R}_{\text{ini}} = \mathbf{R}(x, \alpha_{\text{ini}}) \cdot \mathbf{R}(y, \beta_{\text{ini}}) \cdot \mathbf{R}(z, \gamma_{\text{ini}}). \tag{4.9}$$

The CoM $(\bar{x}_{\text{EAM}}, \bar{y}_{\text{EAM}}, \bar{z}_{\text{EAM}})$ of the imported point cloud of EAM data $\mathbf{P}^0_{\text{EAM}}$ is calculated. A translation matrix $\mathbf{M}_{\text{EAM}}$ is then defined based on this CoM, to align the CoM of $\mathbf{P}^0_{\text{EAM}}$ with the origin. Similarly, the CoM $(\bar{x}_{\text{CT}}, \bar{y}_{\text{CT}}, \bar{z}_{\text{CT}})$ of the point cloud of imported CT contours $\mathbf{P}_{\text{CT}}$ is calculated, and a translation matrix $\mathbf{M}_{\text{CT}}$ is defined accordingly, to shift the origin to the CoM of $\mathbf{P}_{\text{CT}}$.

The composite transformation matrix will then be applied to the original point cloud of imported EAM data $\mathbf{P}^0_{\text{EAM}}$ to obtain the initial point cloud of EAM data $\mathbf{P}^1_{\text{EAM}}$:

$$\mathbf{P}^1_{\text{EAM}} = \mathbf{M}_{\text{EAM}} \cdot \mathbf{M}_{\text{CT}} \cdot \mathbf{R}_{\text{ini}} \cdot \mathbf{P}^0_{\text{EAM}}. \tag{4.10}$$

The $x$-, $y$- and $z$-axes in the coordinate system and the orientation of the three anatomical views (i.e., superior (SUP), left lateral (LL) and anterior-posterior (AP)) are shown in Figure 4.7.

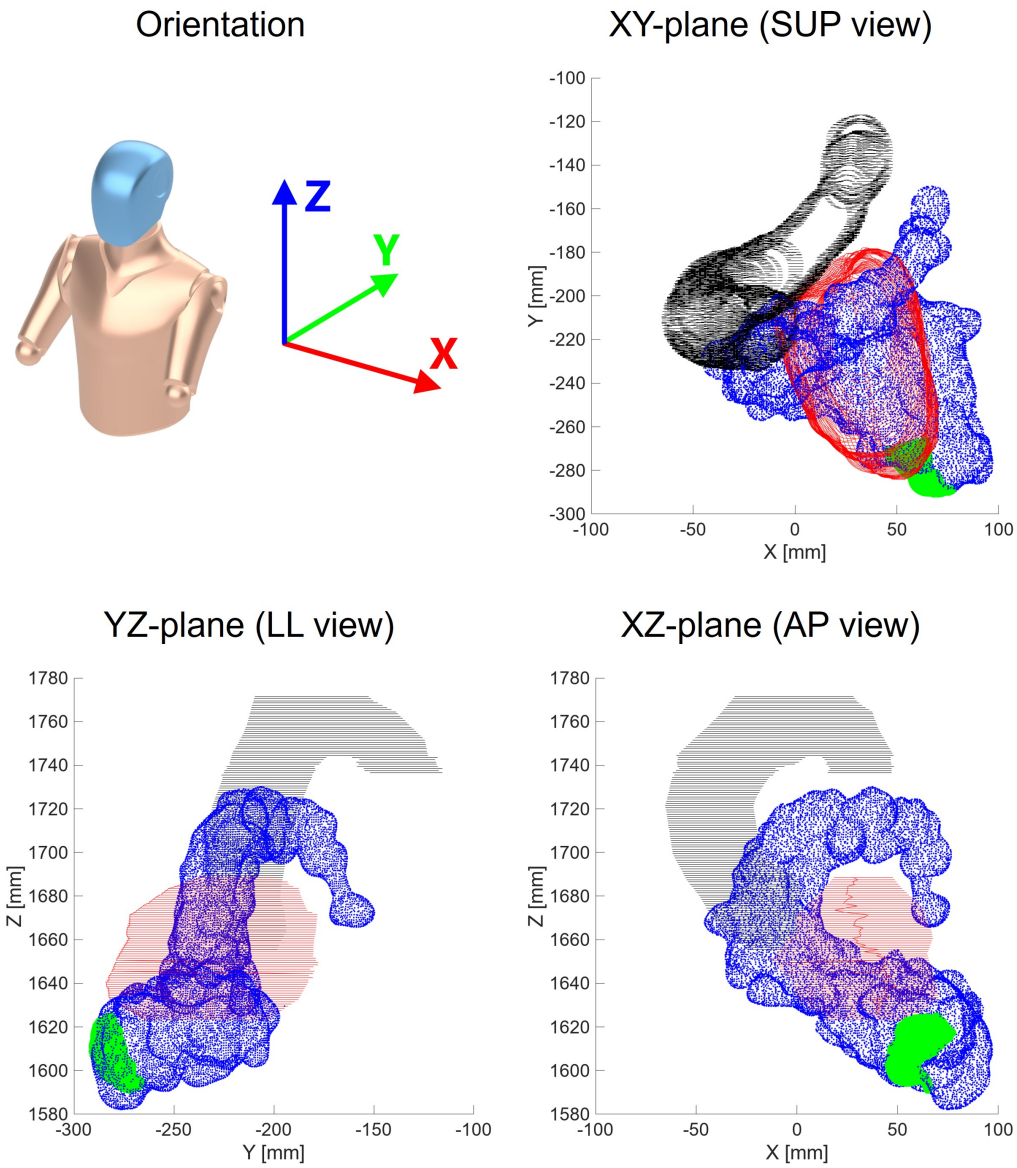


FIGURE 4.7: Orientation of the coordinate system for the 3D-3D registration and three planes for translation and rotation. $x$-axis: right-left direction; $y$-axis: anterior-posterior direction; $z$-axis: inferior-posterior direction. Abbreviations: SUP = superior; LL = left lateral; AP = anterior-posterior.

The initial positions of the EAM point cloud $\mathbf{P}^1_{\text{EAM}}$ and CT contours are shown in Figure 4.8A. At the beginning, the XY-plane, YZ-plane or XZ-plane can be selected. Then, the camera line of sight for the EAM point cloud and CT contours will switch to visualize them in the SUP, LL and AP views, respectively. During registration, the EAM points are moving, while the CT contours of LV and aorta remain fixed. In the selected plane, the EAM point cloud can be translated along the two main axes parallel to the selected plane. Additionally, it can be rotated

about the main axis perpendicular to the plane. The stepsize (unit: mm) and rotation angle increment (unit: degrees) can be adjusted for coarse or fine tuning. During the 3D-3D registration process, the EAM point cloud and CT contours are visualized in real time in the GUI.

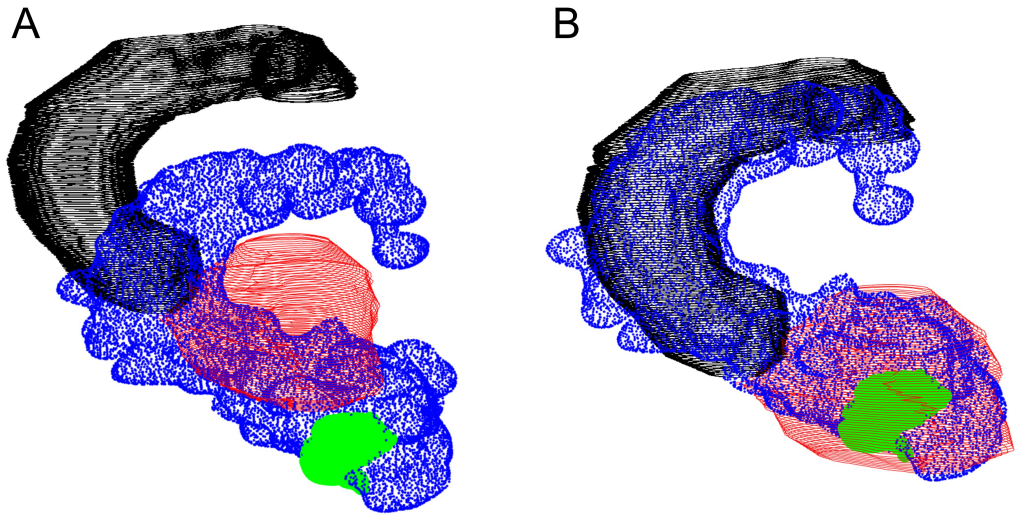


FIGURE 4.8: Representative case of the 3D-3D registration. Blue: left ventricle (LV) and aorta electroanatomical mapping (EAM) points; green: ventricular tachycardia catheter ablation points; red: computed tomography (CT) LV contours; black: CT aorta contours. (A) Position of the EAM point cloud and CT contours before registration. (B) Position of the EAM point cloud and CT contours after registration.

For translations, in the XY-plane (SUP view) and XZ-plane (AP view), the EAM point cloud can be translated along the $x$-axis. The total translation along the $x$-axis in these two planes is defined as $\mathbf{T}_x$. In the XY-plane (SUP view) and YZ-plane (LL view), the EAM point cloud can be translated along the $y$-axis. The total translation along the $y$-axis in these two planes is defined as $\mathbf{T}_y$. In the YZ-plane (LL view) and XZ-plane (AP view), the EAM point cloud can be translated along the $z$-axis. The total translation along the $z$-axis in these two planes is defined as $\mathbf{T}_z$.

For rotations, in the YZ-plane (LL view), the EAM point cloud can be rotated about the $x$-axis, and the rotation matrix is defined as $\mathbf{R}_x(\theta)$. In the XZ-plane (AP view), the EAM point cloud can be rotated about the $y$-axis, and the rotation matrix is defined as $\mathbf{R}_y(\phi)$. In the XY-plane (SUP view), the EAM point cloud can be rotated about the $z$-axis, and the rotation matrix is defined as $\mathbf{R}(z, \psi)$.

Optionally, the ICP algorithm [133] can be applied to iteratively minimize the distance between corresponding points to align the point cloud $\mathbf{P}^1_{\text{EAM}}$ with point cloud $\mathbf{P}_{\text{CT}}$, resulting in a rigid transformation matrix $\mathbf{M}_{\text{ICP}}$ which can be applied

to the EAM point cloud. The composite transformation matrix $\mathbf{M}_{\text{3D-3D}}$ is obtained as:

$$\mathbf{M}_{\text{3D-3D}} = \begin{cases} \mathbf{M}_{\text{ICP}} \cdot \mathbf{R}(x,\theta) \cdot \mathbf{R}(y,\phi) \cdot \mathbf{R}(z,\psi) \cdot \mathbf{T}_x \cdot \mathbf{T}_y \cdot \mathbf{T}_z \cdot \mathbf{M}_{\text{EAM}} \cdot \mathbf{M}_{\text{CT}} \cdot \mathbf{R}_{\text{ini}}, \\ \text{if ICP algorithm is applied} \\ \mathbf{R}(x,\theta) \cdot \mathbf{R}(y,\phi) \cdot \mathbf{R}(z,\psi) \cdot \mathbf{T}_x \cdot \mathbf{T}_y \cdot \mathbf{T}_z \cdot \mathbf{M}_{\text{EAM}} \cdot \mathbf{M}_{\text{CT}} \cdot \mathbf{R}_{\text{ini}}, \\ \text{otherwise} \end{cases} \tag{4.11}$$

and the final registered EAM point cloud $\mathbf{P}^{f}_{\text{EAM}}$ is then obtained as:

$$\mathbf{P}^{f}_{\text{EAM}} = \mathbf{M}_{\text{3D-3D}} \cdot \mathbf{P}^{0}_{\text{EAM}}. \tag{4.12}$$

If needed, the transformation of the EAM point cloud can be reset to its initial position ($\mathbf{P}^{1}_{\text{EAM}}$). During the 3D-3D registration procedure, the registration matrix $\mathbf{M}_{\text{3D-3D}}$ can be exported to a file with the .txt extension for potential documentation or research purposes. The exported file including the registration matrix can also be imported into the software to restore the corresponding position of the EAM point cloud $\mathbf{P}^{f}_{\text{EAM}}$. After the registration, the registered EAM point cloud is shown in Figure 4.8B.

**Project Ventricular Tachycardia Target onto Left Ventricle Contour Planes**

The moved EAM VT ablation points are projected onto the planes of the CT LV contours. For each point in the moved EAM VT ablation point cloud, the nearest $z$-plane from the CT LV points is identified by minimizing the absolute difference in $z$-coordinates. The $z$-coordinate of the specific plane is then assigned to the given point, while its $x$- and $y$-coordinates remain unchanged. This approach outputs a new matrix representing the registered VT target points.

**Project Ventricular Tachycardia Target onto Left Ventricle Point Cloud**

Since the EAM LV point cloud and CT LV contours are acquired using two different modalities, there is variation in the shape of these two LVs. Therefore, the registered VT target points may not locate exactly on the CT LV point cloud (see Figure 4.9A-C). To address this issue, the transformed VT target points can be projected onto the CT LV point cloud using a k-d tree-based search algorithm. In this approach, the moved EAM VT ablation points are defined as the query points, and the CT LV points are defined as the reference points. For each point

in the moved EAM VT ablation point cloud, the nearest $z$-plane in the reference point cloud is identified by minimizing the absolute difference in $z$-coordinates. Within the selected plane, the nearest point from the reference point cloud is then matched. Finally, a new set of points consisting of these matched points is defined as the registered VT target points (see Figure 4.9D-F).

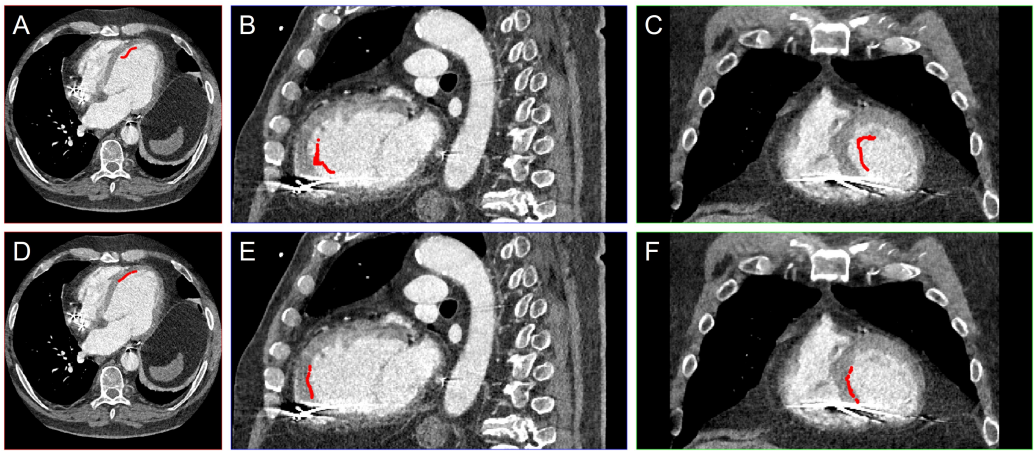


FIGURE 4.9: (A-C) The 3D-3D registered ventricular tachycardia (VT) target points (red) within the left ventricle (LV) blood pool, shown in axial, sagittal and coronal views of the cardiac computed tomography (CT). (D-F) The 3D-3D registered VT target points projected onto the LV point cloud (red), shown in axial, sagittal and coronal views of the cardiac CT.

**Fill the Border of Sparse Ventricular Tachycardia Target Points**

In some cases, only a set of very sparse EAM VT ablation points are defined and saved during the EAM procedure. These VT catheter ablation points are located along the the border of the VT target region, and thus only a small number of ablation points can be read and are applicable for the 3D-3D registration (see Figure 4.10). To enhance the visualization for the registered VT target points, the LV points within the border represented by these VT catheter ablation points can be selected and defined as VT target points.

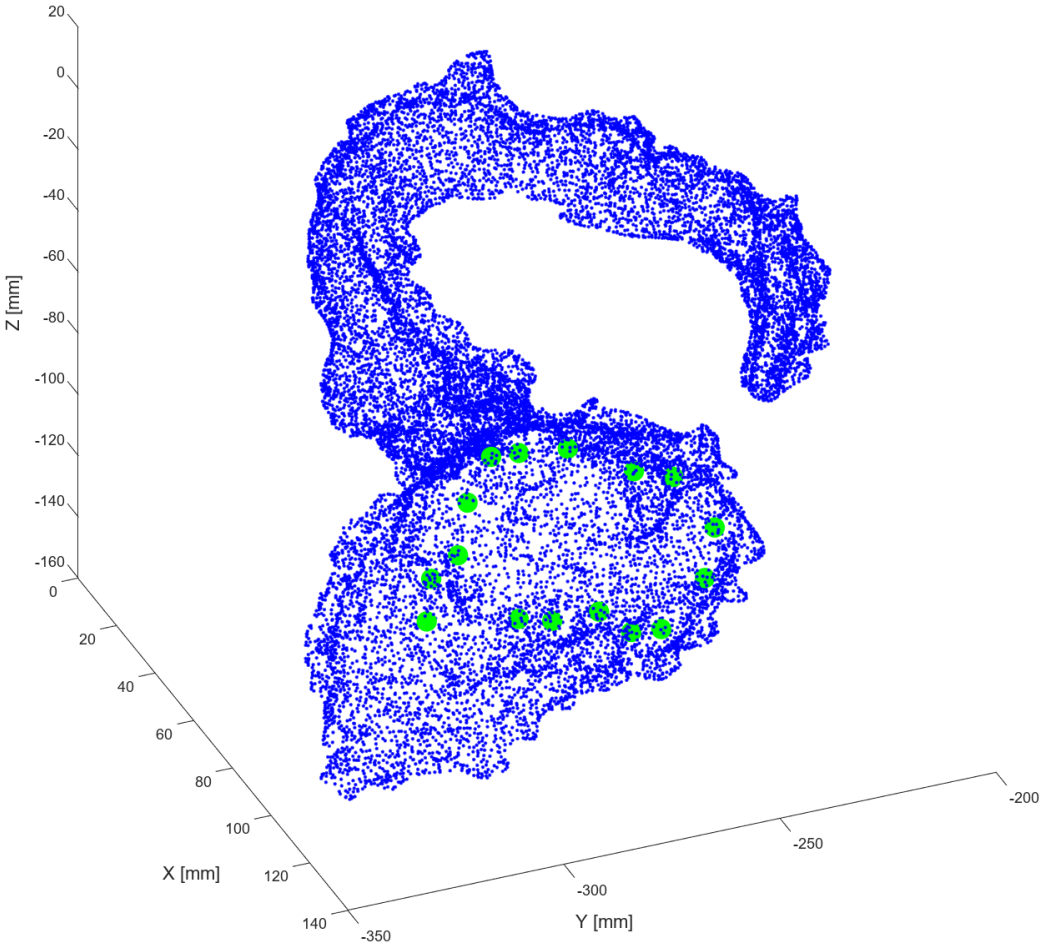


FIGURE 4.10: Electroanatomical mapping left ventricle and aorta points (blue) and a set of sparse ventricular tachycardia catheter ablation points (green).

First, the CoM of the transformed EAM VT ablation points and the CT LV points are calculated. The vector connecting these two CoMs is then determined as $\mathbf{v}_1$. Using this vector and the initial line-of-sight vector $\mathbf{v}_2$ (inferior (INF) view), the axis angle rotation vector $\mathbf{r} = (x, y, z, \theta)$ can be computed. The unit vector $(x, y, z)$ representing the rotation axis is calculated as:

$$(x, y, z) = \frac{\mathbf{v}_1 \times \mathbf{v}_2}{\|\mathbf{v}_1 \times \mathbf{v}_2\|}, \tag{4.13}$$

where $\theta$ is the angle of rotation around the axis $(x, y, z)$, and is calculated using the equation:

$$\theta = \arccos\left(\frac{\mathbf{v}_1 \cdot \mathbf{v}_2}{\|\mathbf{v}_1\|\|\mathbf{v}_2\|}\right). \tag{4.14}$$

Next, the axis angle rotation vector $\mathbf{r}$ is converted into a rotation matrix $\mathbf{R}$ which describes the same rotation:

$$\mathbf{R} = \mathbf{I}_3 + \sin(\theta)\mathbf{K} + (1 - \cos(\theta))\mathbf{K}^2, \tag{4.15}$$

where $\mathbf{K}$ is the skew-symmetric matrix of the axis vector $(x, y, z)$:

$$\mathbf{K} = \begin{pmatrix} 0 & -z & y \\ z & 0 & -x \\ -y & x & 0 \end{pmatrix}. \tag{4.16}$$

Afterwards, the rotation matrix $\mathbf{R}$ is converted into Euler angles $(\alpha, \beta, \gamma)$, representing rotations about the $x$-, $y$-, and $z$-axes, respectively:

$$\alpha = \arctan 2(\mathbf{R}_{3,2}, \mathbf{R}_{3,3}), \tag{4.17}$$

$$\beta = \arcsin(-\mathbf{R}_{3,1}), \tag{4.18}$$

$$\gamma = -\arctan 2(\mathbf{R}_{2,1}, \mathbf{R}_{1,1}). \tag{4.19}$$

The rotation matrix $\mathbf{R}_{\text{fill}}$ is then defined as:

$$\mathbf{R}_{\text{fill}} = \mathbf{R}(x, \alpha) \cdot \mathbf{R}(y, \beta) \cdot \mathbf{R}(z, \gamma). \tag{4.20}$$

In the next step, a bounding box surrounding the LV point cloud $\mathbf{P}_{\text{CT}}$ is defined, and its geometric center is defined as the center using the following equation:

$$\mathbf{C} = \left( \frac{\max(P_x) + \min(P_x)}{2}, \frac{\max(P_y) + \min(P_y)}{2}, \frac{\max(P_z) + \min(P_z)}{2} \right), \tag{4.21}$$

where $\mathbf{C} = (C_x, C_y, C_z)$ represents the center of the bounding box, and $P_x$, $P_y$ and $P_z$ are the $x$-, $y$-, and $z$-coordinates of the LV point cloud $\mathbf{P}_{\text{CT}}$, respectively. A translation matrix $\mathbf{T}_{\text{c}}$ is then defined, to shift the bounding box center of the LV point cloud $\mathbf{P}_{\text{CT}}$ to the origin. Afterwards, the composite transformation matrix $\mathbf{M}_{\text{fill}}$ is given by:

$$\mathbf{M}_{\text{fill}} = \mathbf{R}_{\text{fill}} \cdot \mathbf{T}_{\text{c}}. \tag{4.22}$$

After applying the transformation matrix $\mathbf{M}_{\text{fill}}$ to both the LV point cloud and the registered EAM target point cloud, perpendicular to the current view, the point cloud of the CT LV contours is divided into two sections: front and back. The

transformed EAM target points are displayed as green dots, and only the front section of the LV points is activated and visualized, while the back section of the LV points and the auxiliary aorta points are hidden (see Figure 4.11A).

Afterwards, a set of vertices along the VT catheter ablation points on the two-dimensional (2D) projected view are interactively defined to create a polygonal region of interest (ROI) interactively (see Figure 4.11B). Once the polygonal ROI is created, each vertex can be adjusted for fine-tuning. Next, the indices of the transformed points of CT LV contours of the front section within this customized polygonal ROI are obtained. With these indices, the corresponding points of the original points of CT LV contours are defined as the VT target points, and these points turn red in both the 2D and 3D views (see Figure 4.11C). If needed, the customized polygonal ROI or defined VT target points can be deleted, and the aforementioned steps can be repeated. Otherwise, the defined VT target points are saved as the registered VT target points.

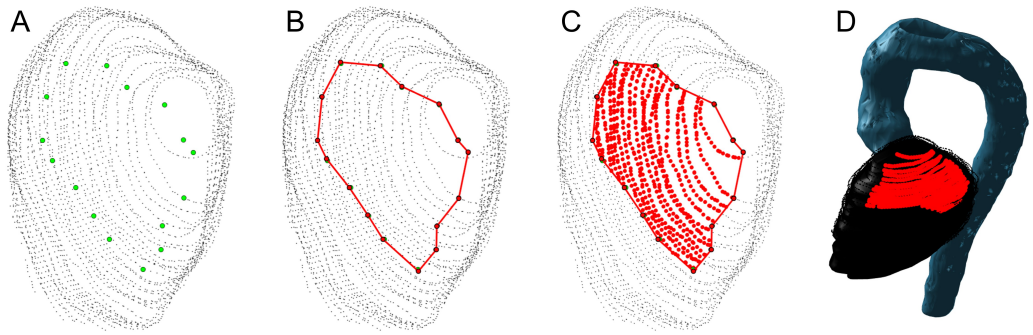


FIGURE 4.11: Representative case of 3D-3D registration for the feature border fill. (A) Computed tomography (CT) left ventricle (LV) points (black) in the front section and registered VT catheter ablation points (green). (B) Visualization of the polygonal region of interest (ROI, red). (C) Defined VT target points (red) within the polygonal ROI. (E) Visualization of the aorta and defined VT target points (red) on the LV structure in the 3D view.

**Data Output**

The $x$-, $y$- and $z$-coordinates of each point in the registered VT target points cannot be directly added to the original RTSS file because radiation TPS typically cannot interpret structures with a POINT value for the DICOM attribute ContourGeometricType. Through manual inspection of the metadata for the original RTSS file, the DICOM attribute ContourGeometricType of the cardiac substructures is assigned as CLOSED_PLANAR. Therefore, for each VT target point, three additional points are defined to generate a square with a side length of 1 mm.

Afterwards, a matrix containing the $x$-, $y$- and $z$-coordinates of these four points is saved to the DICOM metadata ROIContourSequence with the DICOM attribute ContourGeometricType set to CLOSED_PLANAR. Finally, all the registered VT target points are added to the original RTSS file as a new structure and exported as a new RTSS file. The exported RTSS file is compatible with the radiation TPS, and the registered VT target structure can be visualized in the radiation TPS as a reference for cardiac CTV delineation. Additionally, the output VT target structure can be used for quality assurance. The $x$-, $y$- and $z$-coordinates of the registered VT target points can also be saved and exported in comma-separated values (CSV) format.

### 4.3.2 Visualization of the Registered Target

A bounding box surrounding the registered VT target point cloud is defined, and its geometric center is calculated for the initial CT slices in coronal, axial and sagittal views. The registered VT target points are then visualized on the CT slices in these three views. If both cardiac CT and planning CT datasets are imported, the type of visualized CT can be switched. Additionally, the registered VT target, LV and aorta structures are visualized in the 3D view (see Figure 4.12). The visualized CT slices in the three anatomical views (i.e., coronal, axial and sagittal) can be adjusted. If needed, the CT slices in all three anatomical views can be reset to their initial positions. The slice position and the corresponding world position (unit: mm) for the current anatomical views are also displayed in the GUI. The window width and level values for the visualized medical images can be adjusted as needed. Additionally, the coronal, axial, and sagittal views of the images can be displayed individually in the 3D view.

A

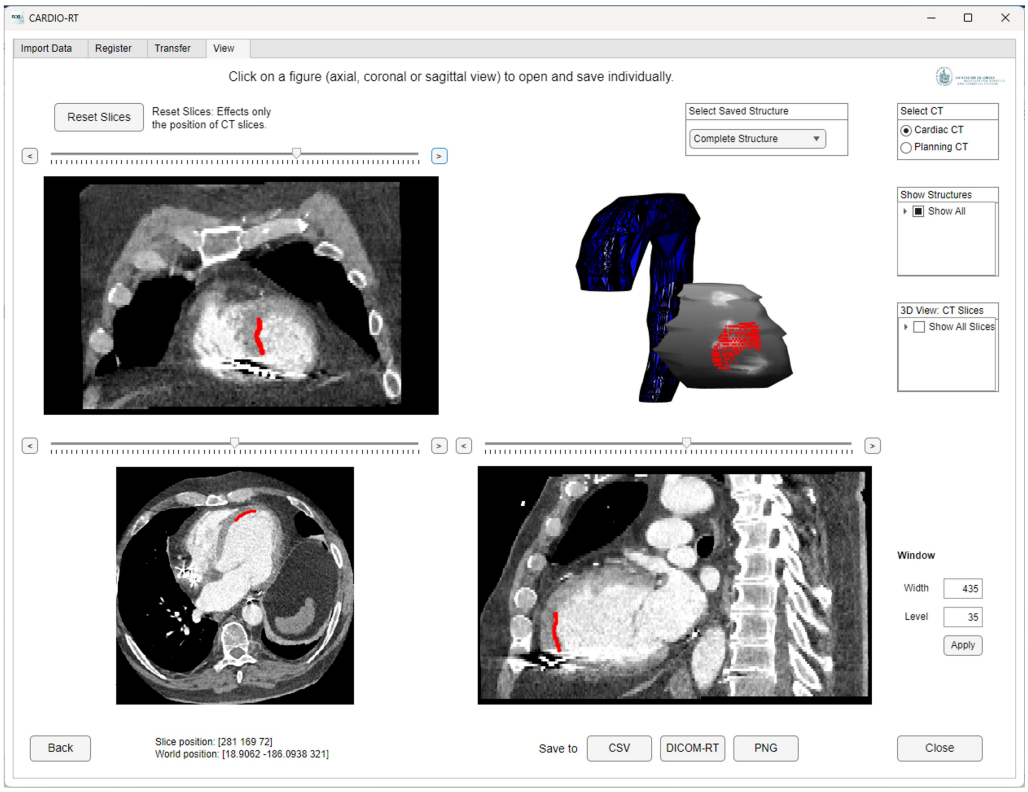


B

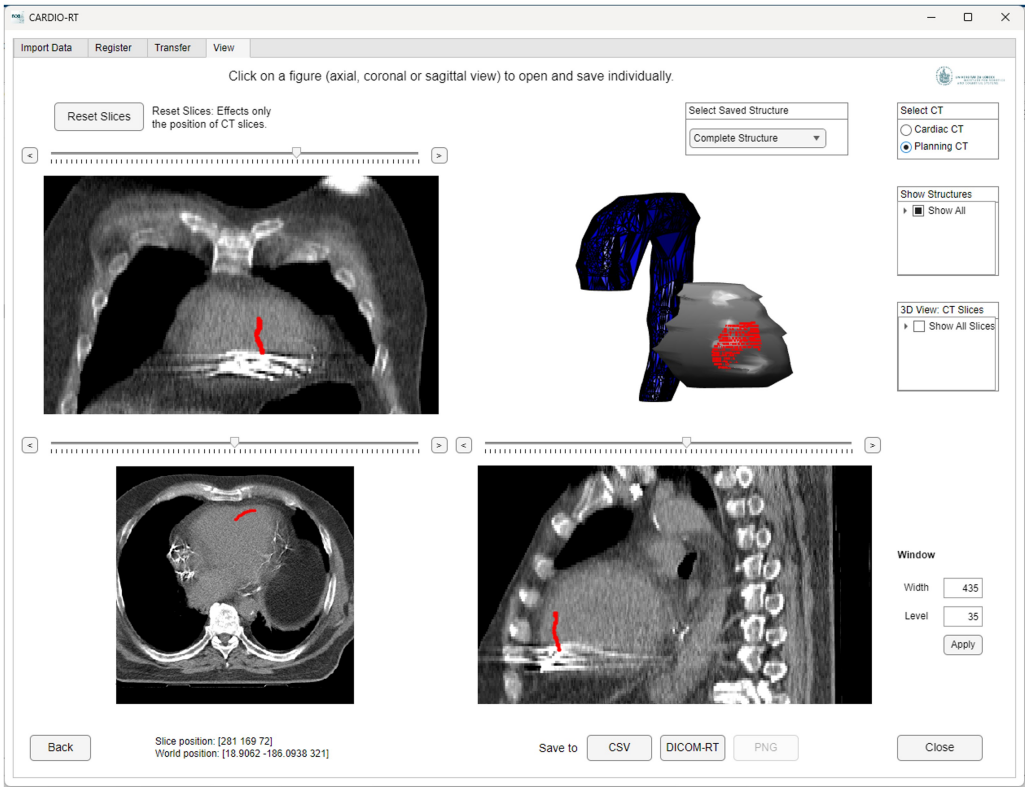


FIGURE 4.12: Representative 3D-3D registered ventricular tachycardia target points (red) on the cardiac computed tomography (CT) (A) and planning CT (B) visualized in the CARDIO-RT software.

## 4.4 2D-3D Registration

### 4.4.1 Registration Workflow

**Data Preparation and Import**

The 2D-3D registration is a versatile method that supports all EAM systems. The EAM sreenshots are captured from the EAM system and saved in PNG or JPG/JPEG format. The VT target region is marked by a cardiac electrophysiologist either directly on the 3D LV structure in the EAM system before capturing screenshot or on the LV in the captured EAM screenshots using any applicable image editing software, such as Windows Paint or Microsoft PowerPoint. At a minimum, the EAM screenshot where the VT target region can be visualized has to be captured. However, it is highly recommended to routinely capture EAM screenshots in all standard anatomical views (i.e., AP, posterior-anterior (PA), right lateral (RL), LL, SUP, INF, right anterior oblique (RAO) 30° and left anterior oblique (LAO) 60°, see Figure 4.13). If the VT target region cannot be fully visualized in a single EAM screenshot, then multiple EAM screenshots showing the VT target region from different views should be marked by the cardiac electrophysiologist. The 2D-3D registration can be performed multiple times, depending on the number of views where the VT target region is visualized and marked. During each 2D-3D registration procedure, one EAM screenshot is imported at a time.

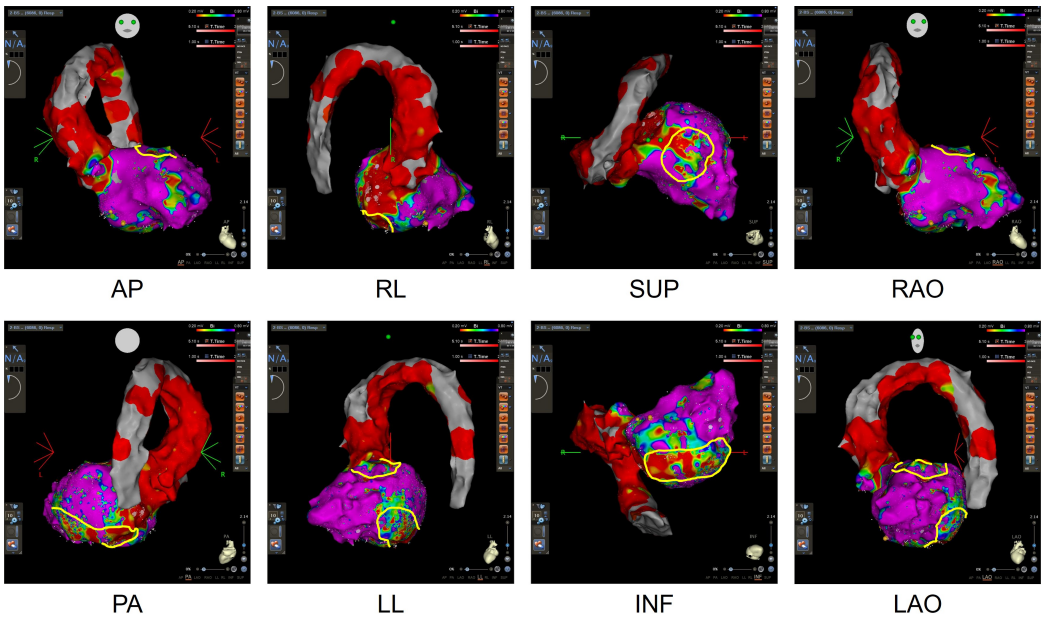


FIGURE 4.13: Representative electroanatomical mapping (EAM) screenshots in standard anatomical views captured from the CARTO 3 system. The left ventricle and aorta structures are mapped, with two ventricular tachycardia target regions marked in the CARTO 3 system as yellow shapes. AP = anterior-posterior; PA = posterior-anterior; RL = right lateral; LL = left lateral; SUP = superior; INF = inferior; RAO = right anterior oblique; LAO = left anterior oblique.

In cases where EAM data are unavailable, 2D fluoroscopic images can serve as an alternative input for the 2D-3D registration method (see Figure 4.14). Since the aorta is not visible in fluoroscopic images, but the coronary arteries are, the coronary arteries can bee contoured from the contrast-enhanced cardiac CT at the end-diastolic phase and used as reference structures for the 2D-3D registration method (see Figure 4.15).

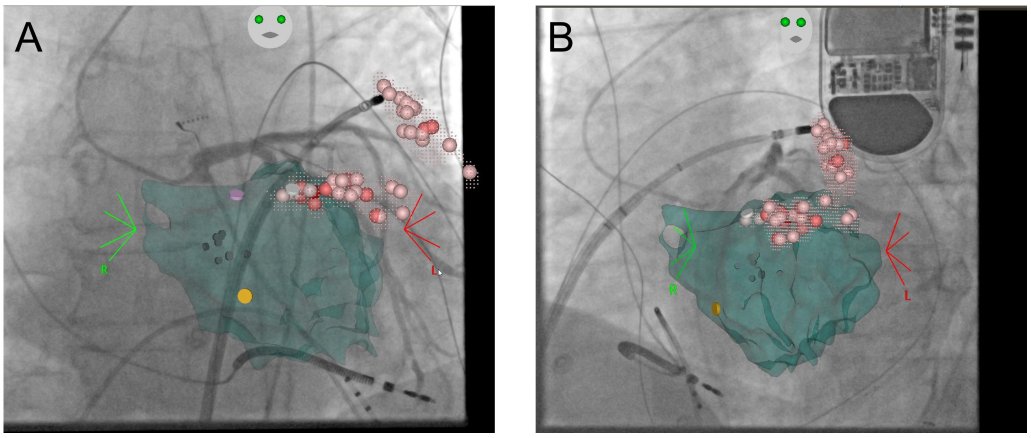


FIGURE 4.14: Representative fluoroscopic screenshots captured from the CARTO 3 system. (A) Standard anterior-posterior (AP) view. (B) Non-standard left anterior oblique (LAO) view (49°). The endocardial left ventricle is shown in cyan, while the catheter ablation points are represented as pink spheres. This STAR case was performed in Erlangen, Germany, and only 2D CARTO 3 fluoroscopic images from the standard AP view and the non-standard LAO view (49°) were available.

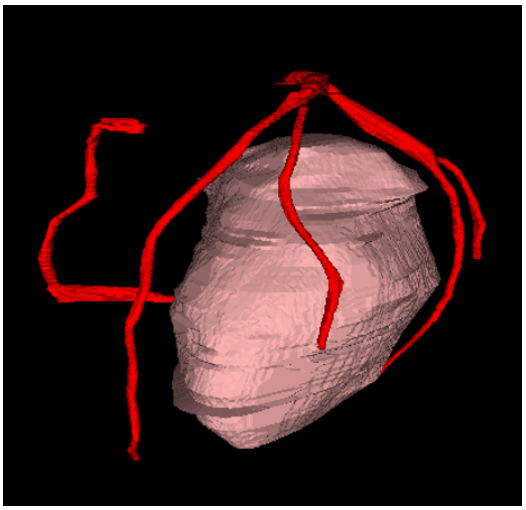

FIGURE 4.15: Computed tomography contours of the endocardial left ventricle (pink) and coronary arteries (red).

For CT scans, either the planning CT, the cardiac CT, or both should be imported. The CT slices are exported in DICOM format from the radiation TPS and then imported as a volume into the CARDIO-RT software.

The RTSS file including the cardiac substructures (i.e., LV, aorta, etc.) is imported, and the LV and aorta contours (if available) are imported as individual point clouds. Importing the aorta as an auxiliary structure can enhance the accuracy of the 2D-3D registration, as it can serve as a registration reference. For the LV structure from the RTSS file, the points forming the contours on some slices

may be sparse. As described in section 4.2.1, an LV point cloud with higher density is generated (see Figure 4.2).

After importing all required and optional data, if both the planning CT and cardiac CT datasets are imported, it is checked whether the cardiac CT is already registered to the planning CT. If not, the cardiac CT can be registered to the planning CT (see section 4.6.2).

**Ventricular Tachycardia Target Registration**

The 2D-3D registration process includes EAM-CT LV registration and VT target points definition. Figure 4.16 illustrates the workflow of the 2D-3D registration.

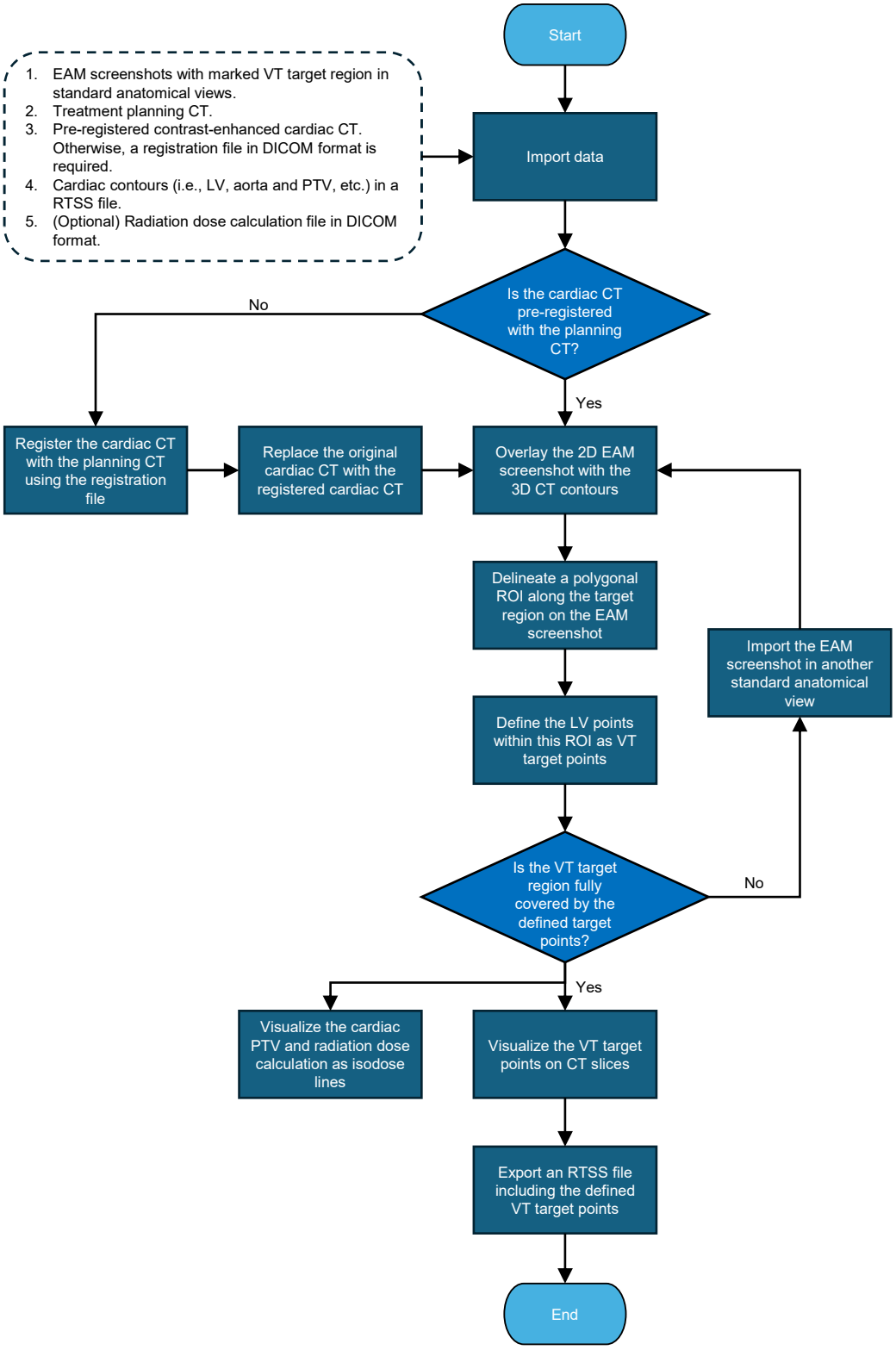


FIGURE 4.16: 2D-3D registration workflow. See main text for details. Abbreviations: EAM = electroanatomical mapping; VT = ventricular tachycardia; CT = computed tomography; DICOM = Digital Imaging and Communications in Medicine; LV = left ventricle; PTV = planning target volume; RTSS = radiotherapy structure set; ROI = region of interest.

For EAM-CT LV registration, the LV in the EAM screenshot and the LV in the RTSS file are overlaid. The orientation of the standard anatomical views used in the CARDIO-RT software is shown in Figure 4.18A. It should be noted that the definitions on the SUP view are inconsistent across different EAM systems. In RHYTHMIA HDx and EnSite EAM systems, the SUP view is consistent, with the left side on the left and the right side on the right. However, in the CARTO 3 system, the SUP view is point-symmetrical, with the left and right directions reversed, which actually represents the caudal (CAU) view.

Initially, a standard anatomical view for the CT contours is defined, which should be the same as the currently imported EAM screenshot (Figure 4.18A). Since the VT patient is positioned on two different couches in the cardiac catheterization laboratory and the CT scanner, there might be considerable angular deviations between the LV point cloud from the RTSS file and the LV structure in the EAM screenshots in a specific standard anatomical view. To diminish such angular deviations, the rotation feature of the CARDIO-RT software can be used (see Figure 4.17). For each axis, the rotation offsets $offset_x$, $offset_y$ and $offset_z$ (unit: degrees) about the three axes are defined, and the value for angle increment is defined to enable faster adjustments or fine-tuning. To avoid misoperation, only the rotation about the axis perpendicular to the current standard anatomical view is possible. The direction of rotation about each axis follows the conventional right-hand rule (see Figure 4.18A). The rotation feature can also be applied if the imported EAM screenshot is in a non-standard anatomical view, such as the representative case with an LAO 49° view (see Figure 4.14).

The rotation offsets $\theta_x$, $\theta_y$ and $\theta_z$ about the $x$- $y$- and $z$-axes are defined as:

$$\theta_x = \pi \cdot \frac{offset_x}{180}, \quad \theta_y = \pi \cdot \frac{offset_y}{180}, \quad \theta_z = \pi \cdot \frac{offset_z}{180}. \tag{4.23}$$

Afterwards, the rotation offsets will be applied to the corresponding rotation matrix for the standard anatomical views, and the rotation matrix $\mathbf{R}_{\text{view}}$ is defined as one of the matrices below:

$$\mathbf{R}_{\text{AP}} = \mathbf{R}(x, \frac{\pi}{2}) \cdot \mathbf{R}(x, \theta_x) \cdot \mathbf{R}(y, \theta_y) \cdot \mathbf{R}(z, \theta_z), \tag{4.24}$$

$$\mathbf{R}_{\text{PA}} = \mathbf{R}(x, \frac{\pi}{2}) \cdot \mathbf{R}(z, \pi) \cdot \mathbf{R}(x, \theta_x) \cdot \mathbf{R}(y, \theta_y) \cdot \mathbf{R}(z, \theta_z), \tag{4.25}$$

$$\mathbf{R}_{\text{SUP}} = \mathbf{R}(y, \pi) \cdot \mathbf{R}(x, \theta_x) \cdot \mathbf{R}(y, \theta_y) \cdot \mathbf{R}(z, \theta_z), \tag{4.26}$$

$$\mathbf{R}_{\mathrm{INF}} = \mathbf{I}_4 \cdot \mathbf{R}(x, \theta_x) \cdot \mathbf{R}(y, \theta_y) \cdot \mathbf{R}(z, \theta_z), \tag{4.27}$$

$$\mathbf{R}_{\mathrm{CRA}} = \mathbf{R}(x, \pi) \cdot \mathbf{R}(x, \theta_x) \cdot \mathbf{R}(y, \theta_y) \cdot \mathbf{R}(z, \theta_z), \tag{4.28}$$

$$\mathbf{R}_{\mathrm{CAU}} = \mathbf{R}(z, \pi) \cdot \mathbf{R}(x, \theta_x) \cdot \mathbf{R}(y, \theta_y) \cdot \mathbf{R}(z, \theta_z), \tag{4.29}$$

$$\mathbf{R}_{\mathrm{RL}} = \mathbf{R}(x, \frac{\pi}{2}) \cdot \mathbf{R}(z, \frac{\pi}{2}) \cdot \mathbf{R}(x, \theta_x) \cdot \mathbf{R}(y, \theta_y) \cdot \mathbf{R}(z, \theta_z), \tag{4.30}$$

$$\mathbf{R}_{\mathrm{LL}} = \mathbf{R}(x, \frac{\pi}{2}) \cdot \mathbf{R}(z, \frac{3\pi}{2}) \cdot \mathbf{R}(x, \theta_x) \cdot \mathbf{R}(y, \theta_y) \cdot \mathbf{R}(z, \theta_z), \tag{4.31}$$

$$\mathbf{R}_{\mathrm{RAO}} = \mathbf{R}(x, \frac{\pi}{2}) \cdot \mathbf{R}(z, \frac{\pi}{6}) \cdot \mathbf{R}(x, \theta_x) \cdot \mathbf{R}(y, \theta_y) \cdot \mathbf{R}(z, \theta_z), \tag{4.32}$$

$$\mathbf{R}_{\mathrm{LAO}} = \mathbf{R}(x, \frac{\pi}{2}) \cdot \mathbf{R}(z, -\frac{\pi}{3}) \cdot \mathbf{R}(x, \theta_x) \cdot \mathbf{R}(y, \theta_y) \cdot \mathbf{R}(z, \theta_z). \tag{4.33}$$

As explained in Equation 4.21, a rectangular bounding box surrounding the point cloud of the CT LV contours is defined, and its geometric center is used as the center for rotation. Afterwards, the LV and aorta point clouds are transformed according to the composite transformation matrix $\mathbf{M}_{\mathrm{view}}$:

$$\mathbf{M}_{\mathrm{view}} = \mathbf{R}_{\mathrm{view}} \cdot \mathbf{T}_{\mathrm{c}}. \tag{4.34}$$

Then, the LV and aorta point clouds are visualized and projected onto the imported EAM screenshot. An interactive rectangular ROI is created surrounding the projected LV point cloud (see Figure 4.18B). This rectangular ROI is draggable and scalable, and the point clouds are moved and scaled with it simultaneously. Based on the location and profile of the LV and aorta structures from the CT and EAM data, the visualized LV point cloud is moved, scaled and rotated until it overlays the LV structure in the EAM screenshot appropriately (see Figure 4.18C). The position of the visualized LV and aorta point clouds can be reset as needed during the overlaying procedure.

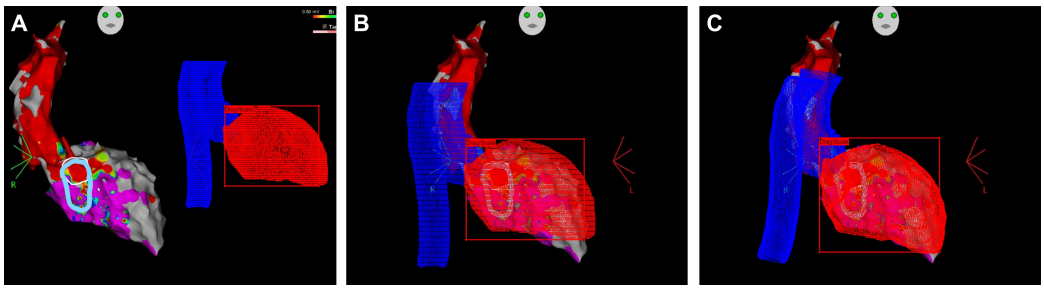


FIGURE 4.17: Representative case of the rotation function for the 2D-3D registration. The ventricular tachycardia target region is marked as a light blue shape on the electroanatomical mapping screenshot from the right anterior oblique (RAO, 30°) view. Red: left ventricle (LV) point cloud; blue: aorta point cloud. (A) The LV and aorta point clouds before overlay. (B) The overlaid LV and aorta point clouds with translation and scale only. (C) The LV and aorta point clouds with additional rotation about the $y$-axis.

Next, specific points in the LV point cloud from the RTSS file are defined as VT target points. Based on the previously defined geometric center of the bounding box, perpendicular to the current standard anatomical view, the point cloud of the CT LV contours is divided into two sections: front and back. In the current view, only the front section of the LV points is activated and visualized on the imported EAM screenshot as black dots, while the back section of the LV points and the auxiliary aorta points are hidden (see Figure 4.18D). Afterwards, a set of vertices (red) along the previously marked VT target region on the EAM screenshot are interactively defined to create a polygonal ROI interactively (see Figure 4.18E). Once the polygonal ROI is created, each vertex can be adjusted for fine-tuning. Next, the indices of the transformed points of CT LV contours of the front section within this customized polygonal ROI are obtained. With these indices, the corresponding points of the original points of CT LV contours are defined as VT target points, and these points turn red in both 2D and 3D views (see Figure 4.18F and G). The customized polygonal ROI or the defined VT target points can be deleted, and the steps can be repeated if modifications are needed. Otherwise, the defined points are saved as the registered VT target.

If the VT target region cannot be completely visualized from a single EAM screenshot in a specific standard anatomical view, the VT target registration procedure can be performed multiple times. The registered VT target points from each procedure are then combined to form the final registered VT targets, which can be visualized in the GUI and exported in an RTSS file.

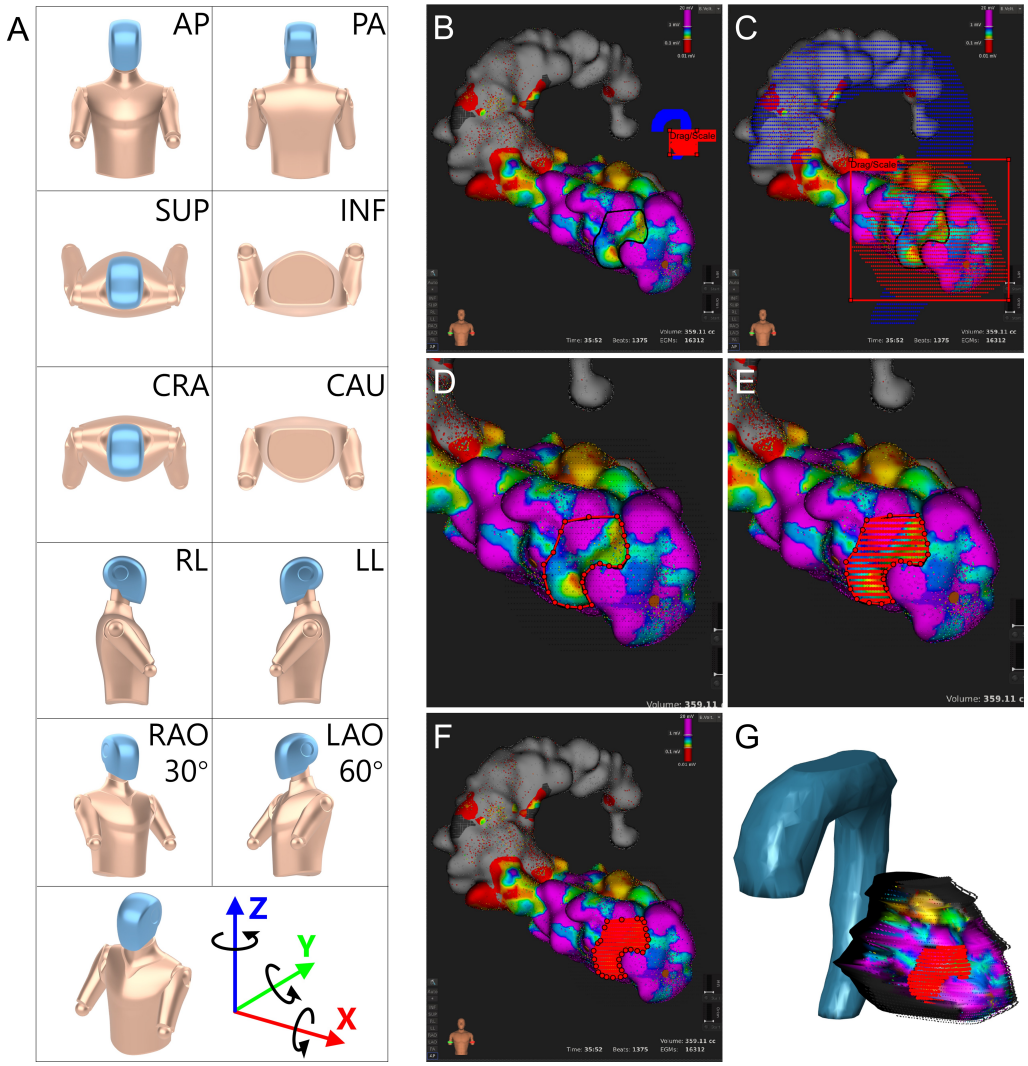


FIGURE 4.18: Orientation of the standard anatomical views and rotation directions about the *x*-, *y*- and *z*-axes (A) and a representative case for the 2D-3D registration method. (B) The position of left ventricle (LV) (red) and aorta (blue) point clouds before registration. (C) The position of LV and aorta point clouds after registration. (D) Generation of a polygonal region of interest (ROI, red) by defining some points (red) along the marked ventricular tachycardia (VT) target region (black) on the electroanatomical mapping screenshot in the anterior-posterior view. (E) Visualization of the aorta and LV structures in the 3D view. (F) Selected LV points (red) within the polygonal ROI as the VT target points. (G) Visualization of the aorta and selected LV points (red) on LV structure and structures in the 3D view. Abbreviations: AP = anterior-posterior; PA = posterior-anterior; SUP = superior; INF = inferior; CRA = cranial; CAU = caudal; RL = right lateral; LL = left lateral; RAO = right anterior oblique; LAO = left anterior oblique.

### Data Output

The *x*-, *y*- and *z*-coordinates of each point in the registered VT target points cannot be directly added to the original RTSS file because radiation TPS typically

cannot interpret structures with a POINT value for the DICOM attribute ContourGeometricType. Through manual inspection of the metadata for the original RTSS file, the DICOM attribute ContourGeometricType of the cardiac substructures is assigned as CLOSED_PLANAR. Therefore, for each VT target point, three additional points will be defined to generate a square with a side length of 1 mm.

Afterwards, a matrix containing the $x$-, $y$- and $z$-coordinates of these four points is saved to the DICOM metadata ROIContourSequence with the DICOM attribute ContourGeometricType set to CLOSED_PLANAR. Finally, all the registered VT target points are added to the original RTSS file as a new structure and exported as a new RTSS file. The exported RTSS file is compatible with the radiation TPS, and the registered VT target structure can be visualized in the radiation TPS as a reference for cardiac CTV delineation. Additionally, the output VT target structure can be used for quality assurance. The $x$-, $y$- and $z$-coordinates of the registered VT target points can also be saved and exported in CSV format.

### 4.4.2 Visualization of the Registered Target

A bounding box surrounding the registered VT target point cloud is defined, and its geometric center is calculated for the initial CT slices in coronal, axial and sagittal views. The registered VT target points are then visualized on the CT slices in these three views. If both cardiac CT and planning CT datasets are imported, the type of visualized CT can be switched. Additionally, the registered VT target, LV and aorta structures are visualized in the 3D view (see Figure 4.19). The visualized CT slices in the three anatomical views (i.e., coronal, axial and sagittal) can be adjusted. If needed, the CT slices in all three anatomical views can be reset to their initial positions. The slice position and the corresponding world position (unit: mm) for the current anatomical views are also displayed in the GUI. The window width and level values for the visualized medical images can be adjusted as needed. Additionally, the coronal, axial, and sagittal views of the images can be displayed individually in the 3D view.

A

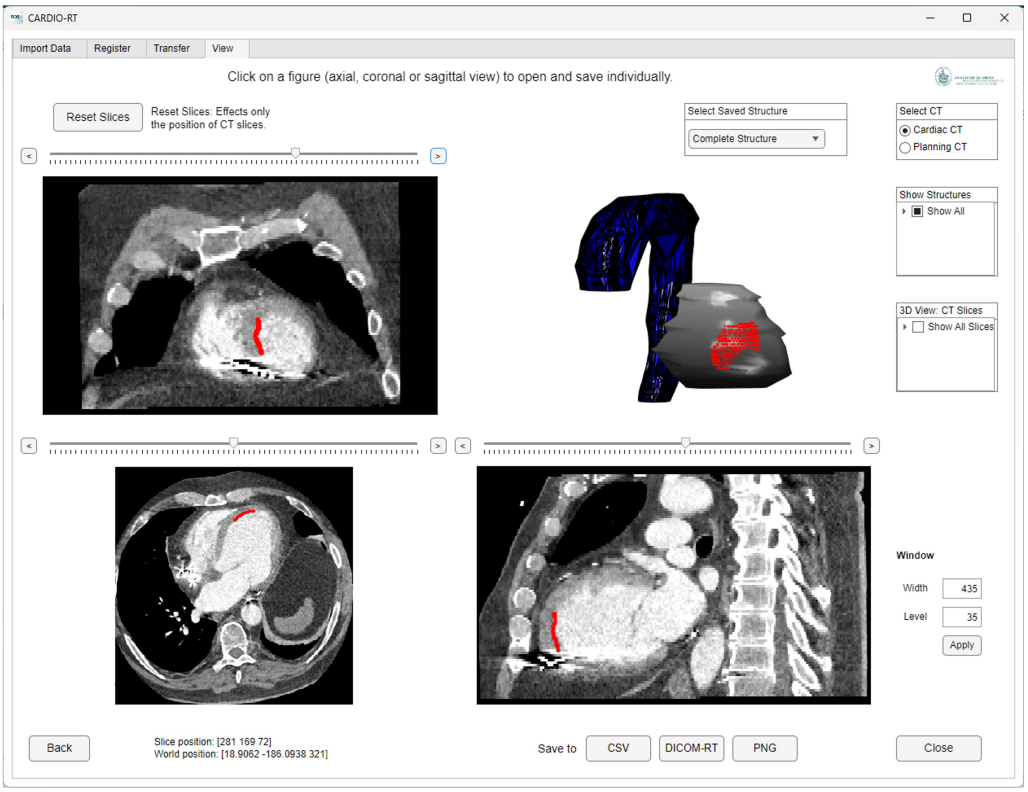


B

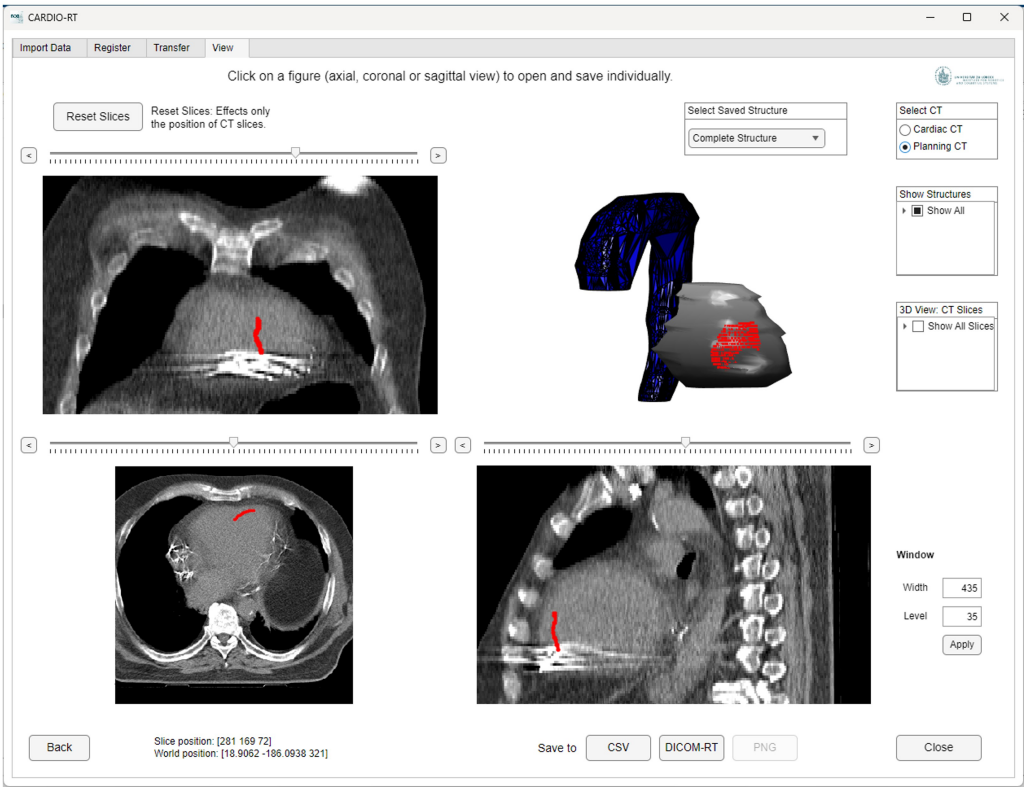


FIGURE 4.19: Representative 2D-3D registered ventricular tachycardia target points (red) on the cardiac computed tomography (CT) (A) and planning CT (B) visualized in the CARDIO-RT software.

If multiple EAM screenshots are used for VT target registration, the anatomical views of the EAM screenshots used for VT target registration can be selected, then the corresponding registered VT target points from that view are visualized on the CT slices and in the 3D view.

## 4.5 Significance of Aorta Mapping

As demonstrated in section 4.4, the VT target region can be transferred from the EAM screenshots to the treatment planning CT using the 2D-3D registration method in the CARDIO-RT software. In typical EAM procedures, mapping the aorta structure is not a standard routine. However, the aorta structure can serve as a registration reference during the VT target transfer procedure. This analysis aims to assess whether including the aorta as secondary structure for aligning EAM and CT data improves the VT target registration for STAR therapy.

### 4.5.1 Inter- and Intra-Observer Variability Analysis

Retrospectively, multi-center, non-randomized data of VT patients who underwent STAR therapy between 2019 and 2022 in Germany were analyzed. EAM data with the aorta mapped and contrast-enhanced cardiac CT were used for the 2D-3D registration method, with (aorta group) and without (standard group) the usage of the mapped aorta. The VT target registrations were conducted for six patients' datasets by three observers, with each registration repeated twice for both tests (with and without the aorta structure). Inter- and intra-observer variabilities were assessed using the DSC, change in surface area, distance of CoM and rotation about the main axes during registration.

### 4.5.2 Results

Table 4.1 presents the inter- and intra-observer variabilities for the 2D-3D registration method. Integrating the aorta led to a reduction of the inter-observer variability as measured by an increase of mean DSC values from 0.760 to 0.799 ($p = 0.007$). Additionally, a trend toward reduced intra-observer variability was observed in the aorta group for the DSC (0.868 vs 0.885; $p = 0.384$) and a reduction of standard deviation from 0.091 to 0.062.

Furthermore, a reduction in variation for all rotational components was detected: $x$-axis (RL) from 4.88° to 3.89°, $y$-axis (AP) from 6.30° to 4.65°, and $z$-axis (superior-inferior (SI)) from 5.84° to 3.30°. Similarly, the mean change in surface

TABLE 4.1: Inter- and intra-observer variabilities for the 2D-3D registration method, comparing electroanatomical mapping data with and without the aorta structure. Abbreviations: DSC = Dice-Sørensen coefficient; CoM = center of mass; SD = standard deviation.

| | | DSC | | Change in surface area (%) | | Distance of CoM (mm) | |
|---|---|---|---|---|---|---|---|
| | | Mean | SD | Mean | SD | Mean | SD |
| Intra-observer variability | Without aorta | 0.868 | 0.091 | 10.64 | 17.09 | 3.890 | 5.133 |
| | With aorta | 0.885 | 0.062 | 6.28 | 4.68 | 3.064 | 1.855 |
| Inter-observer variability | Without aorta | 0.760 | 0.111 | 15.38 | 16.53 | 6.617 | 5.213 |
| | With aorta | 0.799 | 0.103 | 12.70 | 8.51 | 4.917 | 2.479 |

area and the mean distance of the CoM were reduced from 15.4% and 6.62 mm in the standard group to 12.7% and 4.92 mm in the aorta group.

## 4.6 Additional Functions

### 4.6.1 Visualize Cardiac Target Volume and Dose Calculation

During a typical STAR treatment, the cardiac PTV and radiosurgery dose calculation are generated by the clinician. The cardiac target volume such as the PTV structure is saved in the RTSS file, and the radiosurgery dose calculation is exported as a single file in DICOM format. Both datasets can be imported and visualized in the software, allowing the observer to check the consistency between the registered VT target points/LV segment(s) and the PTV structure/dose calculation. In this way, the CARDIO-RT software serves as a tool for physicians to perform STAR quality assurance.

Once the VT target points or 17 LV segments are registered and visualized in the GUI, the RTSS file including the cardiac PTV structure can be imported. The PTV structure is visualized simultaneously with the registered VT target points/LV segment(s) on the cardiac CT slices in coronal, axial and sagittal views (see Figure 4.20).

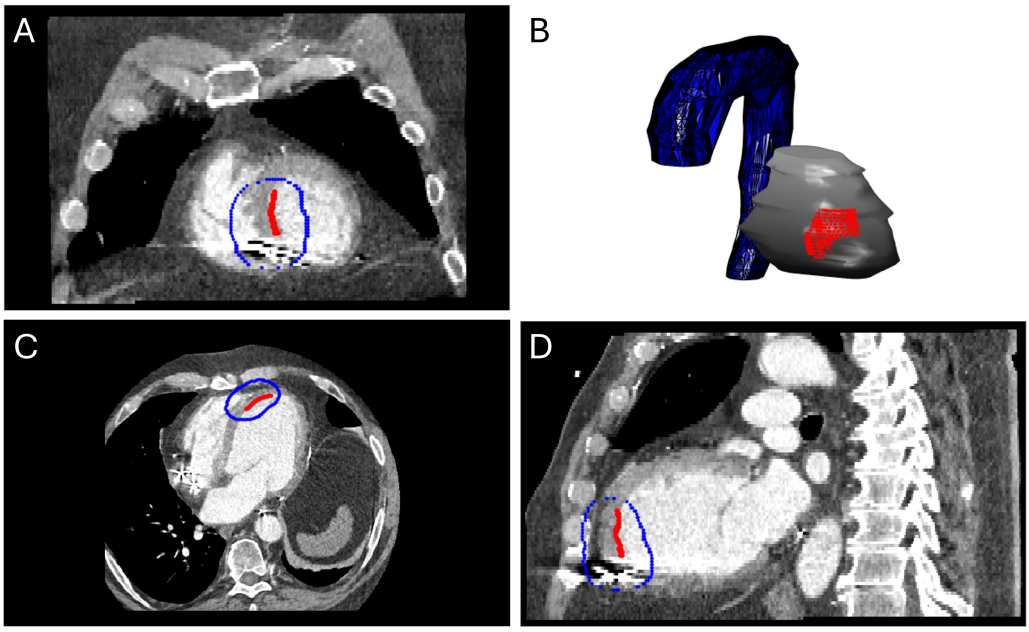


FIGURE 4.20: Representative case of the visualization of the planning target volume (blue) and 2D-3D registered ventricular tachycardia target points (red) in coronal (A), 3D (B), axial (C) and sagittal (D) views.

Additionally, the radiosurgery dose calculation file can be read and visualized as isodose lines, along with the visualization of transferred VT target. The volume of dose calculation is read from the DICOM file as a 3D array. Similar to the CT volume, the first and second dimensions represent the values of dose calculation in axial view, while the third dimension represents slices (along the $z$-axis). The origin of the dose volume, pixel spacing and slice thickness can also be extracted from the DICOM metadata of the dose calculation file. In the axial view of the CT volume, the current slice number of the CT volume being visualized in the GUI is extracted. The difference in the origins of dose and CT slices is converted to grid units by dividing by the pixel spacing to determine where the dose slice starts relative to the CT slice. Then, the end position for the dose slice, in terms of the grid units of CT slice is obtained. Finally, evenly spaced grid points in both $x$ and $y$ directions are generated as two 2D matrices representing the dose slice, and the isodose lines are visualized on the corresponding CT slice (see Figure 4.21).

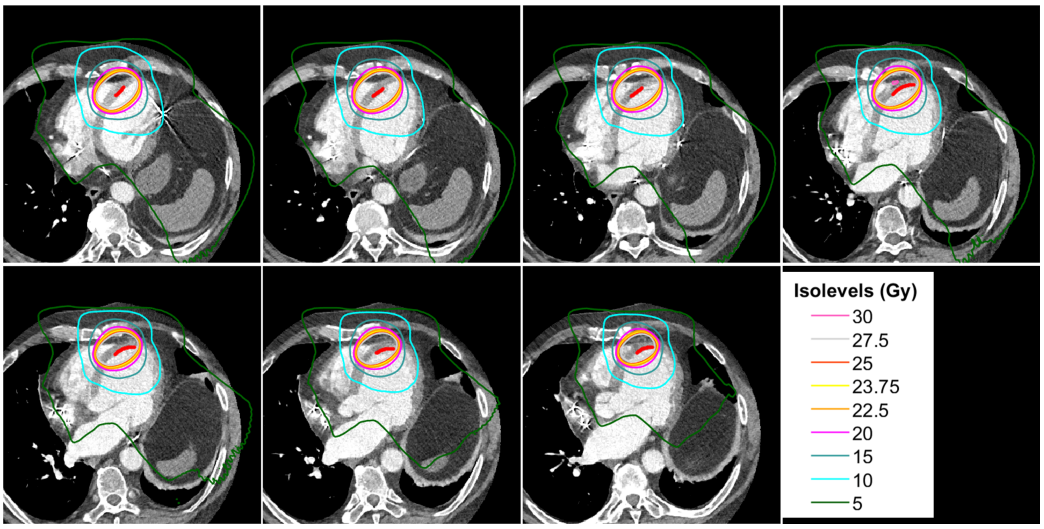


FIGURE 4.21: Representative case of the dose calculation visualization with the 2D-3D registered ventricular tachycardia target points (red) on the cardiac computed tomography slices in axial view.

### 4.6.2 Register Cardiac CT with Planning CT

STAR treatment is performed on the planning CT. However, in some cases, the cardiac CT is not registered with the planning CT, making it not feasible to visualize the cardiac substructures from the RTSS file as well as the 3D-3D/2D-3D registered VT target points or registered 17 LV segments on the cardiac CT (see Figure 4.22A). To resolve this issue, the cardiac CT can be rigidly registered to the planning CT using the radiosurgery registration file in DICOM format.

First, a set of planning CT scans and a set of cardiac CT scans are imported as two 3D volumes. During the registration process, the planning CT volume is fixed, while the cardiac CT volume is moving. The translation matrix $\mathbf{T}_{\text{cardiac}}$ is extracted from the DICOM metadata attribute PatientPositions of the cardiac CT volume, while the translation matrix $\mathbf{T}_{\text{planning}}$ is extracted from the DICOM metadata attribute PatientPositions of the planning CT volume. The transformation matrix $\mathbf{M}_{\text{RE}}$ is read from the DICOM radiosurgery registration file, and the composite transformation matrix $\mathbf{M}_{\text{warp}}$ for the geometric transformation of the CT volume is then defined as:

$$\mathbf{M}_{\text{warp}} = \mathbf{T}_{\text{cardiac}} \cdot \mathbf{M}_{\text{RE}} \cdot (-1) \cdot \mathbf{T}_{\text{planning}}. \tag{4.35}$$

Afterwards, the cardiac CT volume is warped based on the transformation matrix

$\mathbf{M}_{\text{warp}}$ and registered to the planning CT. During the registration, spatial reference information, such as voxel size, pixel spacing and slice thickness, is incorporated to ensure accuracy. Bicubic interpolation is used to transform cardiac voxel intensities smoothly. After registration, the warped cardiac CT will be saved as multiple files in DICOM format at a defined path for potential future use. Afterwards, in the CARDIO-RT software, the previous imported cardiac CT volume is replaced with the new registered cardiac CT volume for visualization in the GUI. The registered cardiac CT with the visualization of the LV and aorta structures is shown in Figure 4.22B-E.

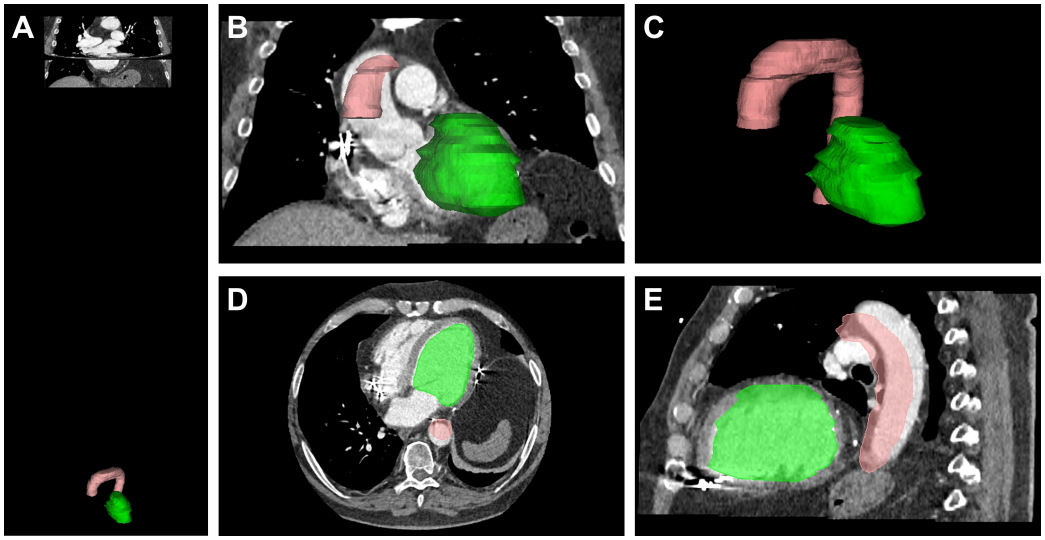


FIGURE 4.22: Representative case of the rigid registration between the cardiac computed tomography (CT) and planning CT. Green: left ventricle (LV); pink: aorta. (A) Visualization of the LV and aorta structures in coronal view of the cardiac CT before registration. (B) Visualization of the LV and aorta structures in coronal view of the registered cardiac CT. (C) Visualization of the LV and aorta structures in the 3D view. (D) Visualization of the LV and aorta structures in axial view of the registered cardiac CT. (E) Visualization of the LV and aorta structures in sagittal view of the registered cardiac CT.

### 4.6.3 Generate Transmural Target

The function for generating a transmural VT target is applicable to both the 3D-3D and 2D-3D registration methods. Since these registration methods register the defined VT target from the EAM data on either the endocardial or epicardial LV structure, the registered VT target structure does not represent a transmural cardiac CTV. To enhance the visualization of the registered VT target structure in the radiation TPS and assist t in finalizing the cardiac CTV, the registered VT target structure can be extended transmurally. To do so, it needs to be determined

whether the transmural VT targets should be generated on the endocardial or epicardial LV structure, or based on the input myocardium thickness.

If the previously imported RTSS file contains both, endocardial and epicardial LV structures, it needs to be determined whether the transmural VT target structure should be created on the endocardial or epicardial LV, depending on which LV structure is used for 3D-3D/2D-3D registration. For example, if the VT target structure is created on the endocardial LV, the corresponding transmural VT target points are generated on the epicardial LV structure. Conversely, if the VT target structure is created on the epicardial LV structure, the transmural VT target points are located on the endocardial LV structure. This LV structure is imported as a 3D point cloud and used for projecting the 3D-3D/2D-3D registered VT target points.

Alternatively, if only one LV structure (endocardial or epicardial) is available from the previously imported RTSS file, a value for the LV myocardium thickness (unit: mm) is defined based on the patient's characteristics or the LV myocardium thickness obtained from the CT data. A new point cloud is then generated by dilating or shrinking the original LV point cloud using the input LV myocardium thickness, representing the epicardial or endocardial LV structure as an approximation. The CoM of the imported LV point cloud is calculated, and a 3D vector for dilating or shrinking is determined based on this CoM. Afterwards, this vector is applied to the imported LV point cloud to generate a dilated or shrunk LV point cloud. The new LV point cloud is then used for projecting the 3D-3D or 2D-3D registered VT target points.

For each point in the registered VT target points, the nearest point in the projected LV point cloud is identified using the k-d tree search algorithm. Next, the CoMs of both, the registered VT target points and the nearest points in the projected LV points, are calculated. Afterwards, for each point in the registered VT target points, a 3D vector connecting these two CoMs is generated. The point in the projected LV point cloud with the smallest Euclidean distance to this registered VT target point is identified and defined as a projected VT target point. In the end, a set of points in the projected LV point cloud is defined as the projected VT target points (see Figure 4.23).

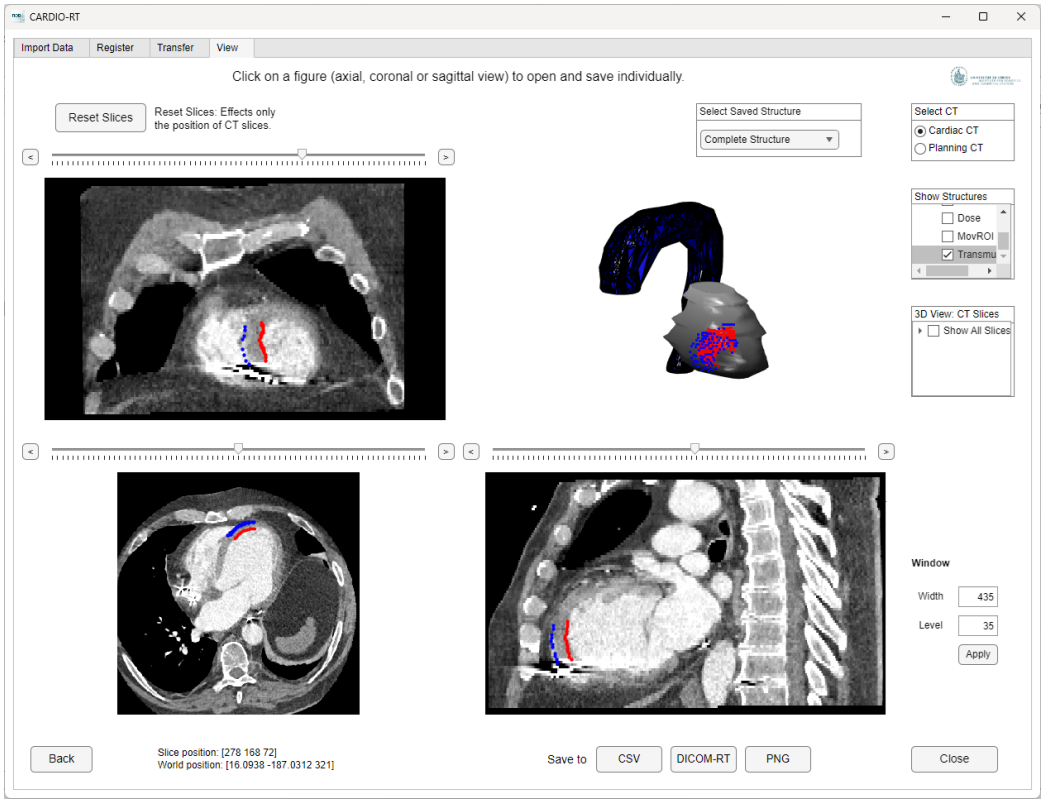


FIGURE 4.23: Representative case of the generation of transmural ventricular tachycardia (VT) target points (blue) based on the 2D-3D registered VT target points (red) and a left ventricle myocardium thickness of 10 mm, approximated from the corresponding cardiac computed tomography.

Similar to the 3D-3D/2D-3D registered VT target structure, the transmural VT target points are added as a new structure to the original RTSS file and exported, along with the 3D-3D/2D-3D registered VT target structure, in a new RTSS file.

## 4.7 Discussion

In this chapter, a stand-alone software named CARDIO-RT including three practical semi-automatic VT target registration methods between EAM systems and radiation TPS for STAR is demonstrated. It includes the AHA 17-segment model registration, 3D-3D registration and 2D-3D registration methods. This software has a GUI and has been developed and maintained within the MATLAB App Designer development environment. The software is compatible with Windows, Linux, and Mac operating systems. The three registration methods follow a structured workflow, reducing additional workload when switching between them. It can serve as a quality assurance tool for prospective STAR treatments, as well as retrospective analysis of STAR cases.

Since the AHA 17-segment model is designed for the LV myocardium, it applies only to STAR cases where the VT target is in the LV. However, the 3D-3D and 2D-3D registration methods can also be applied to cases where the VT substrate is in the RV, as long as the required EAM data of the RV is obtained during catheter procedures. Additionally, the registration methods support not only CT scans, but also MRI images.

The 17-segment model registration enables the division of the LV myocardium structure into 17 segments based on the AHA 17-segment model in real time. This method can assist clinicians in visualizing specific LV segments on the cardiac CT, determining whether the initial targeted LV segments are appropriate, and make any necessary adjustments. The targeted LV segments can serve as a reference for delineating the cardiac CTV in the radiation TPS. However, it should be noted that relying solely on the AHA 17-segment model for VT target transfer will most likely lead to a larger cardiac CTV, as the expected CTV is not located exactly in some of the LV segments [89]. Additionally, this method can be used for segment-specific cardiac motion analysis and other AHA 17 LV segments-based studies. To perform this method, contouring of the aorta structure is essential, as it serves as a landmark for segmenting the LV myocardium. In case the aorta structure is not contoured, the $x$-, $y$- and $z$-coordinates of the aortic valve center can be obtained from the CT scans and manually input into the software, where it is visualized as a sphere for reference instead.

The CARDIO-RT 3D-3D registration method can transfer the catheter ablation points exported from three EAM systems - RHYTHMIA HDx, CARTO 3 and EnSite - in vendor-specific data formats to the radiation TPS. Compared to the AHA 17 segment model registration, the 3D-3D registration method can achieve a more accurate target transfer as long as the catheter ablation points are well defined by the cardiac physiologist during EAM procedures and properly exported. If the cardiac substructures (i.e., LV, aorta) and the VT target structure are mapped and exportable as specific file(s), other EAM systems can be easily integrated into the CARDIO-RT software.

For the versatile 2D-3D registration method, since the only required input from the EAM systems are screenshots in standard anatomical views in PNG or JPG/JPEG format, it addresses the limitations of earlier AHA 17-segment model and 3D-3D EAM mesh data registration methods by eliminating reliance on proprietary vendor-specific data formats exported from different EAM systems. Moreover, 2D fluoroscopic screenshots captured by the CARTO 3 system can also

be used for 2D-3D registration, with coronary arteries serving as the registration reference since the aorta structure is not well visualized. In recent years, the novel disposable non-invasive mapping system, CardioInsight 3D mapping vest (Medtronic, Minneapolis, Minnesota, USA), has been developed and employed in some clinical trials to treat VT [134]–[136]. The vest is connect to the CardioInsight workstation to capture ECGI data from the body surface for identifying VT substrate, despite its insufficient resolution for precise VT target localization compared to conventional EAM procedures [137]. Technically, the 2D-3D registration method can also transfer the VT target marked on ECGI screenshots to the treatment planning imaging data. Additionally, the 2D-3D registration method has potential for applications in other radiotherapy treatments within the human body where the target is identifiable using 2D imaging data. Currently, due to the absence of ground truth for the transferred VT target, cross-validation with a 3D-3D registration method is recommended to ensure the VT target transfer accuracy.

The proposed VT target registration methods are semi-automatic rather than fully automatic due to strict accuracy requirements in clinical applications. Automatic registration methods may not be sufficiently reliable, as the LV structures are derived from two distinct modalities - contoured from contrast-enhanced CT and mapped from EAM systems - which may result in considerable shape differences and data incompleteness (e.g., the aorta may be unmapped, or the LV may be only partially mapped during EAM procedures). These discrepancies can lead to inaccuracies in fully automatic registration, making it unsuitable for clinical use. In contrast, the semi-automatic registration methods proposed in this study have demonstrated practical feasibility on real-world STAR datasets [131], [138]. They provide the necessary flexibility, allowing clinicians to refine the registration process based on their expertise and the specific characteristics of each STAR case, ensuring both accuracy and clinical applicability. To further ensure the accuracy and performance of the VT target registration, it is recommended to acquire all required data for the three registration methods and determine the final VT target based on their outputs.

Mapping the aorta structure is not a standardized routine procedure during EAM attempts in clinical practice. However, the aorta structure can serve as a reference for registration in the AHA 17-segment model registration, 3D-3D registration and 2D-3D registration. Additionally, for the 2D-3D registration method, as shown in Table 4.1, mapping the aorta reduces both inter- and intra-observer variabilities when transferring the VT target from the EAM system to the radiation

TPS, thereby could potentially improve the dose delivery accuracy and patient outcomes in STAR therapy. In most cases, EAM data are already available during STAR treatment planning procedure due to prior catheter ablation attempts for VT. Therefore, mapping the aorta during EAM procedures is highly recommended to avoid repeated invasive catheter procedures solely for aorta mapping.

It has been reported that the thickness of ventricular wall could help identify cardiac CTV within myocardium regions with a thickness of less than 5 mm [139]–[141]. These regions of myocardium thinning are often associated with VT isthmuses and substrates. Based on this concept, the inHEART online platform (Pessac, France) has been developed, which is able to segment the cardiac CT to visualize the wall thickness to aid in identifying potential VT substrates using MUSIC with proprietary algorithms [110]. However, the effectiveness and robustness of identifying VT substrates using wall thickness maps derived from cardiac CT require further evaluation.

Currently, there is no commercial or research tool with CE or FDA certification, and there is an absence of ground truth for the registered VT target. It would be beneficial to cross-validate the CARDIO-RT software with other VT target registration solutions to evaluate its effectiveness. Additionally, cardiac phantoms have been developed to facilitate STAR in VT patients [142], [143]. The customized computerized imaging reference systems dynamic cardiac phantom (Sun Nuclear, Melbourne, USA) with synthetic LV structure has been designed for end-to-end STAR treatments test [142]. This cardiac phantom allows for typical EAM procedures and the definition of various cardiorespiratory motion patterns. In the future, the accuracy of the proposed VT target registration methods in the CARDIO-RT software could potentially be evaluated using this phantom, where a ground truth for the transferred VT target on the synthetic LV structure can be defined.

**Limitations**

The DICOM attributes of the metadata of the newly added 17 LV segments and registered VT target structure in the output RTSS file have been carefully verified and assigned to ensure compatibility with the corresponding radiation TPS. The readability of the output RTSS file has been confirmed in multiple versions of commonly used radiation TPS in clinical practice, including Eclipse (Varian Medical Systems, Palo Alto, California, USA), Monaco (Elekta AB, Stockholm,

Sweden), Precision (Accuray Inc., Sunnyvale, California, USA), RayStation (RaySearch Laboratories AB, Stockholm, Sweden) and ViewRay (ViewRay, Inc., Oakwood Village, Ohio, USA). However, it has been noticed that certain TPS may specifically verify some DICOM metadata attributes of the newly added structure in the RTSS file. Therefore, if the output RTSS file is unreadable by the TPS, it is helpful to check the radiation TPS log file and the DICOM metadata attributes of the original cardiac substructures (e.g., LV, aorta, etc.).

Additionally, the CARDIO-RT software may have potential bugs. Evaluating the three VT target registration methods in the software on additional cases, both, prospectively and retrospectively, could further enhance their robustness. The CARDIO-RT software is continually updated and refined to address potential bugs and improve user-friendliness.

## 4.8 Chapter Summary

In this chapter, three practical VT target registration methods from the CARDIO-RT software, namely the AHA 17-segment model registration, 3D-3D registration and 2D-3D registration, are demonstrated. The aim of this chapter was to address research question Q1.

The AHA 17-segment model registration is able to divide the LV myocardium structure contoured from the cardiac CT into 17 segments according to the 17-segment model as defined by the AHA. This model is specifically designed for the LV. The 3D-3D registration method currently supports three EAM systems commonly used in clinical practice: CARTO 3, RHYTHMIA HDx and EnSite. It can process raw data including the LV, aorta (optional) and catheter ablation points exported from the EAM system in the respective vendor-specific data formats. The software then registers the catheter ablation points to the radiation treatment planning imaging data as VT target structure. For 2D-3D registration, the software transfers the VT target region marked on the EAM screenshots in PNG or JPG/JPEG format in standard anatomical views (i.e., AP, PA, RL, LL, SUP, INF, RAO 30° and LAO 60°) to the radiation treatment planning imaging data. All three VT target registration methods can export the registered VT target or 17 LV segments as an RTSS file compatible with the radiation TPS and other medical image processing software. The VT target transferred by the CARDIO-RT software can serve as a reference for cardiac CTV delineation in the radiation TPS, and these VT target registration methods have potential for applications in quality assurance process in STAR.

Since currently there is no ground truth for the registered VT target, cross-validating the target registration methods in the CARDIO-RT software with other VT target registration solutions would help evaluate the effectiveness. Additionally, the accuracy of the proposed VT target registration methods can further be assessed on a cardiac phantom, where a ground truth for the transferred VT target on the synthetic LV structure can be defined.

# Chapter 5

# Validations of Target Registration Methods

As introduced in the previous chapter, the CARDIO-RT software offers three practical VT target registration methods. This chapter validates the CARDIO-RT VT target registration methods by employing them in the quality assurance process for STAR treatment planning within the RAVENTA trial, and by cross-validating the 2D-3D registration method against the 3D-3D registration method from the 3D Slicer extension EAMapReader [90]. Section 5.2 and section 5.3 provide the answers to the research questions Q2 and Q3 mentioned in section 1.1, respectively.

## 5.1 Scientific Contributions

In section 5.2, the newly developed practical software CARDIO-RT introduced in the previous Chapter 4 is validated as a quality assurance tool for cardiac CTV generation in the STAR treatment planning procedure for VT. The semi-automatic AHA 17-segment model registration, 3D-3D registration and 2D-3D registration methods in the software were successfully confirmed for 5 VT patients who underwent STAR treatments in a multi-center setup within the German RAVENTA trial. The registration software could serve as a quality assurance tool to provide a second opinion on the validity of manual or other method for VT target transfer in STAR. In particular, the versatile 2D-3D registration method, which is compatible with any EAM platform, addresses the limitations of earlier published 3D-3D registration methods related to EAM raw data acquisition and format inconsistency.

Parts of section 5.2 have been published in [138], and parts of section 5.3 have been published in [131].

In section 5.3, a cross-validation study was conducted for the first time between two novel, conceptually different, semi-automated VT target registration approaches for STAR: the 2D-3D registration method (introduced in section 4.4) in the CARDIO-RT software [138] and the 3D Slicer extension EAMapReader [90], which follows the concept of 3D-3D VT target registration. The VT target registration using both methods was performed on 10 cases of VT patients who underwent STAR treatment. The results showed that both methods produced nearly identical 3D cardiac CTV structures, indicating their reliability for quality assurance and VT target transfer from the EAM system to the radiation TPS. This reliability helps prevent mistargeting and supports standardized cardiac CTV creation workflows in STAR treatment.

## 5.2 Validation for Quality Assurance

Quality assurance of the VT target definition in the radiation TPS conducted as a pre-treatment verification during treatment planning for VT could ensure the treatment performance and patients' outcomes in STAR [2], [4], [6], [17], [29], [101], [103]. However, there is currently no commercial product with CE or FDA certification for dedicated and (semi-)automatic VT target transfer from the EAM system to the radiation TPS. As discussed in section 3.1, the basis for precise cardiac CTV structure definition for STAR is accurate image registration between the EAM data and CT contours. This section aimed to assess the performance of the CARDIO-RT software including three VT target registration methods as a quality assurance tool using real-world VT patient data within the RAVENTA trial, and to provide the answer to the research question Q2 mentioned in section 1.1.

### 5.2.1 Data Acquisition and Patient Characteristics

The CARDIO-RT software was evaluated in 5 STAR centers. According to the RAVENTA trial protocol [29] and current consensus [144], STAR treatment was considered for patients with VT refractory to dose-escalated antiarrhythmic drug therapy and where catheter ablation was deemed inappropriate - either due to failure of one or more previous catheter ablation to suppress VT, or because catheter ablation was infeasible. Five individual VT cases, one from each center, were included during the development phase of the CARDIO-RT software.

At the time of treatment for case 1, the 2D-3D registration method had not yet been completed, so only the 3D-3D registration method was available, with the

2D-3D registration applied retrospectively. For cases 3 and 4, structural analyses were conducted to compare the manually transferred VT target with the VT target generated using the 2D-3D registration. In case 4, the EAMapReader extension [90] within the 3D Slicer software was additionally employed. The fifth case examined the target transfer for a patient with an unsuccessful STAR procedure.

In this study, the participating experts (electrophysiologists, radiation oncologists and medical physicists) at each center were trained at the national workshop for STAR in Germany and/or had previous experience with STAR. Each center provided case data including general medical information of the patient including epicrisis, 12-lead surface ECG, EAM data and contrast-enhanced cardiac CT. The patient characteristics can be found in Table 5.1). Detailed case histories for the 5 patients are provided in AppendixB.

TABLE 5.1: Patient characteristics. Abbreviations: LVEF = left ventricular ejection fraction; VT = ventricular tachycardia; ICD = implantable cardioverter-defibrillator; STAR = stereotactic arrhythmia radioablation; EAM = electroanatomical mapping; LV = left ventricle; CTV = clinical target volume.

| Patient | 1 | 2 | 3 | 4 | 5 |
|---|---|---|---|---|---|
| Age (years) | 68 | 52 | 66 | 61 | 60 |
| Sex (m,f) | m | f | m | m | m |
| Cardiac condition | Non-ischemic dilated cardiomyopathy | Non-ischemic dilated cardiomyopathy | Ischemic cardiomyopathy | Non-ischemic dilated cardiomyopathy | Ischemic cardiomyopathy |
| LVEF (%) | 45-45 | 45 | 35 | 25 | 15 |
| VT/origin | Recurrent, anteroseptal | Septal-apical, most likely epicardial origin | Recurrent, monomorphic | Basal-anterior and basal-inferolateral | Recurrent, monomorphic |
| Combined antiarrhythmic therapy | Beta-blocker and amiodarone | Beta-blocker and amiodarone | Beta-blocker and amiodarone | Beta-blocker, amiodarone and mexiletine | Beta-blocker and amiodarone |
| Inappropriate ICD shocks | No | No ICD | No | No | No |
| Catheter ablation history | 4 endo- and epicardial, 2 endocardial catheter ablations | 3 endocardial and 2 epicardial catheter ablations | 5 endocardial catheter ablations | 4 endocardial and 1 epicardial catheter ablations | 2 endocardial catheter ablations (1 after failed STAR) |
| Repeated catheter ablation not possible due to | Failure of several recent procedures | Failure of several recent procedures | Failure of several recent procedures | Failure of several recent procedures | Failure of several recent procedures |
| System used for EAM | RHYTHMIA HDx | EnSite | CARTO 3 | CARTO 3 | CARTO 3 |
| Targeted LV segment | 8, 13 and 14 | 7, 8, 13 and 14 | 4 | 1, 4, 5, 8 and 11 | 7, 8, 12 and 13 |
| CARDIO-RT tool used for target registration | 3D-3D registration | 2D-3D registration | 2D-3D registration | Only applied retrospectively | Only applied retrospectively |
| CTV ($cm^3$) | 12.9 | 16.9 | 29.5 | 38.1 | 14.9 |

### 5.2.2 Target Registration

For each patient, EAM data for the cardiac chamber of interest were obtained using one of the three EAM systems: CARTO 3, RHYTHMIA HDx or EnSite.

A time-resolved thoracic treatment planning CT was acquired as STAR treatment planning imaging data. Additionally, ECG-gated contrast-enhanced cardiac CT was obtained in the diastolic phase. The VT target region for STAR was manually determined by the electrophysiologists at each center. Using all the available clinical information (i.e., 12-channel ECG and EAM), the VT target was contoured on several EAM screenshots in standard anatomical views (i.e., AP, PA, RL, LL, SUP, INF, RAO and LAO). The myocardium was contoured on the ECG-gated contrast-enhanced CT and registered with the planning CT. The 3D CTVs were then created on the planning CT by the interdisciplinary teams based on the defined VT target regions [15]. This delineation procedure was performed in the radiation TPS available at each STAR center, including Velocity and Eclipse v15 (Varian, Palo Alto, California, USA), Monaco (Elekta, Stockholm, Sweden) and Precision (Accuray, Sunnyvale, California, USA).

The CARDIO-RT software was employed as a quality assurance tool to verify the accuracy of the CTV transfer. In cases where significant modifications were needed, the initial manually transferred CTV was re-evaluated by the interdisciplinary team (cases 1-4). For case 5, the software was applied retrospectively using the EAM data acquired after STAR. Figure 5.1 provides an overview of the workflow for EAM-treatment planning imaging data verification.

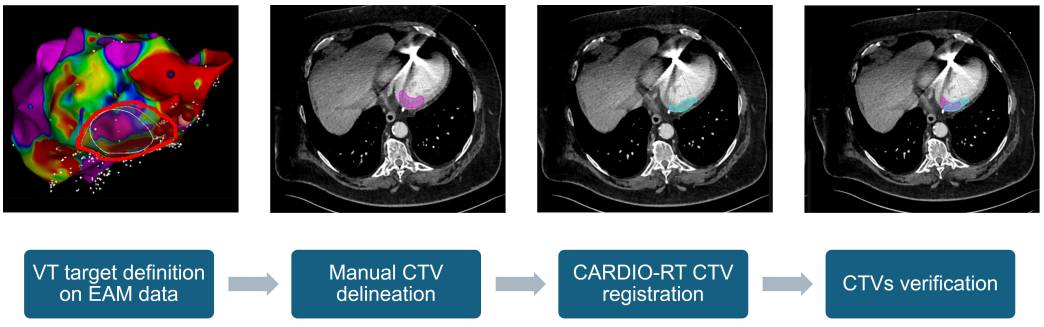


FIGURE 5.1: Workflow of ventricular tachycardia (VT) target identification, manual clinical target volume (CTV) delineation, CARDIO-RT electroanatomical mapping (EAM)-treatment planning imaging data registration and verification during quality assurance process.

### 5.2.3 Structure Analysis

Cardiac CTVs were manually transferred from the EAM data to the planning CT. CTV transfer by 3D-3D registration to the planning CT as well as transfer to the 17-segment model was conducted semi-automatically. All 2D-3D, 3D-3D, and 17-segment model registrations were checked and/or performed by the study center.

CTVs generated by manual transfer and using CARDIO-RT (2D-3D and 3D-3D) were compared for cases 3 and 4. These comparisons were analyzed in Velocity (version 3.2.1, Varian, Palo Alto, California, USA) regarding structure characteristics including volume, surface size, localization, DSC and surface distance metrics by the means of mean, median, standard deviation and HD [15]. The DSC ranges from 0 to 1, where 0 indicates no overlap and 1 indicates perfect overlap.

### 5.2.4 Validation Results

The employed EAM-treatment planning imaging data transfer method and associated information for the 5 cases analyzed with the CARDIO-RT software are presented in Table 5.2. The target transfer workflow was based on the availability of CARDIO-RT at the time of STAR treatment and the EAM system used at the STAR treatment center.

TABLE 5.2: EAM-treatment planning imaging data transfer in the 5 patient cases. Abbreviations: LV = left ventricle. *Based on the American Heart Association 17-segment model.

| Case | Target transfer methods | Targeted (partial) LV segments* | Adjustments after CARDIO-RT assessment |
|---|---|---|---|
| 1 | Manual, adapted by 3D-3D | 8, 13 and 14 | Minor adjustments |
| 2 | Manual, adapted by 2D-3D | 7, 8, 9, 13 and 14 | Minor adjustments |
| 3 | Manual, adapted by 2D-3D and 3D-3D | 4 | Yes, see structure analysis |
| 4 | Manual, confirmed by 2D-3D | 1, 4, 5 and 6 | Applied retrospectively |
| 5 | Manual | 13, 14 and 17 | Applied retrospectively |

**Case 1**

In case 1, EAM identified two possible VT target regions in the anteroseptal region of the LV and proximity of an aneurysm of the LV in the basolateral region. Based on the location of the previous catheter ablations and the VT morphology, it was decided to treat only the left anteroseptal region (see Figure 5.2A). Figure 5.2B-D illustrates the EAM points (LV, aorta and catheter ablation points) and CT contours (LV and aorta) before and after 3D-3D registration, as described in section 4.3. The registered catheter ablation points (Figure 5.2E-G) serve as reference for generating the final cardiac CTV (Figure 5.2H-K). Based on 4D CT, STAR treatment was planned by adapting the CTV generated through the 3D-3D registration.

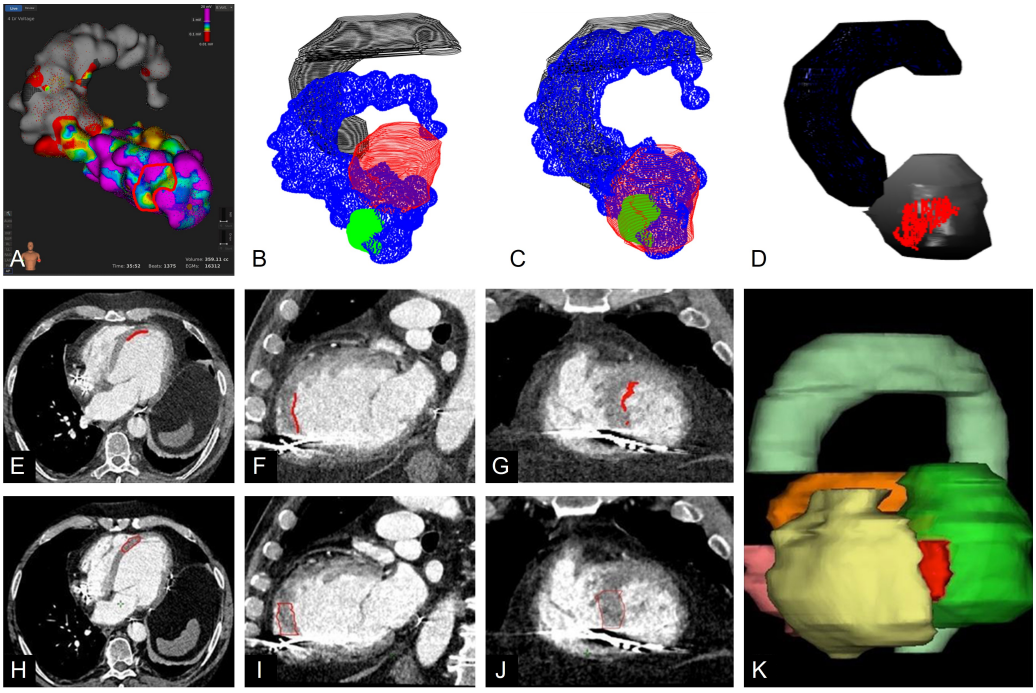


FIGURE 5.2: Case 1. (A) Electroanatomical mapping (EAM) data with the marked ventricular tachycardia (VT) target region (red) in anterior-posterior view from RHYTHMIA HDx system. (B) Computed tomography (CT) contours (red: left ventricle, LV; black: aorta) and EAM points (blue: LV and aorta; green: catheter ablation points) before 3D-3D registration. (C) CT contours and EAM points after 3D-3D registration. (D) 3D view of the LV, aorta and 3D-3D registered target points (red). (E-G) Axial, sagittal and coronal views of the cardiac CT with the 3D-3D registered VT target points. (H-J) Axial, sagittal and coronal views of the cardiac CT with the final cardiac clinical target volume (CTV, red). (K) 3D view of the CTV (red) and cardiac substructures (light green: aorta; green: LV; yellow: right ventricle; rose: right atrium; orange: left atrium).

**Case 2**

In case 2, cardiac MRI and contrast-enhanced CT data from the systolic and diastolic phases were used for CTV verification and plausibility checks due to scarring from myocarditis and multiple catheter ablations (Figure 5.3B and C). The CT and MRI data suggested slightly different regions as potential targets. The 2D-3D registration was performed using an EAM screenshot and confirmed the results of the manually created CTV (Figure 5.3F-H). The final CTV was determined as the union of the target regions identified on CT and MRI data (Figure 5.3J-L).

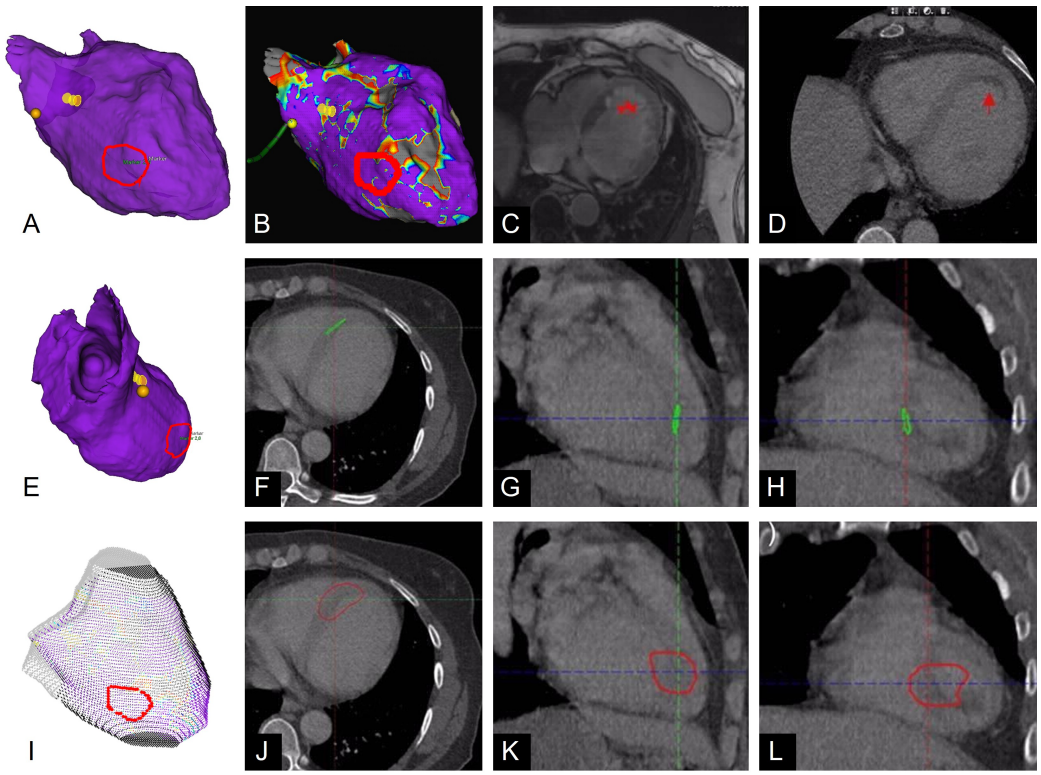


FIGURE 5.3: Case 2. (A, B, E) Electroanatomical mapping data with the ventricular tachycardia (VT) target region (red) in anterior-posterior and left lateral views from EnSite NavX system. (C) Pre-stereotactic arrhythmia radioablation contrast-enhanced cardiac computed tomography (CT) in systolic phase. Red arrow: septal-apical hypoattenuation indicating fibrosis/scarring. (D) 3.0 Tesla cardiac magnetic resonance imaging, transaxial navigated 3D fast low angle shot magnetic resonance imaging sequence with inversion recovery showing pronounced late gadolinium enhancement indicating cardiac fibrosis/scarring. (F-H) Axial, sagittal and coronal views of the cardiac CT with 2D-3D registered VT target (green). (I) 3D view of the left ventricle point cloud and the 2D-3D registered VT target points (red). (J-L) Axial, sagittal and coronal views of the planning CT with the final cardiac clinical target volume (red).

**Case 3**

In case 3, a large low voltage area was recorded in the inferior, septal, basal and mid-ventricular regions of the LV using the CARTO 3 system. Programmed ventricular stimulation with the ICD reproducibly induced sustained monomorphic VT with an exit site in the inferior basal scar area, corresponding to LV segment 4 (Figure 5.4A and E). STAR was performed using the manually transferred CTV, which was adapted through 2D-3D and 3D-3D registrations. A comparison between CTVs generated by manual, 2D-3D and 3D-3D registrations showed high variation (Table 5.3), with the smallest CTV observed for 3D-3D registration, followed by manual registration and the largest for 2D-3D registration. Surface area

measurements also varied across registration methods, with the smallest surface area reported for 3D-3D transfer and the largest for manual transfer. Axial, sagittal and coronal locations of the center differed among the registration methods. Using 2D-3D registered CTV as the reference, the 3D-3D result demonstrated higher conformity and a smaller HD compared to manual registration.

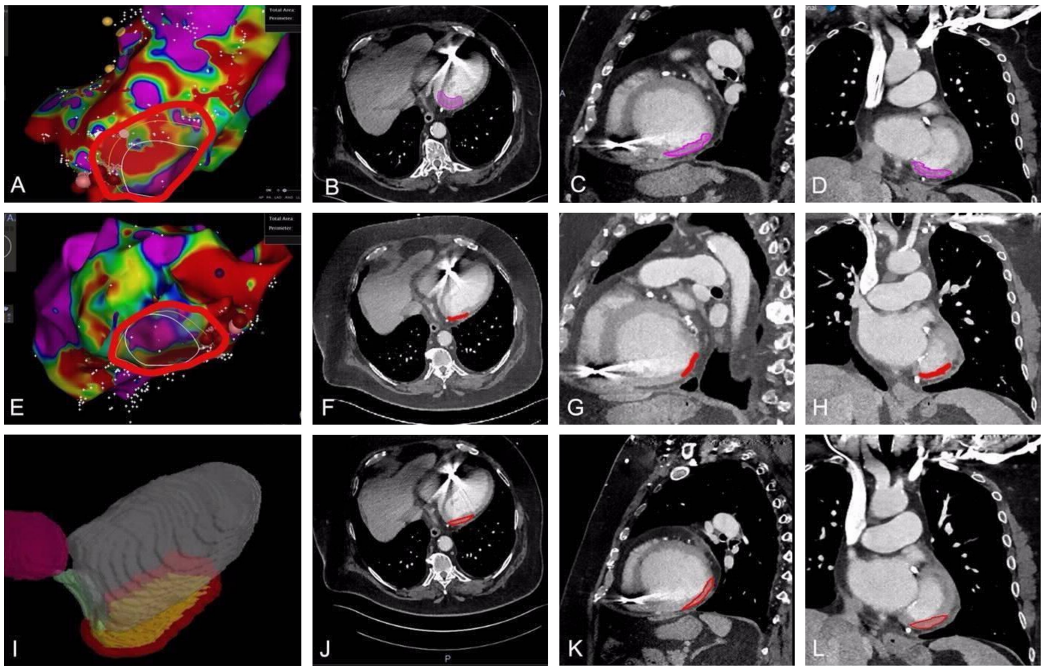


FIGURE 5.4: Case 3. (A, E) Electroanatomical mapping (EAM) data with the ventricular tachycardia target region (red) in inferior and posterior-anterior views from CARTO 3 system. (B-D) Axial, sagittal and coronal views of the cardiac computed tomography (CT) with manually transferred clinical target volume (CTV, magenta). (F-H) Axial, sagittal and coronal views of the cardiac CT with the 2D-3D registered CTV (red). (I) 3D view of the registered CTV. (J-L) Axial, sagittal and coronal views of the cardiac CT with the final CTV (red).

TABLE 5.3: Structure analysis for cases 3 and 4. Abbreviations: CTV = clinical target volume; DSC = Dice-Sørensen coefficient; HD = Hausdorff distance.

| | Case 3 | | | Case 4 | |
|---|---|---|---|---|---|
| CTV transfer method | Manual | 2D-3D | 3D-3D | Manual | 2D-3D |
| CTV ($cm^3$) | 13.0 | 21.0 | 10.4 | 94.9 | 34.3 |
| Surface area ($mm^2$) | 5845 | 4757 | 3421 | 13297 | 8775 |
| Center axial | 56.8 | 53.0 | 51.5 | 8.7 | 8.7 |
| Center coronal | 33.9 | 30.6 | 24.1 | 43.5 | 40.5 |
| Center sagittal | 20.3 | 32.7 | 30.7 | 34.7 | 41.5 |
| DSC | 0.47 | Reference | 0.55 | 0.51 | Reference |
| Mean surface distance (mm) | 4.19 | Reference | 2.19 | 3.90 | Reference |
| Median surface distance (mm) | 2.22 | Reference | 1.37 | 2.59 | Reference |
| Standard deviation of surface distance (mm) | 4.43 | Reference | 2.60 | 3.80 | Reference |
| HD (mm) | 21.0 | Reference | 17.4 | 24.4 | Reference |

**Case 4**

In case 4, a large low voltage zone encompassing the anterior, posterolateral, inferior, and basal regions of the LV suggested an epicardial substrate with endocardial exits at these locations (Figure 5.4A-C). The EAM-defined VT target covering the basal low voltage zone was transferred to the CT. A transmural ITV and PTV were created, accounting for respiratory motion (Monaco, Elekta AB). The EAM-treatment planning imaging transfer was validated by 2D-3D registration. A comparison between manual and 2D-3D registered CTVs showed a DSC of 0.5 for the CTV structures (Table 5.3). As shown in Figure 5.6, the 2D-3D registered CTV (yellow) is centrally positioned within the manually defined CTV structure (green).

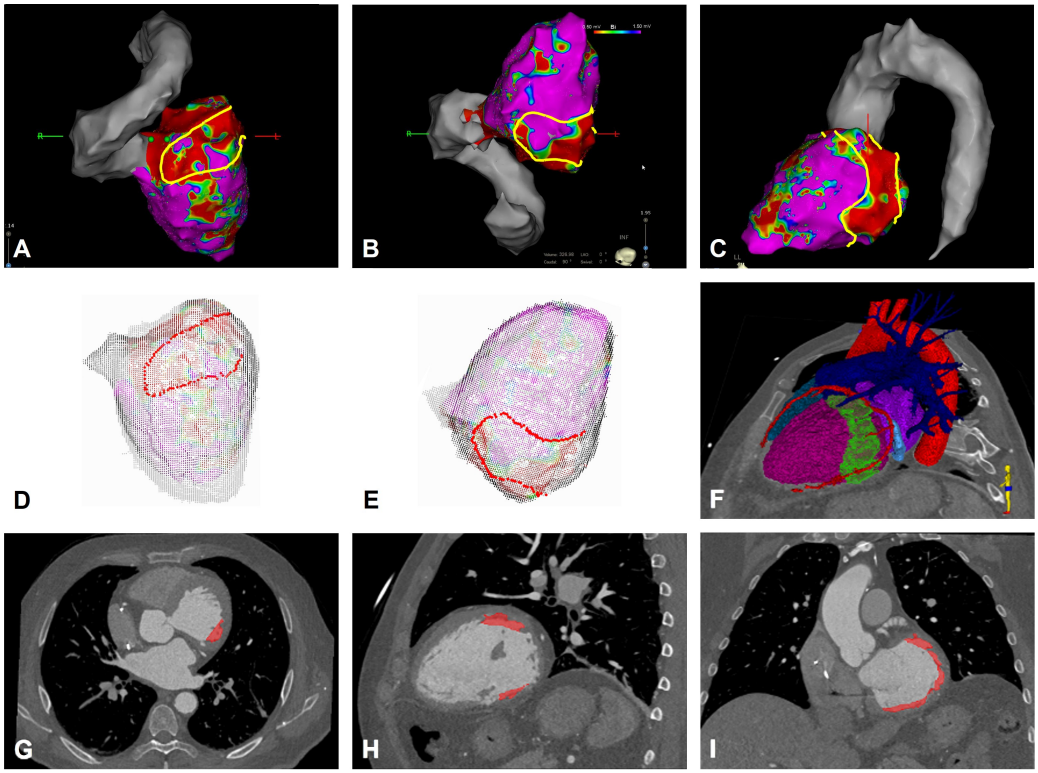


FIGURE 5.5: Case 4. (A-C) Electroanatomical mapping data with the marked ventricular tachycardia (VT) region (yellow) in superior (SUP), inferior (INF) and left lateral (LL) views from CARTO 3 system. (D, E) SUP and INF views during the 2D-3D registration with the defined VT target points (red). (F) A 3D rendering (LL view) of the resulting clinical target volume (CTV, green) shown in the context of the cardiac chambers and great vessels, as segmented from the cardiac computed tomography (CT). (G-I) Axial, sagittal and coronal views of the cardiac CT with the final CTV (red).

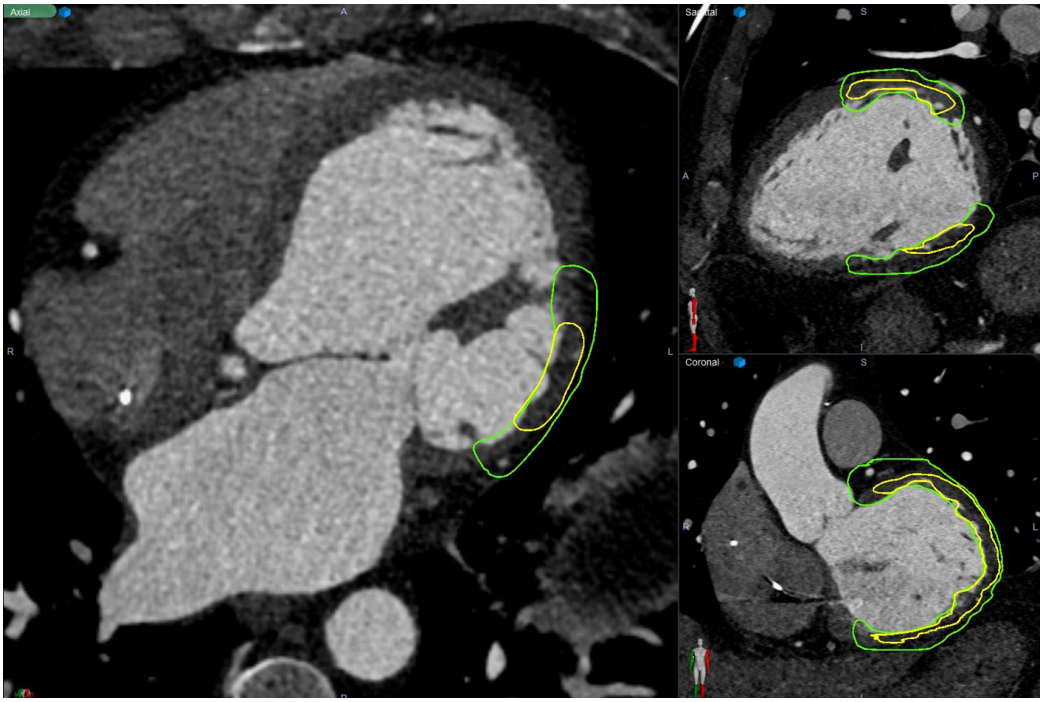


FIGURE 5.6: Manually defined clinical target volume (CTV, green) and the 2D-3D registered CTV (yellow) for case 4, shown on the cardiac computed tomography in axial, sagittal and coronal views.

**Case 5**

In case 5, the cardiac CTV was defined by manual registration. A comparison of the manually defined CTV with the CTV generated by the CARDIO-RT software was not possible before STAR, as the software was unavailable at the time of treatment and a complete EAM could not be acquired due to an LV apical thrombus. Despite STAR, sustained VT recurred with recurrent conversion attempts. Therefore, an additional invasive catheter ablation was performed three weeks after STAR in LV segment 7, successfully terminating the VT. Retrospectively, CARDIO-RT registration was performed using the EAM data from the successful catheter ablation, and accordance with the CTV defined as the STAR target was observed (Figure 5.7). Retrospective structure analysis using CARDIO-RT showed that STAR was performed more apically relative to the successful catheter ablation region.

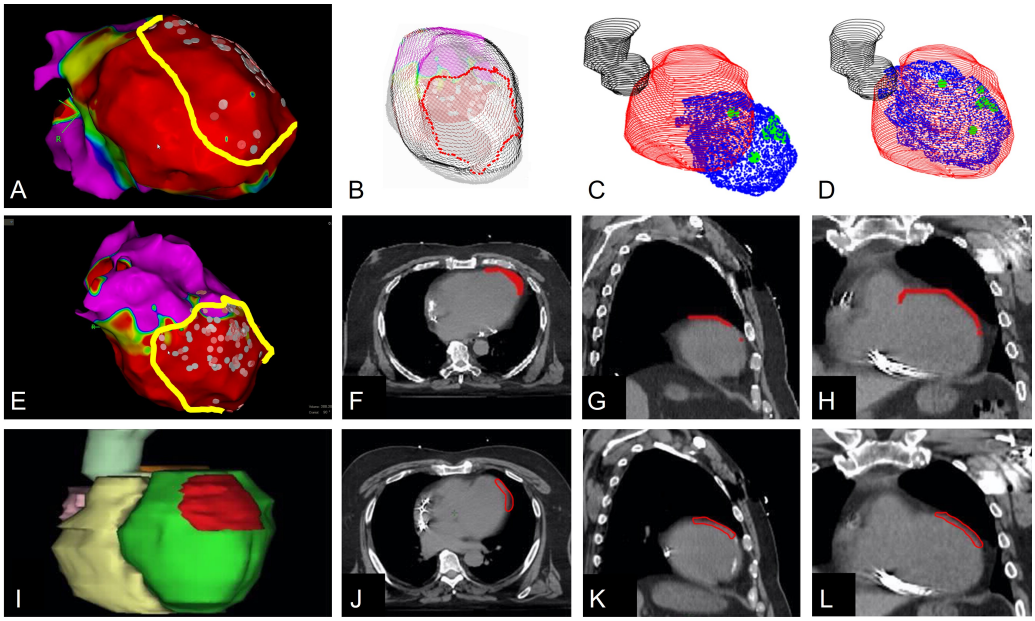


FIGURE 5.7: Case 5. (A, E) Electroanatomical mapping (EAM) data with the marked ventricular tachycardia (VT) target region (yellow) in superior and anterior-posterior views from CARTO 3 system. (B) 3D view of the left ventricle (LV) point cloud and the 2D-3D registered VT target points (red). (C) Computed tomography (CT) contours (red: LV; black: aorta) and EAM data (blue: LV; green: ablation points) before the 3D-3D registration. (D) CT contours and EAM data after the 3D-3D registration. (F-H) Axial, sagittal and coronal CT slices with marked (red) region by 2D-3D match; (I) 3D structures from the planning CT with final clinical target volume (CTV, red), LV (green), right ventricle (yellow) and aorta (light green). (J-L) Axial, sagittal and coronal CT slices with the final treated CTV (red, without assistance of the CARDIO-RT software).

### 5.2.5 Discussion

In this study, the CARDIO-RT VT target registration methods introduced in Chapter 4 were clinically validated in quality assurance process for STAR treatment planning for VT. The software allows the import and analysis of EAM data from all major clinical systems, supporting screenshots and raw data exported from commonly used EAM systems in clinical practice (i.e., RHYTHMIA HDx, CARTO 3 and EnSite). The AHA 17-segment model registration, 3D-3D registration and 2D-3D registration in the software were successfully confirmed for 5 VT patients who underwent STAR treatments in a multi-center setup within the German RAVENTA trial [29]. The three practical VT target registration approaches could serve as a quality assurance tool to provide a second opinion on the validity of manual or other methods for VT target transfer in STAR. In particular, the versatile 2D-3D registration method, which is compatible with any EAM platforms, overcomes the difficulties and limitations of earlier published 3D-3D

registration methods related to EAM mesh data acquisition and EAM raw data format inconsistency.

The CARDIO-RT software was designed with an intuitive GUI that guides users through a structured workflow. Feedback from participating centers highlighted its ease of use, requiring minimal additional training and no extensive prior experience with similar systems. The uniform workflow is compatible with any EAM and CT system combinations, eliminating additional workload when switching between systems. This feature is particularly valuable in multi-center trials, where heterogeneous data from various systems are analyzed and compared. Additionally, no external visualization software is required as the CARDIO-RT software allows for 3D visualization of semi-automatically generated cardiac CTV structure with anatomical cardiac substructures such as the LV and aorta.

Some previous approaches have relied on using mesh data to register EAM-treatment planning imaging data [90], [93], [113]. In contrast, the newly developed 2D-3D registration method in CARDIO-RT eliminates the need for dealing with proprietary data formats exported from different EAM systems that the input needed from EAM systems are screenshots in standard anatomical views. Since these proprietary vendor-specific data formats are not readily well documented, they often require deduction and reverse engineering from exported files [90]. Additionally, the format of exported EAM data can change unpredictably, as observed during the update of CARTO 3 system from version 6 to version 7.

Compared to relying solely on the AHA 17-segment model in the CTV definition workflow [87], the CARDIO-RT software enables more precise VT target transfer by highlighting the exact VT substrate defined on the EAM data. Future features, such as incorporating ECG data as suggested in a previous publication [145], can be easily integrated into the software. The proposed CARDIO-RT software can seamlessly fit into the preparatory workflow before STAR treatment. STAR is characterized by its rigorous requirements for high precision and advanced technological quality [146], [147]. With expert consensus emphasizing the need for standardized protocols and specialized centers conducting STAR within clinical trials [144], the proposed software addresses previous uncertainties in the EAM-treatment planning imaging registration data by ensuring quality assurance for manually transferred VT targets.

Within the RAVENTA trial, the CARDIO-RT software was successfully applied to 5 STAR cases for VT patients, illustrating the current diversity of

EAM systems (RYTHMIA HDx, CARTO 3, and EnSite) and the range of EAM-treatment planning imaging data registration methods used in this field. In cases 1 and 3, the manually transferred cardiac CTV structure was modified after analysis with CARDIO-RT. For patients 3 and 4, manual transfer, 3D-3D registration (for case 3) and 2D-3D registration methods were performed and compared. The significant variation in the examined parameters, particularly in the extent and localization of the target region, highlights the differences observed between the manual transfer method and semi-automatic transfer methods. This finding highlights the limited accuracy of manual target transfer, even when performed and approved by an interdisciplinary team with experienced expertise in the field [15]. In Case 4, the CARDIO-RT 2D-3D registration method was compared with the previously published 3D Slicer extension EAMapReader with the 3D-3D registration concept [90], demonstrating a high degree of agreement in transferred CTVs between both approaches. The aorta structure was also obtained in both the EAM data and the CT contours, providing an additional spatial validation for the registration outcome. In case 5, CARDIO-RT provided retrospective verification using newly acquired EAM data, revealing why the prior STAR procedure may not have been successful: segment 7 was not targeted during the previous STAR procedure, which ultimately led to a permanent cessation of VTs.

Using CARDIO-RT, the previously reported discrepancies in the degree of agreement of the cardiac CTV definition on the EAM and the CT could be addressed [15]. The semi-automated EAM-treatment planning imaging registration enables quality assurance of the manually transferred cardiac CTV structure, reducing clinician-dependent inconsistencies and enhancing the safety and robustness of the VT target registration. This approach facilitates standardized STAR treatment planning processes that are less dependent on the expertise of the treating center. This advance in the VT treatment by STAR may promote a more widespread use of this technique by facilitating the employed workflow and ensuring a high-quality standard. Additionally, this software may furthermore be used to obtain a detailed statistical analysis of previously performed STAR treatments, allowing retrospective assessments of VT target transfer accuracy and dose-response analyses. Retrospective findings of incorrectly transferred VT target could help explain VT recurrence. A successful treatment, despite a retrospective analysis identifying areas that should have been targeted but were spared, could enhance the understanding of STAR treatment target definition.

**Limitations**

Due to limited data availability, a complete validation of the three VT target registration methods in the CARDIO-RT software was not performed on all cases in this study. Specifically, in cases 1 and 2, the manually transferred cardiac CTV was adjusted using CARDIO-RT analysis, but as the manually transferred CTV was not stored, structural CTV comparisons were not possible. In case 5, EAM data prior to STAR could not be included. Moreover, since STAR is still a novel therapeutic option for VT, the number of patients is limited, and no large-scale clinical trial has been conducted so far [148].

## 5.3 Cross-Validation

As shown in Chapter 4 and section 3.1, that although several novel semi-automatic VT target registration tools have been developed, there is a lack of studies to evaluate and cross-validate different VT target registration approaches using real-world VT patient data. Such studies are essential to assess the accuracy and conformity of different VT target registration tools for STAR. EAMapReader is a novel semi-automated VT target transfer extension within the open-source 3D Slicer software with the concept of 3D-3D registration. Due to the fundamentally different concepts between the 2D-3D registration from the CARDIO-RT software and the 3D-3D registration from the EAMapReader extension, it can be hypothesized that a systematic error is highly unlikely when performing both registration methods on a same dataset. Therefore, a cross-validation study is conducted to investigate the conformity between these two approaches. Given that freehand manual VT target transfer is prone to considerable inter-observer variability [15], [16], the manual delineated VT target is unsuitable to be used as ground truth. Therefore, in this cross-validation study, the registered VT target structure generated by each approach serves as ground truth for the other. This section provides the answer to the research questions Q3 mentioned in section 1.1.

This study aimed to compare the results of two novel, conceptually different, in-house-developed semi-automated VT target registration software solutions for STAR [90], [138]. These two solutions transfer VT target surface regions defined in EAM space to a 3D cardiac CTV defined on contrast-enhanced ECG-triggered cardiac CT in the radiation TPS. Both target transfer approaches have been previously published [90], [138] and are described below. The target transfer using both methods was performed by two independent investigators, blinded to each

other's results. The resulting cardiac CTVs were compared by a third investigator in a core lab using two complementary software packages: Velocity (Varian Medical System, Palo Alto, California, USA) and ADMIRE (Elekta, Stockholm, Sweden). Figure 5.8 illustrates the workflow of the study design.

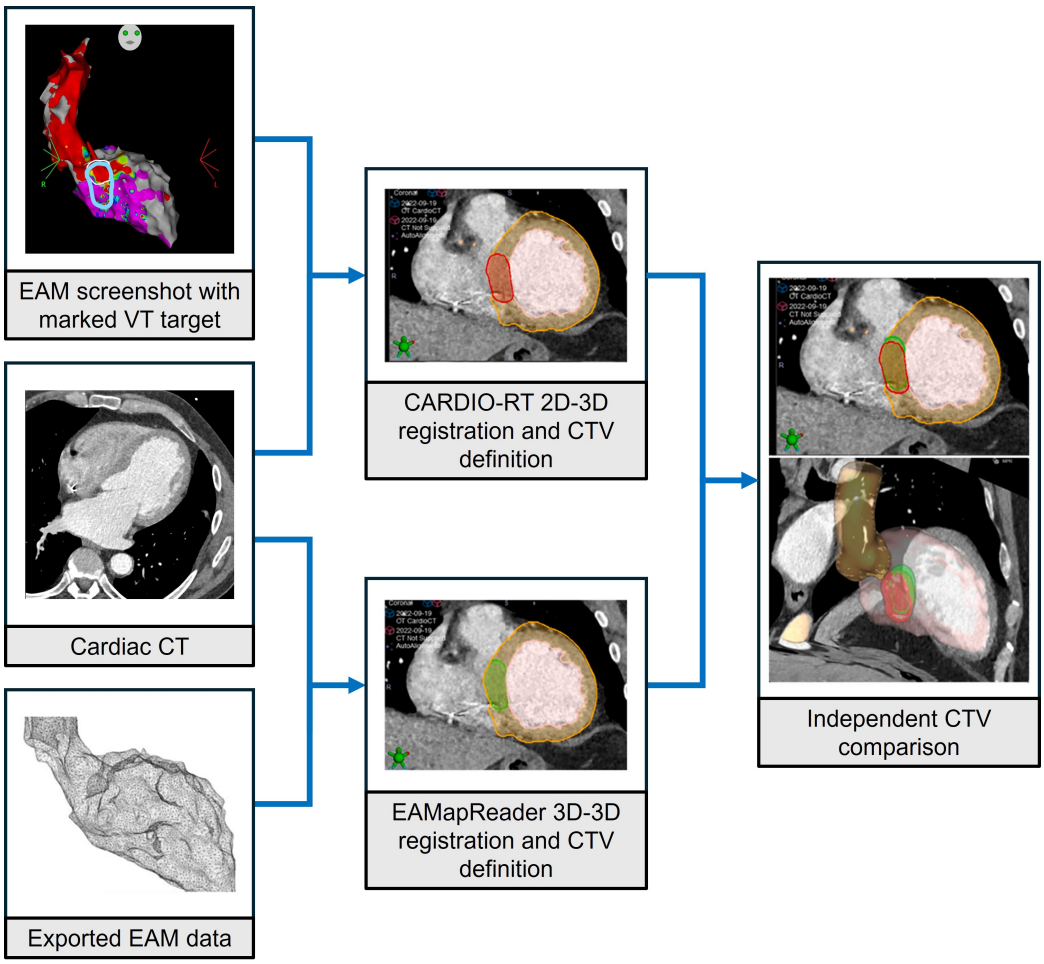


FIGURE 5.8: Study design and analysis workflow. See main text for details. Abbreviations: EAM = electroanatomical mapping; VT = ventricular tachycardia; CT = computed tomography; CTV = clinical target volume.

### 5.3.1 Data Acquisition and Patient Characteristics

Patients underwent STAR within the RAVENTA trial [29] or as compassionate use following consensus guidelines [80], [144]. Pseudonymized data were collected from the treating centers. Ethics approval was obtained for the coordinating center (reference number D555/18, see Appendix A) and each local site and/or for the STAR benchmark studies (D476/19 and D483/21). Informed consent to pseudonymized data sharing was obtained before treatment.

ECG-gated contrast-enhanced cardiac CTs per local protocol were acquired as part of treatment planning. The contrast-enhanced cardiac CT used was the scanner-determined "best diastolic" volume. This corresponds well to the EAM data, which acquires point locations during diastole. EAMs were created either during VT catheter ablation attempts or as dedicated STAR procedure. The choice of EAM system was at the discretion of the treating center: RHYTHMIA HDx, CARTO 3 Version 7 or Ensite NavX.

EAM screenshots were captured on the EAM workstation. For the CARDIO-RT 2D-3D registration, standard anatomical views were obtained. For the EAMapReader 3D-3D registration, any angulation providing a clear view of the VT target region (standard projections or oblique views) was used. Additionally, the EAM raw data were exported in their respective proprietary file formats. The target on the EAM screenshot, marked by the treating cardiac electrophysiologist, was used as input for both approaches.

For each patient case, cardiac structures including the contrast-filled LV blood pool, LV myocardium, aorta and RV cavity [5] were segmented from the contrast-enhanced CT by the local cardiologist or radiation oncologist and exported as in a RTSS file. This radiotherapy structure set and the contrast-enhanced CT (both in DICOM format), EAM screenshots with delineated VT targets (in PNG or JPG/JPEG format), and exported EAM data (vendor-specific file format), were used as common inputs for both registration methods. The transfer for each method was performed by an experienced team consisting of a physiologist/cardiologist, a radiation oncologist, a medical physicist, and an engineer.

Detailed patient characteristics are summarized in Table 5.4. All 10 patients have been treated with a single dose of 25 Gy prescribed to the surrounding isodose surface while adhering to critical structure constraints according to the RAVENTA trial protocol [29]. Baseline demographics, STAR planning and delivery details, and initial clinical follow-up data have been previously reported for some of these patients [4], [100], [124].

TABLE 5.4: Patient characteristics. Abbreviations: EAM = electroanatomical mapping; LV = left ventricle; RV = right ventricle. *Based on the American Heart Association 17-segment model.

| Patient | EAM system | Targeted (partial) LV segments* | Aorta/RV mapped | Clinical trial or compassionate use |
|---|---|---|---|---|
| 1 | CARTO 3 | 1 | Yes | Compassionate use |
| 2 | RHYTHMIA HDx | 6 and 12 | Yes | RAVENTA |
| 3 | EnSite | 8 | No | RAVENTA |
| 4 | CARTO 3 | 1 and 7 | Yes | Compassionate use |
| 5 | CARTO 3 | 1, 5, 6 and 11 | Yes | RAVENTA |
| 6 | RHYTHMIA HDx | 8 | No | RAVENTA |
| 7 | CARTO 3 | 5 and 11 | No | RAVENTA |
| 8 | CARTO 3 | 2, 3 and 8 | No | RAVENTA |
| 9 | RHYTHMIA HDx | 8 and 13 | Yes | RAVENTA |
| 10 | CARTO 3 | 2 and 3 | Yes (also RV) | RAVENTA |

### 5.3.2 Independent Target Registration

**EAMapReader 3D-3D Registration**

3D-3D registration was performed using the open-source 3D Slicer software for medical image analysis (version 5.0.3, 3D Slicer contributors, https://www.slicer.org/) and the EAMapReader extension [90], [91]. Briefly, the 3D EAM was registered to the endocardial structure of the LV, contoured on the contrast-enhanced CT (slice thickness: 0.8-1.0 mm), through manual alignment followed by an ICP optimization to minimize the distance between the structures. This process resulted in a rigid (6-degrees-of-freedom) 3D transformation. Where available, EAM of the aorta or the right ventricle were used as additional registration reference to reduce rotational ambiguity and enhance robustness.

The registration of the EAM to the contrast-enhanced CT produces a transformation matrix, which can be decomposed into sequential rotations around the

principal axes. Euler angles about the left–right, anterior-posterior and inferior-superior axes were calculated from the final registration matrix.

After registration, a target structure was contoured directly onto the EAM in 3D Slicer to re-create the target surface delineated on the corresponding EAM screenshots. Since the VT substrate may locate at any depth within the LV myocardium, and catheter ablation failures are often attributed to inaccessible substrates deep in the LV myocardium, a transmural target volume is typically used for STAR. To create a transmural target volume from the endocardial target surface on the EAM, the full myocardial thickness was added to the target surface. This thickness was defined during segmentation using thresholding and grow-from-seed algorithms. The resulting target structure was smoothed with a Gaussian smoothing kernel with a 3 mm width according to the CT slice thickness identically in both workflows (see Figure 5.9).

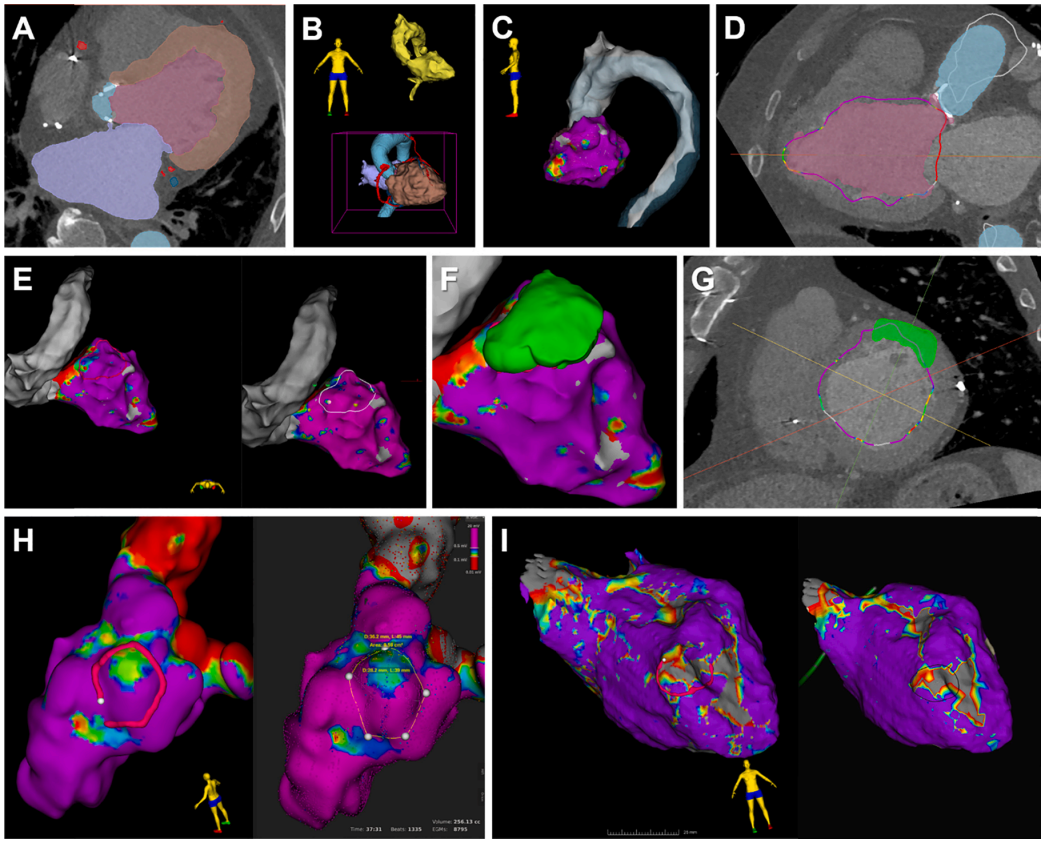


FIGURE 5.9: Representative case of 3D-3D registration followed by target creation using 3D Slicer software and the EAMapReader extension. (A) Contouring of relevant cardiac structures. Magenta: left ventricle (LV) cavity; light blue: aorta; brown: LV myocardium. (B) 3D representation of the segmentation and geometry of the electroanatomical mapping (EAM, yellow). (C, D) 3D rendering (C) and short-axis reformation (D) of the EAM data (LV and aorta) after rigid registration with the segmentation. (E) Side-by-side view of the imported EAM in 3D Slicer (left) and the corresponding screenshot from the CARTO 3 EAM system (right). The white shape in the EAM screenshot (right) is the predefined ventricular tachycardia target. Note the corresponding contouring in progress (red) on the imported model (left). (F, G) Final transmural cardiac clinical target volume (green). While (A-G) demonstrate a case using the CARTO 3 EAM system, other EAM systems lead to similar results. (H) Corresponding step to panel (E) in a case using RHYTHMIA HDx system. (I) Corresponding step to panel (E) in a case using EnSite NavX system.

**CARDIO-RT 2D-3D Registration**

2D-3D registration was performed using the CARDIO-RT software, which enables the registration of CT volumes of the respective cardiac chamber with EAM screenshots in standard anatomical views. EAM screenshots with the marked target region were imported into CARDIO-RT, along with the RTSS file containing the segmentations of the LV blood pool and other cardiac substructures from

the contrast-enhanced cardiac CT (see Figure 5.10). The screenshots were overlaid onto a corresponding projection of the CT segmentations, and the segmentation was translated and rotated to achieve an optimal match. The rotation angles about the three principal axes were recorded for later analysis. Once registration was complete, the marked target region on the screenshot was delineated on the registered segmentation, resulting in a point cloud on the segmentation surface. These points were then saved into the original RTSS file and converted into a 3D CTV in the cardiac CT space by extending transmurally across the LV myocardium and smoothed with a 3 mm radius, as described above.

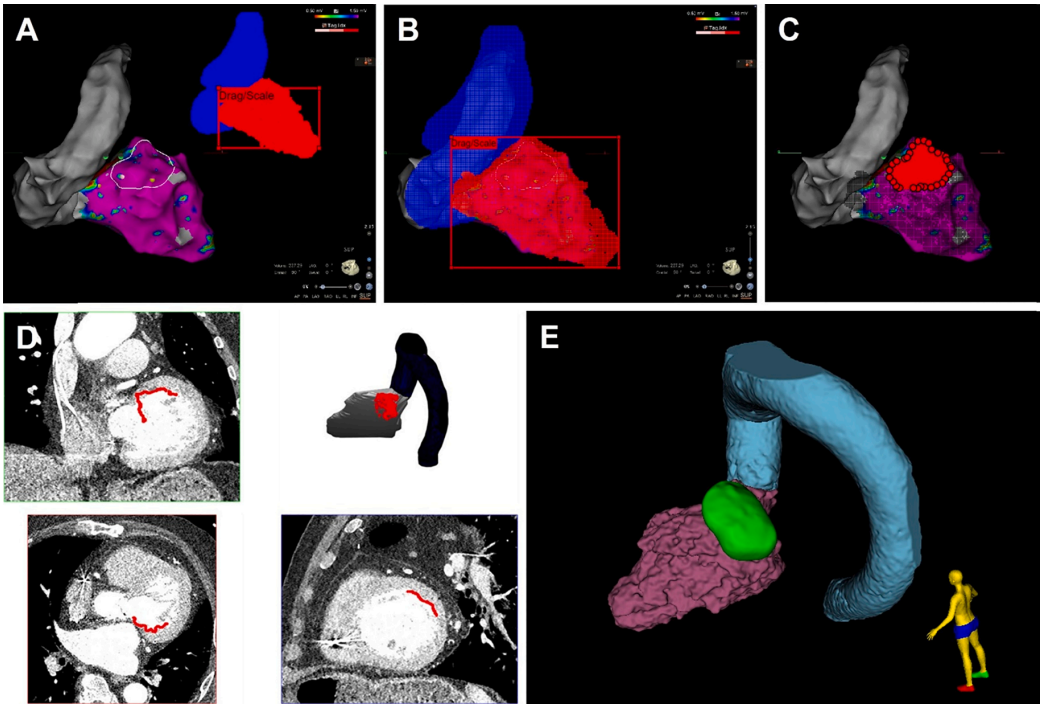


FIGURE 5.10: Representative case of 2D-3D registration followed by target creation using CARDIO-RT and 3D Slicer softwares. (A) CARTO 3 electroanatomical mapping (EAM) screenshot and the computed tomography (CT) point clouds of left ventricle (LV) blood pool (red) and aorta (blue) used as additional registration reference before registration. The EAM screenshot and CT-based point clouds are both visualized from superior view, and the white shape in the EAM screenshot is the predefined ventricular tachycardia (VT) target. (B) Registered EAM screenshot and CT contours. (C) Target points on the LV blood pool defined by delineated polygon along the intended target. (D) Registered VT target (red) on the cardiac CT slices and 3D view of the LV, aorta and VT target. (E) Transmural cardiac clinical target volume (green) according to the 2D-3D output.

### 5.3.3 Structure Analysis

The resulting 3D CTVs, independently generated by the blinded investigators using both methods, were transferred to a core lab and imported into commercial software for dedicated 3D structure analysis (Velocity, version 3.2.1, Varian Inc., Palo Alto, USA). Structure characteristics were analyzed and compared to evaluate overlap and similarity, including structure volumes, surface areas, distances and differences between the 3D CoM, conformity index (DSC, range 0–1), geometric structure similarity (independent of overlap) and surface distance metrics (median surface distance and HD). The median surface distance represents the median of the nearest-neighbor distances between points on both structures, while the HD is the maximum distance between the two structures. In addition, sensitivity (proportion of identical voxels) and specificity were evaluated [15], [149]. A second dedicated research software solution (ADMIRE, V3.47, Elekta, Stockholm, Sweden) was utilized to independently validate the results and analyze additional parameters of structure agreement, as reported previously [149].

Continuous variables were compared, and differences were evaluated using the t-test or the Mann-Whitney test, as appropriate. It should be noted that the number of cases lacks the power to identify statistical significance in minor differences. However, descriptive statistics allow for the evaluation of whether the magnitude of observed differences is of clinical significance. Statistical analysis was performed using R (version 4.0.5) within the RStudio environment (version 1.3, Posit Software, Boston, Massachusetts, USA). Values are given as mean ± standard deviation unless noted otherwise.

### 5.3.4 Cross-Validation Results

Complete datasets were obtained for 10 patients, and registration using both approaches was successfully completed. In six patients, EAM of the thoracic aorta was available and used in combination with the LV for registration with the corresponding structures on the contrast-enhanced CT. For the remaining four cases, alternative landmarks such as partial EAM of the right ventricular outflow tract or the endocardial impressions of the left ventricular papillary muscles, were used to reduce rotational ambiguity around the LV long axis.

All cases resulted in comparable and highly similar 3D CTVs in terms of size and anatomical position (see Figure 5.11 and Figure 5.12). The volumes and surface areas of the CTV structures were comparable, without significant differences:

14.88 ± 11.72 $cm^3$ versus 15.15 ± 11.35 $cm^3$ (p = 0.54) and 44.29 ± 33.63 $cm^2$ versus 46.43 ± 35.13 $cm^2$ (p = 0.18) for 3D-3D and 2D-3D registrations, respectively. The mean difference in volumes and surface areas were 0.37 ± 1.81 $cm^3$ and 2.14 ± 4.67 $cm^2$, respectively. Comparing both structures, the DSC was 0.84 ± 0.04, with sensitivity of 0.86 ± 0.05 and specificity of 0.96 ± 0.02. The median surface distance between the structures was 0.53 ± 0.37 mm, and the HD was 6.91 ± 2.26 mm. The distance between the 3D CoM was 3.62 ± 0.99 mm, and the geometrical volume similarity regardless of volume coordinates was 0.94 ± 0.05. All variables available in both analysis software packages were identical. Detailed results are presented in Table 5.5.

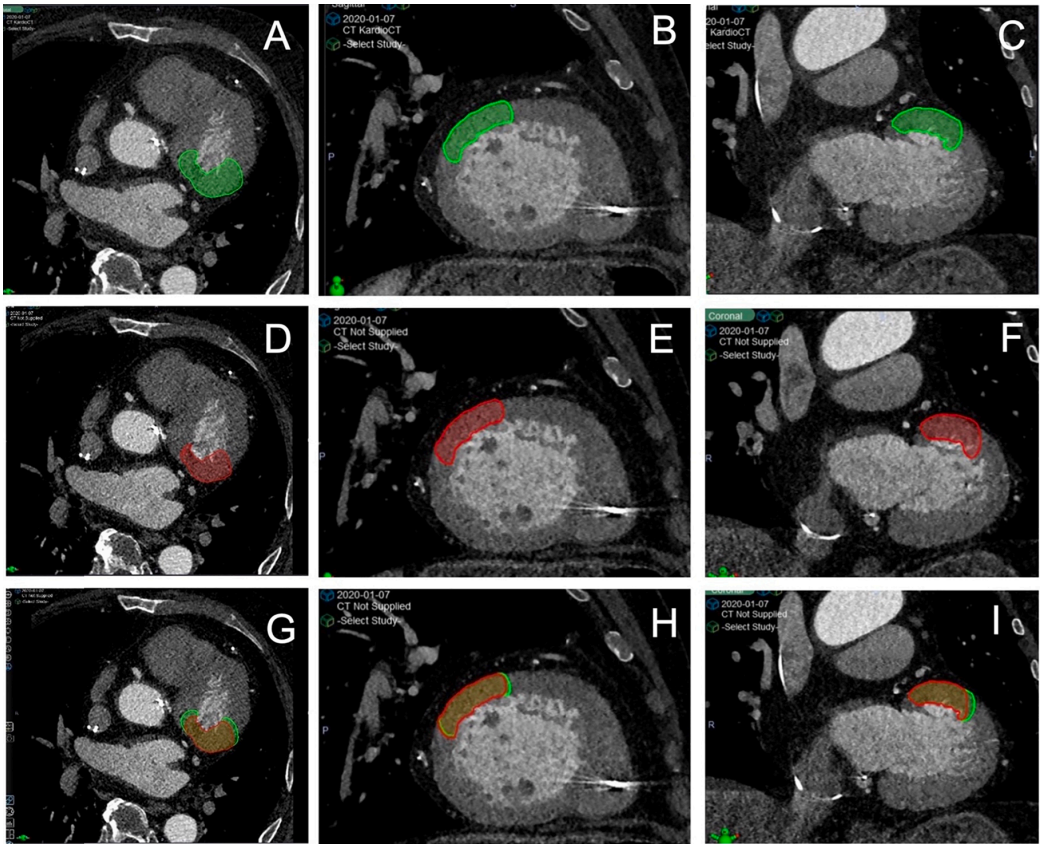


FIGURE 5.11: Axial, sagittal and coronal views of cardiac computed tomography with a representative transferred transmural cardiac clinical target volume (CTV). (A-C) CTV transferred by EAMapReader 3D-3D registration (green). (D-F) CTV transferred by CARDIO-RT 2D-3D registration (red). (G-I) Overlay both CTV structures.

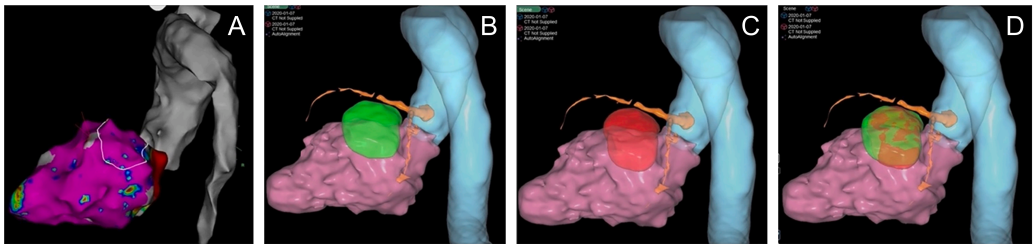


FIGURE 5.12: (A) Electroanatomical mapping screenshot with marked ventricular tachycardia target region (white shape). (B) 3D view of the cardiac CTV transferred by 3D-3D registration (green). (C) 3D view of the cardiac clinical target volume (CTV) transferred by CARDIO-RT 2D-3D registration (red). (D) Overlay of both CTV structures. Magenta: left ventricular blood pool; blue: aorta; orange: coronary arteries.

TABLE 5.5: Structure analysis results. Abbreviations: HD = Hausdorff distance; DSC = Dice-Sørensen coefficient; 3D CoM = three-dimensional center of mass; CTV = clinical target volume; RV = right ventricle; SD = standard deviation. °Cases with no additional map of the aorta/RV. *Mean difference of generated volumes -0.37 $cm^3$, 95 % confidence interval [-1.66 $cm^3$; 0.93 $cm^3$], p-value = 0.5366. ** Mean difference of generated surfaces -2.14 $cm^2$, 95 % confidence interval [-5.48 $cm^2$; 1.20 $cm^2$], p-value = 0.181.

| Case | Volume ($cm^3$)* | | Surface area ($cm^2$)** | | Overlap/similarity parameters | | | | | | |
|---|---|---|---|---|---|---|---|---|---|---|---|
| | 3D-3D | 2D-3D | 3D-3D | 2D-3D | DSC | Median surface distance (mm) | HD (mm) | 3D CoM difference (mm) | Volume similarity | Sensitivity | Specificity |
| 1 | 18.85 | 16.37 | 48.73 | 47.26 | 0.90 | 0.0 | 5.30 | 2.34 | 0.92 | 0.82 | 0.99 |
| 2 | 8.64 | 8.32 | 27.15 | 26.38 | 0.84 | 0.67 | 6.04 | 4.16 | 0.98 | 0.82 | 0.97 |
| 3° | 2.18 | 2.47 | 10.28 | 10.05 | 0.84 | 0.63 | 4.87 | 1.44 | 0.94 | 0.89 | 0.96 |
| 4 | 31.77 | 33.01 | 76.13 | 72.94 | 0.88 | 0.68 | 7.39 | 2.91 | 0.98 | 0.90 | 0.96 |
| 5 | 40.72 | 39.11 | 130.47 | 138.33 | 0.78 | 0.79 | 11.55 | 4.62 | 0.98 | 0.77 | 0.98 |
| 6° | 6.68 | 9.78 | 25.84 | 35.17 | 0.76 | 0.81 | 10.99 | 4.17 | 0.81 | 0.93 | 0.94 |
| 7° | 15.42 | 18.56 | 47.37 | 55.93 | 0.83 | 0.0 | 8.12 | 4.23 | 0.91 | 0.92 | 0.96 |
| 8° | 6.99 | 6.54 | 25.80 | 24.74 | 0.86 | 0.0 | 4.31 | 4.31 | 0.97 | 0.84 | 0.98 |
| 9 | 8.82 | 8.73 | 26.53 | 26.45 | 0.84 | 0.65 | 5.96 | 3.70 | 1.00 | 0.84 | 0.97 |
| 10 | 8.78 | 9.64 | 24.57 | 27.01 | 0.84 | 1.07 | 4.54 | 4.29 | 0.95 | 0.88 | 0.94 |
| Mean | 14.88 | 15.25 | 44.29 | 46.43 | 0.84 | 0.53 | 6.91 | 3.62 | 0.94 | 0.86 | 0.96 |
| SD | 11.72 | 11.35 | 33.63 | 35.13 | 0.04 | 0.37 | 2.46 | 0.99 | 0.05 | 0.05 | 0.02 |

For cases where neither the aorta nor the RV was available on the EAM data, greater differences in the CTVs were expected due to rotational ambiguity and the conceptually different approaches of the two registration methods. Indeed, the case with the lowest DSC (0.76) lacked both the aorta and RV in the EAM. However, no statistically significant differences in distances or similarity metrics were identified when comparing cases with additional aorta or RV to those without.

During both CT scanning and EAM procedures, the patient is positioned head-first-supine. Differences in body posture such as arms above the head for CT, and variations in diaphragm position can induce some rotation of the heart within the body, along with minor differences in patient positioning. To investigate the necessity of routinely accounting for rotation, the degree of rotation about the three principal patient axes was calculated for each case with both registration methods. As expected, the rotation was similar between these two registration methods, but varied widely across cases, ranging from negligible to over 20°about two axes (see Figure 5.13).

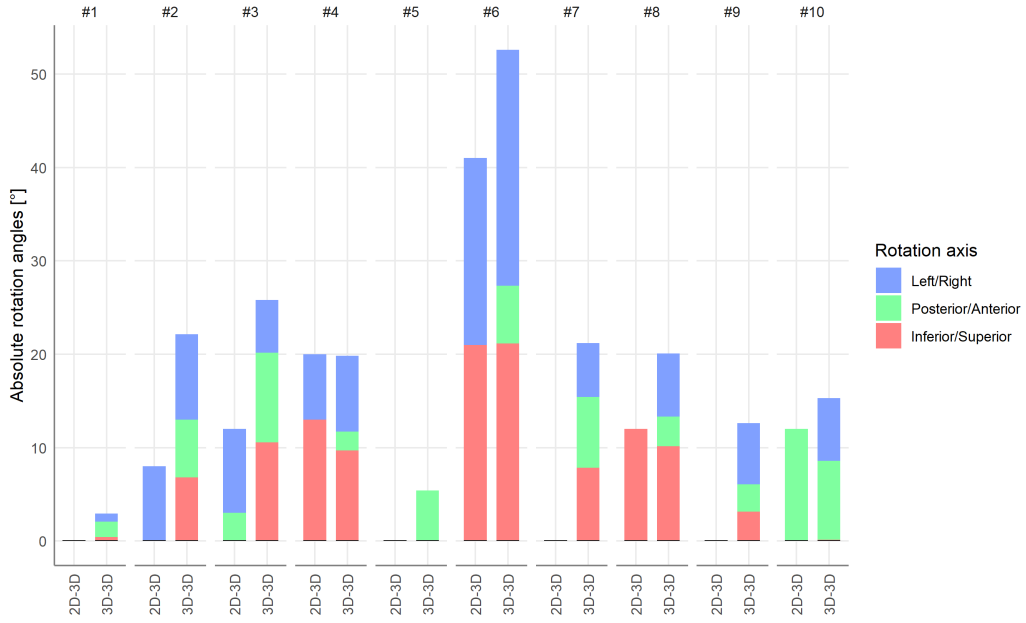


FIGURE 5.13: Absolute rotation angles about the three axes.

### 5.3.5 Discussion

This study cross-validated two conceptually different VT target registration methods for STAR for the first time - CARDIO-RT 2D-3D registration [138] and

EAMapReader 3D-3D registration [90] - on case data from 10 STAR-treated patients either within the RAVENTA trial [4], [29] or as compassionate use following consensus guidelines [80], [144]. Each approach effectively serves as a ground truth for the other, enabling cross-validation of both registration methods. Because of their fundamentally different concepts (2D-3D and 3D-3D), systematic error is considered highly unlikely. It was confirmed that both registration methods were technically feasible on all datasets, regardless of the EAM systems used and local cardiac CT acquisition protocols. The similarity metrics of the cardiac CTV structures registered using these two methods indicated excellent similarity.

STAR, as a novel and non-invasive bailout alternative option for refractory VT, its primary goal is to deliver precisely focused high-dose radiation beams to treat specific targets in the heart while minimizing exposure to the surrounding OAR. The VT target transfer from EAM system to radiation TPS for STAR is a complex and multidisciplinary task [5], [150]–[153]. The initial step, conducted by cardiac electrophysiologists, involves identifying the critical VT target region in the LV using the EAM. The primary objective is to identify the critical isthmus of the reentry circuit or, less commonly, the focal origin of the arrhythmia [102], [154]. Standard clinical practice involves using 3D EAM systems to map the arrhythmia substrate and mechanism [9]. However, for STAR, the target's precise location and extent are defined as a surface on the 3D endocardial or epicardial LV structure in the EAM system. In this technical cross-validation study, the VT target region is assumed to be a predefined input, and the focus is on methods to transfer the specified target from the EAM to the cardiac CT.

Early STAR studies utilized anatomical landmarks, such as the LV apex and aortic valve [1], [2], [155]–[157], or the AHA 17-segment model [25] to manually create the EAM-defined target structure in the radiation treatment planning CT. However, defining the true LV apex on CT is inherently challenging [86], and manual methods for transferring VT target from the EAM system to the TPS have demonstrated poor inter-operator consistency. Even when conducted by experienced clinicians, the resulting CTVs exhibited significant variability in both localization and extent, with 3D CoM differences reaching up to 35 mm and DSC as low as 0.02 [15]. These differences can cause clinically significant issues, as demonstrated by targeting errors in STAR that result in missed VT substrate areas and VT recurrence [18]. To enhance the robustness of target transfer, semi-automated tools were developed to achieve high-accuracy registration of the EAM-defined target to radiation TPS [90], [93]. These workflows and subsequent studies [94], [97], [113] utilized the 3D geometry of the EAM to align it

with a 3D structure of the corresponding cardiac chamber contoured from the CT. Although the technical implementations vary slightly between these tools, primarily in the range of usable 3D EAM data and, in some cases, reliance on closed-source third-party software, the fundamental concept of 3D-3D registration remains consistent across these workflows.

Validation of these methods was limited by the absence of baseline reference data, and because all implementations employed similar concept of 3D-3D registration, common confounders inherent to the methods could not be excluded. The implementation of the CARDIO-RT 2D-3D registration method [138] enabled cross-validation between two conceptually different VT target transfer approaches for the first time. The CARDIO-RT 2D-3D registration and EAMapReader 3D-3D registration methods were feasible for different EAM systems and CT acquisition protocols, and showed high agreement with near-identical CTV structures and localization with a median 3D CoM difference of 3.6 mm and a median DSC of 0.84. Therefore, it indicated that both the 2D-3D registration method (CARDIO-RT software) and the 3D-3D registration method (EAMapReader extension) can be used for quality assurance and VT target transfer from the EAM system to the radiation TPS reliably in STAR treatment, to avoid mistargeting and offer standardized cardiac CTV creation workflows.

**Limitations**

The sample size used in this cross-validation study is relatively small with only 10 STAR patient datasets within the RAVENTA framework. The limited number of cases prevented further analyses, such as comparing different mapping systems for registration accuracy or identifying predictors for better agreement. However, the datasets represented a wide range of EAM systems used in clinical practice. Validation studies with larger cohorts such as the STOPSTORM consortium [5], or investigations into inter-observer variation for each approach are warranted.

Although magnetic navigation EAM systems demonstrate high spatial accuracy and electrophysiological studies remain the only modality capable of identifying electrophysiologic substrates, other imaging modalities such as cardiac MRI and CT scans, can also identify potential VT substrates. In this study, relatively recent EAM maps (no older than four weeks) were available for all cases. The CARDIO-RT software used in this study also supports semi-automatic AHA LV segment-based targeting. However, in the RAVENTA study, segment-based targeting was avoided to keep the cardiac CTV small and minimize toxicity risks.

It is important to recognize that EAM-to-cardiac-CT transfer is not the only potential source of targeting errors. Since the cardiac CT needs to be registered with the non-contrast cardiac average planning CT, this registration process may introduce additional errors. However, this registration process is typically supported by extracardiac structures, which generally ensure robust alignment.

Additionally, both the CARDIO-RT and EAMapReader are research tools that have not yet been approved for routine clinical use. However, given the experimental nature of STAR, these tools are particularly suitable for clinical trials.

## 5.4 Chapter Summary

In this chapter, the stand-alone in-house software CARDIO-RT including three VT target registration methods, AHA 17-segment model registration, 3D-3D registration and 2D-3D registration, was assessed as a quality assurance tool and in a cross-validation study. This chapter addressed research questions Q2 and Q3.

The CARDIO-RT VT target registration methods were successfully applied to 5 STAR cases for VT patients in the quality assurance process demonstrating the current diversity of EAM systems (RYTHMIA HDx, CARTO 3 and EnSite) and the range of EAM-treatment planning imaging registration methods employed in the field of STAR. Particularly, the newly developed 2D-3D registration method in the CARDIO-RT software addresses the challenges and limitations of previous 3D-3D EAM mesh data registration methods by eliminating reliance on proprietary vendor-specific data formats exported from different EAM systems. The successful transfer of the EAM to the planning CT using 2D-3D registration enabled a highly accurate definition of the previously identified VT substrates. The search question Q2 was addressed in this section.

Additionally, a cross-validation study between two conceptually different VT target registration approaches, namely the 2D-3D registration method in the CARDIO-RT software and the EAMapReader extension within the 3D Slicer software with the concept of 3D-3D registration, was conducted based on case data for 10 STAR-treated VT patients. These two methods demonstrated good agreement with a DSC value of $0.84 \pm 0.04$, and are thus suitable for VT target transfer, quality assurance and analysis in STAR treatment. Semi-automated software solutions have the potential to minimize operator-dependent errors during cardiac CTV delineation in STAR treatment planning procedure, simplifying and harmonizing the cardiac target volume definition process across clinical studies. The search question Q3 was addressed in this section.

# Chapter 6

# Patient- and Segment-Specific Cardiac Motion Estimation

In the previous chapters, the CARDIO-RT software including conceptually different VT target registration methods for STAR as well as the validations were discussed. Once the cardiac CTV structure is define in the radiation TPS, the cardiac ITV needs to be created, representing the CTV with an additional margin to compensate for a known or estimated range of internal motion during the STAR treatment. This requires detailed knowledge of the dynamic behavior of the heart due to cardiac motion and respiratory motion.

In this chapter, an ECG-gated cardiac CT based patient- and segment-specific cardiac motion estimation method was proposed. This chapter begins with the scientific contributions in section 6.1. Then, the patient data preparation (section 6.2), the CT image registration method (section 6.3), the cardiac motion estimation method (section 6.4) and the statistical analysis method (section 6.5) are introduced. These are followed by the results of estimates of cardiac motion for the cardiac CTV, all 17 LV segments as well as the ICD lead tip, and the accordance of the ICD lead tip motion with the cardiac CTV/LV segment motion in section 6.6. Finally, this chapter ends with a discussion in section 6.7 and a chapter summary in section 6.8. This chapter provides the answer to the research question Q4 mentioned in section 1.1.

## 6.1 Scientific Contributions

In this chapter, a patient- and segment-specific cardiac motion estimation method based on ECG-gated contrast-enhanced breath-hold cardiac CT has been achieved as proof-of-concept, by using an intensity-based non-rigid automatic

Parts of this chapter have been published in [132].

image registration method. In addition, the motion range of the ICD lead tip was also calculated for evaluation of accordance with the cardiac CTV and AHA 17 LV segments motion.

When adequate respiratory motion management strategies, such as gating, DIBH or tracking, are employed, the information on patient- and segment-specific cardiac motion is significantly helpful for estimating an appropriate individualized cardiac ITV margin for STAR. Additionally, the proposed cardiac motion estimation method could help identify VT patients with larger cardiac motion who would particularly benefit from active motion management strategies. These can greatly enhance the accuracy of radiation delivery in STAR treatment for VT. The analysis containing 10 VT patient data of STAR treatment can also provide reference data for cardiac motion of AHA 17 segments of the LV during STAR treatment planning procedure for VT. Compared to previously published cardiac motion analysis methods, this approach requires only contrast-enhanced breath-hold ECG-gated cardiac CT at end-diastolic and end-systolic phases, which are more readily available in clinical practice and has potential for future clinical use.

In addition, this cardiac motion estimation method has been integrated into the CARDIO-RT software as a module. The proposed method in this chapter also holds potential for other medical image modalities such as MRI and ultrasound.

## 6.2 Data Preparation

Case data for 10 VT patients who underwent STAR based on the RAVENTA trial protocol (NCT03867747) [4], [29] either directly within the RAVENTA study in Germany [29] or within harmonized trials in Austria and Israel (national trial number: 202225964) [30] and/or within the STOPSTORM registry [5] was retrospectively analyzed. All patients received a single dose of 25 Gy prescribed to the surrounding isodose surface, ensuring compliance with critical structure constraints as outlined in the RAVENTA trial protocol [29]. Each patient had one CTV, with the exception of two patients who had two CTVs. Detailed patient characteristics are summarized in Table 6.1.

TABLE 6.1: Patient characteristics. Abbreviations: BMI = body mass index; LVEF = left ventricular ejection fraction; CTV = clinical target volume; LV = left ventricle; CT = computed tomography. * Based on the American Heart Association 17-segment model.

| Patient | Age (years) | Sex (m, f) | BMI ($kg/m^2$) | Cardiac condition | LVEF (%) | Catheter ablation history | CTV ($cm^3$) | Targeted (partial) LV segments* | CT pixel spacing (mm) | CT slice thickness (mm) |
|---|---|---|---|---|---|---|---|---|---|---|
| 1 | 70 | m | 23.6 | Ischemic cardiomyopathy | 23 | 1 | 6.7 | 4 | 0.375 | 0.3 |
| 2 | 84 | m | 29.4 | Ischemic cardiomyopathy | 33 | 3 | CTV 1: 11.4; CTV 2: 21.1 | CTV 1: 4, 5 and 11; CTV 2: 1 and 7 | 0.389 | 0.4 |
| 3 | 61 | m | 39.8 | Ischemic cardiomyopathy | 35 | 2 | 42.8 | 1, 2, 7 and 8 | 0.460 | 0.4 |
| 4 | 74 | m | 23.2 | Non-ischemic cardiomyopathy Dilated cardiomyopathy, valvular defect (tricuspid, mitral) | 35 | 0 | 8.3 | 6, 11 and 12 | 0.463 | 0.5 |
| 5 | 62 | m | 28.4 | Dilated cardiomyopathy, valvular defect (mitral), atrial fibrillation | 35 | 3 | 11.5 | 2, 3 and 9 | 0.479 | 1.0 |
| 6 | 61 | m | 26.1 | Dilated cardiomyopathy, valvular defect (tricuspid, mitral) | 46 | 3 | 4.4 | 6 and 12 | 0.461 | 0.5 |
| 7 | 75 | m | 31.0 | Dilated cardiomyopathy | 25 | 5 | 83.3 | 1, 5, 6, 7, 11 and 12 | 0.490 | 0.8 |
| 8 | 72 | m | 33.1 | Ischemic cardiomyopathy | 25-30 | 3 | 31.2 | 5, 6, 11 and 12 | 0.422 | 0.6 |
| 9 | 64 | m | 19.9 | Non-ischemic cardiomyopathy | 32 | 2 | CTV 1: 8.2; CTV 2: 17.6 | CTV 1: 3 and 4; CTV 2: 1 and 6 | 0.336 | 0.3 |
| 10 | 59 | m | 26.5 | Non-ischemic cardiomyopathy | 25 | 2 | 44.4 | 1, 6, 7, 12 | 0.387 | 0.4 |

A contrast-enhanced breath-hold cardiac CT dataset with retrospective ECG gating was acquired, with reconstructions of the end-diastolic and end-systolic phases included as part of the treatment planning for STAR. Cardiac substructures, with special emphasis on LV myocardium and aorta, were contoured on the cardiac CT at the end-diastolic phase in the radiotherapy TPS by experienced senior physicians. In cases where the LV myocardium structure was not available, the TotalSegmentator extension (version 2.4.0) [158], [159] within the open-source 3D Slicer software (version 5.6.2) [91] was used for LV myocardium structure segmentation. The LV myocardium structure was then divided into 17 segments according to the AHA 17-segment model [25], using the in-house software CARDIO-RT [131], [138]. The CTV was predefined based on the electroanatomical maps with geometry created in end-diastole during sinus or slow-paced rhythm as previously described [29]. The contrast-enhanced cardiac CT datasets were in DICOM format, and the cardiac substructures were exported in an RTSS file.

All patients had at least one ICD lead positioned in the RV near LV segment 14, and 5 patients had an additional ICD lead positioned in the right atrium. The tip of the ICD lead in the RV was manually segmented in the cardiac CT at both end-diastolic and end-systolic phases using the 3D Slicer software and exported in an RTSS file. In order to diminish the uncertainty and variability in identifying the exact voxel of the ICD lead tip, the following steps were performed. First, the ICD lead structures in cardiac CT volumes at both end-diastolic and end-systolic phases were manually segmented by growing from seeds and smoothing. Next, in the cardiac CT volumes at the end-diastolic/end-systolic phase, select a voxel at the top of the ICD lead structure, then grow the selected voxel with a margin size of 5.0 mm to obtain a sphere. Afterwards, apply the Boolean logical operator AND between the ICD lead structure and the sphere to obtain the ICD lead tip with a length of 5.0 mm.

## 6.3 Intensity-Based Non-Rigid Automatic Image Registration

The 3D cardiac CT volumes at the end-diastolic and end-systolic phases were registered using the MATLAB intensity-based non-rigid automatic image registration function from the Image Processing Toolbox™ [160], resulting in a 4D

displacement field. For the image registration procedure, the cardiac CT volume at the end-diastolic phase was displaced, while the cardiac CT volume at the end-systolic phase was fixed. The output 4D displacement field contained displacements (unit: pixels) along the $x$-axis (RL), $y$-axis (AP) and $z$-axis (SI). The displacements in millimeters can then be determined based on the CT pixel spacing and slice thickness, and were treated as estimates of cardiac motion of the cardiac substructures within one cardiac cycle. Figure 6.1 illustrates the workflow of the proposed cardiac motion estimation methods in this study. Figure 6.2 shows the motion vectors representing the deformation of a CTV point cloud on the LV at the end-diastolic phase.

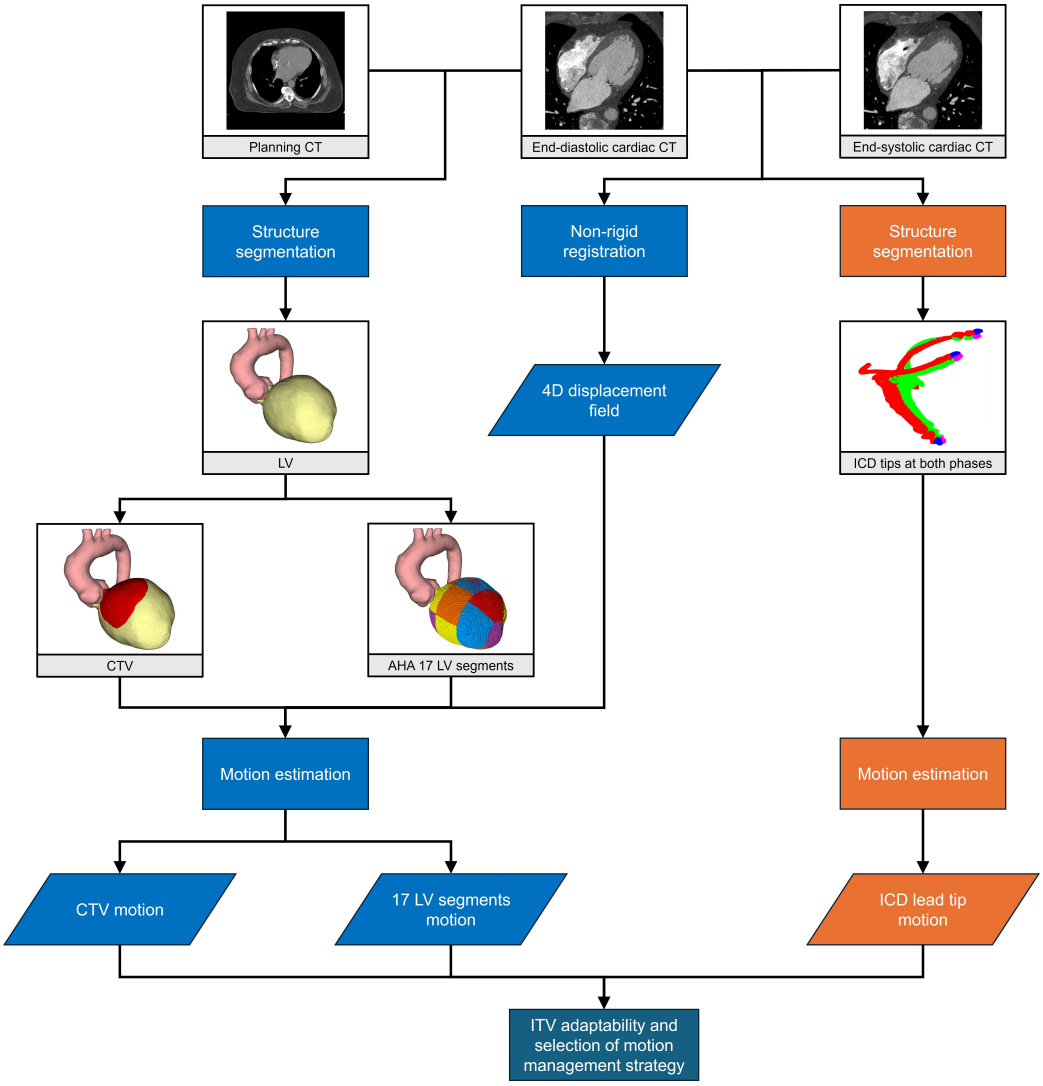


FIGURE 6.1: Diagram of cardiac motion estimation workflow. Processes and data in light blue boxes relate to the cardiac motion of the clinical target volume (CTV) and American Heart Association (AHA) 17 left ventricle (LV) segments, while those in orange relate to implantable cardioverter-defibrillator (ICD) lead tip motion. Abbreviations: CT = computed tomography; ITV = internal target volume.

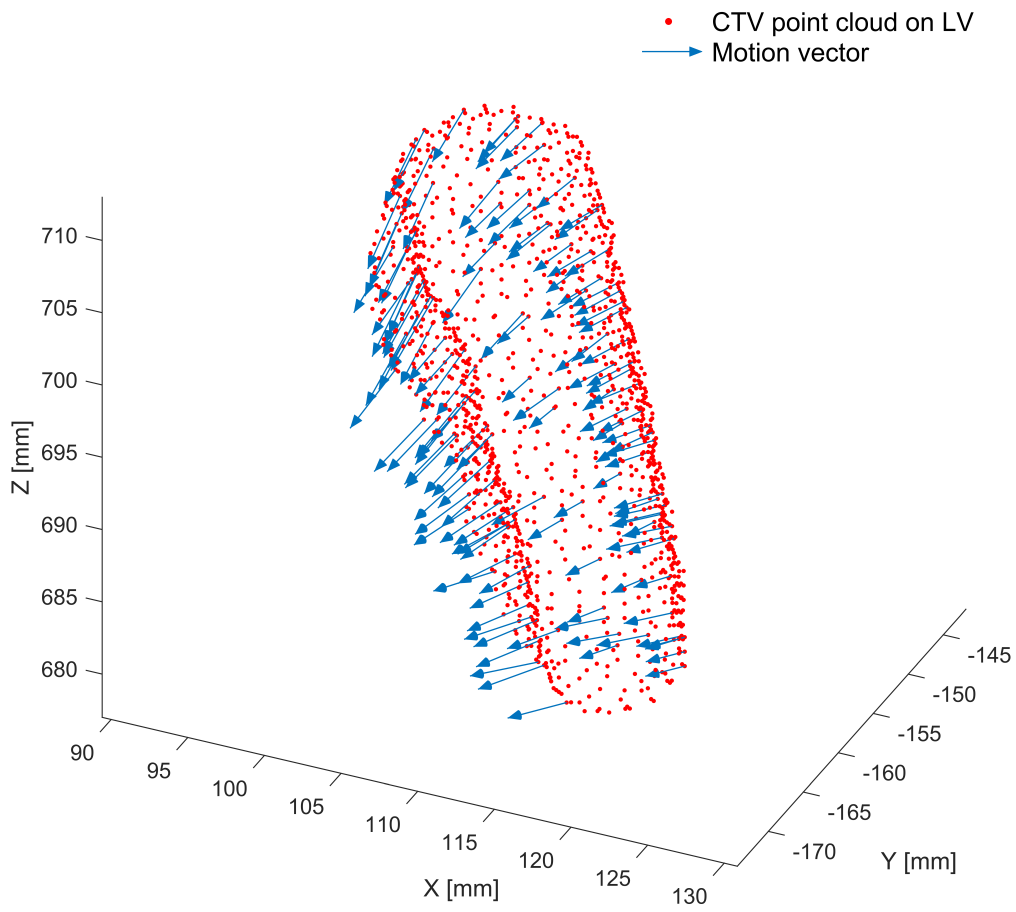


FIGURE 6.2: Motion vectors representing the deformation of a clinical target volume (CTV) point cloud on the left ventricle (LV) at the end-diastolic phase.

Afterwards, the image registration performance was evaluated using the mean squared error (MSE) and Pearson correlation coefficient (PCC) (significance level = 0.05) of the HU for the cardiac CT voxels using MATLAB (version R2022a). A ROI was created in the cardiac CT volumes at both end-diastolic and end-systolic phases which includes the voxels of both the original and displaced LV myocardium structures. The mean squared error (MSE) and PCC ($r$) between the original and displaced ROIs were calculated using the following formulas:

$$\mathrm{MSE} = \frac{1}{N}\sum_{i=1}^{N}\left(I_{\mathrm{original}}(i) - I_{\mathrm{displaced}}(i)\right)^2, \tag{6.1}$$

$$r = \frac{\sum_{i=1}^{N}\left(I_{\mathrm{original}}(i) - \bar{I}_{\mathrm{original}}\right)\left(I_{\mathrm{displaced}}(i) - \bar{I}_{\mathrm{displaced}}\right)}{\sqrt{\sum_{i=1}^{N}\left(I_{\mathrm{original}}(i) - \bar{I}_{\mathrm{original}}\right)^2}\sqrt{\sum_{i=1}^{N}\left(I_{\mathrm{displaced}}(i) - \bar{I}_{\mathrm{displaced}}\right)^2}}, \tag{6.2}$$

where $I_{\text{original}}(i)$ and $I_{\text{displaced}}(i)$ are the intensity values of the $i$-th voxel in the original and displaced ROIs, respectively, $\bar{I}_{\text{original}}$ and $\bar{I}_{\text{displaced}}$ are the mean intensity values of the original and displaced ROIs, and $N$ is the total number of voxels within the ROI.

## 6.4 Estimation of Cardiac Motion

After the image registration procedure, the output 4D displacement field was then applied to the points of the contours of CTV and 17 LV segments, resulting in displaced points of these cardiac substructures. The motion vector of the CoM of the CTV and 17 LV segments from the end-diastolic phase to end-systolic phase was calculated in the right-left (RL), AP, SI and 3D directions.

Given that the motion of the CTV and 17 LV segments is non-rigid due to heart contraction and expansion, the motion of the CoMs within the contoured structures does not fully represent their cardiac motion. Therefore, the motion of each point within the contoured cardiac substructures from the RTSS file was also calculated in the RL, AP, SI and 3D directions. Similarly, since the ICD lead tip can be treated as a rigid object during a cardiac cycle, the CoM motion of the RV ICD lead tip was also calculated for evaluation of accordance with CTV/LV segment motion. For patients with more than one ICD lead in the RV, only the most inferior one (located near LV segment 14) was used for this evaluation.

## 6.5 Statistical Analysis

Statistical analysis was performed using Microsoft Excel (version 2411) and R (version 4.2.1) within the RStudio environment (version 2022.07.2+576). The correlation and significant differences between ICD lead tip motion and CTV motion were assessed using the PCC (significance level = 0.05) and Wilcoxon signed-rank test (significance level = 0.05), while spatial discrepancies with both CTV and LV segment motion were quantified using the Euclidean distance. Values are given as mean ± standard deviation unless noted otherwise.

## 6.6 Motion Estimation Results

### 6.6.1 Evaluation of Image Registration Performance

After the image registration, for the ROI in the cardiac CT volumes, the MSE reduced by 40830 ± 15484 $HU^2$ and the PCC increased from 0.81 ± 0.05 to 0.94 ± 0.02, indicating enhanced similarity between cardiac CT at end-systolic phase and registered cardiac CT at end-diastolic phase.

### 6.6.2 Cardiac Motion Estimation of CTV and 17 Segments

Figure 6.3 presents the cardiac motion of the CoM for individual CTVs and individual CTV points in the RL, AP, SI and 3D directions (detailed numerical data are given in Table 6.2). Comparing cardiac motion of the CoM for the individual CTV with the mean value of the individual CTV points, the difference was 0.3 ± 0.2 mm. The absolute cardiac motion for the CoM was 1.7 ± 1.4 mm in the RL direction, 2.2 ± 1.0 mm in the AP direction, 1.4 ± 1.1 mm in the SI direction, and 3.4 ± 1.4 mm in 3D. Of the 12 CTVs (CoM), 10 exhibited cardiac motion < 5 mm in 3D.

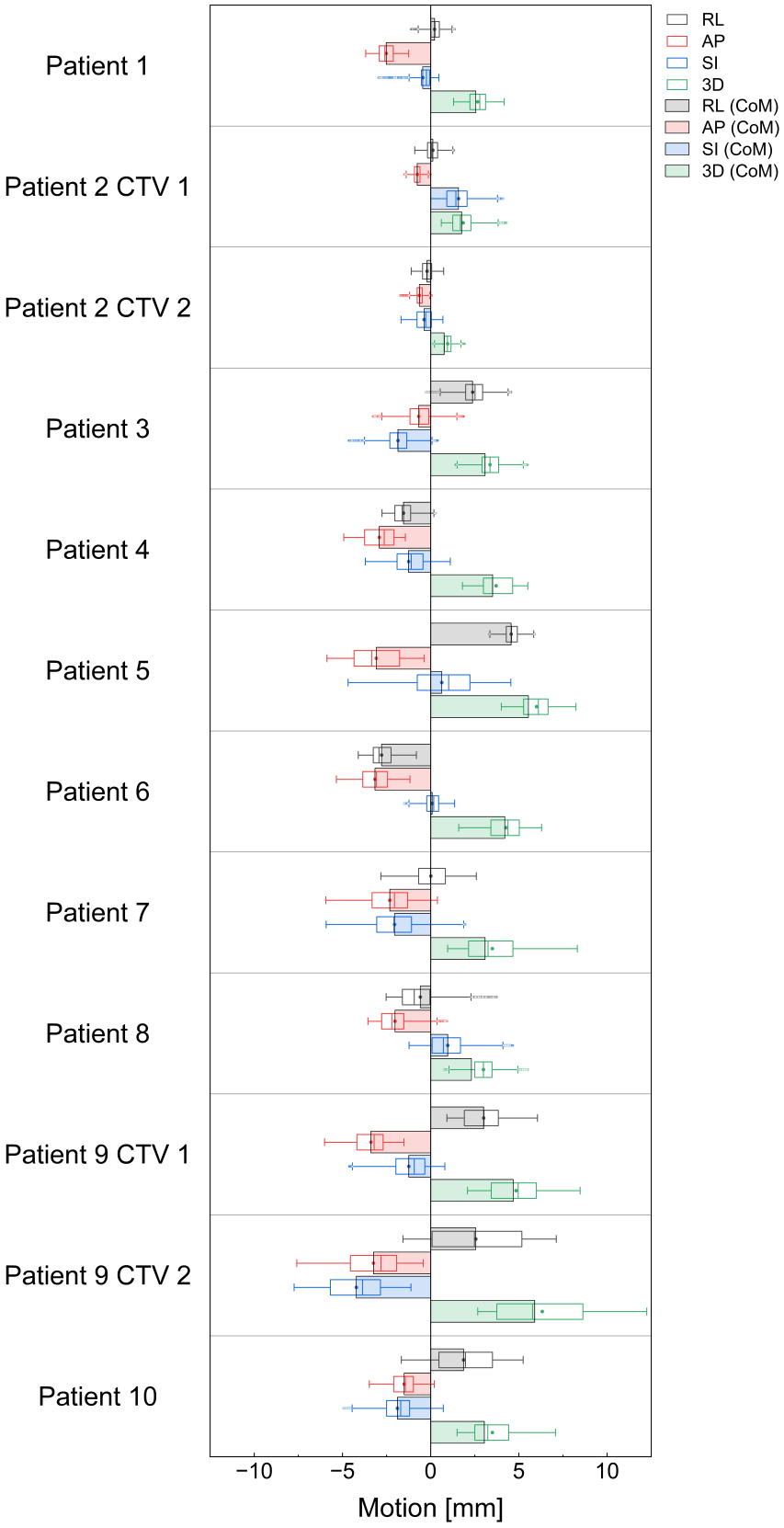


FIGURE 6.3: Cardiac motion of the center of mass (CoM) for individual clinical target volumes (CTVs, bar chart) and individual CTV points (box chart) in the right-left (RL), anterior-posterior (AP), superior-inferior (SI) and 3D directions. Each patient had one CTV, with the exception of patients 2 and 9 with two CTVs. Mean values are shown as dots in the box chart. For the cardiac motion of individual CTV points, the mean and median values are similar and comparable.

Regarding the points of the CTVs, the mean cardiac motion in 3D was < 5 mm in 11 out of 12 CTVs; the cardiac motion of CTV 2 from patient 9 was considerably larger, with a mean value of 6.6 mm.

Among the 10 patients, cardiac motion across the 17 LV segments was < 5 mm in the RL, AP and SI directions, with the exception of patient 5 (segment 4 in the AP direction, segment 6 in the SI direction) and patient 9 (segment 2 in the AP direction, segment 1 in the SI direction). In 3D, cardiac motion of most of the segments was < 5 mm, except patient 4 (segments 3 and 9), patient 5 (segments 1, 2, 4, 5 and 6) and patient 9 (segments 1, 2 and 3; see Figure 6.4). The maximum motion per patient was observed in basal (segments 1, 3, 5 and 6) and mid-cavity (segments 8, 9 and 10) regions of the LV.

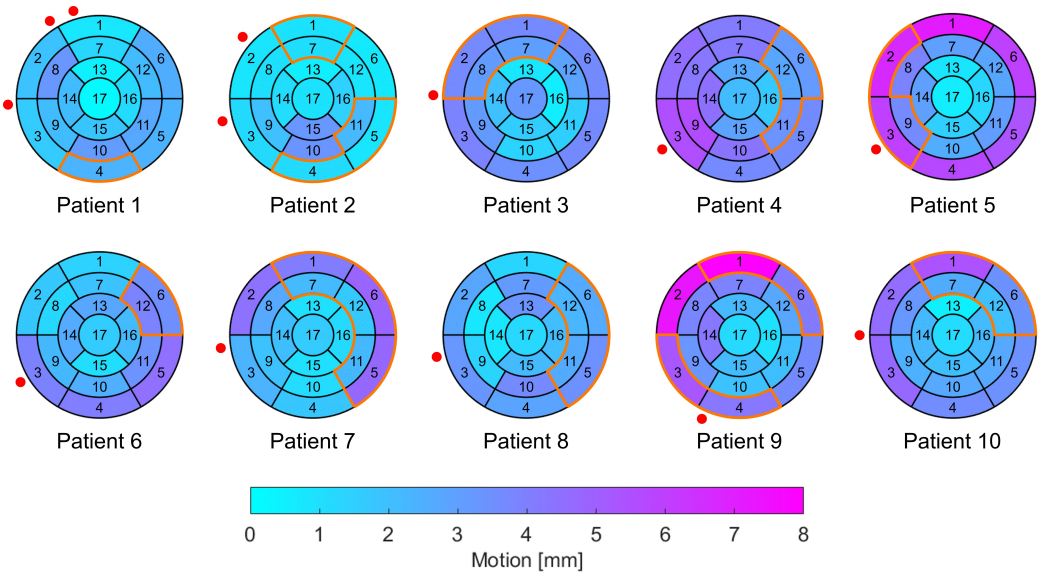


FIGURE 6.4: Cardiac motion of the center of mass for the American Heart Association 17 segments of the left ventricle in 3D on 17-segment bull's-eye maps with the locations of the clinical target volumes (CTVs, orange borders) and implantable cardioverter-defibrillator lead tips (red dots) for each patient. Each patient had one CTV, with the exception of patients 2 and 9 with two CTVs. CTVs are numbered in ascending order from inferior to superior in the manuscript.

### 6.6.3 ICD Lead Tip Motion Estimation and Its Accordance with Cardiac Motion

The motion of the RV ICD lead tips (located near segment 14) in the RL, AP, SI and 3D directions for the 10 patients can be found in Table 6.2. The absolute motion of the ICD lead tips was 3.5 ± 2.8 mm in the RL direction, 1.5 ± 1.2 mm in the AP direction, 1.9 ± 1.2 mm in the SI direction and 4.9 ± 2.2 mm in 3D. Comparing the ICD lead tip motion and CTV motion (CoM), the PCC values showed

TABLE 6.2: Cardiac motion of the clinical target volume (CTV) points and the center of mass (CoM) for each patient. Positive values indicate motion in the left, posterior, and superior directions, while negative values indicate motion in the right, anterior, and inferior directions. Abbreviations: RL = right-left; AP = anterior-posterior; SI = superior-inferior.

| CTV | Direction | Min (mm) | Max (mm) | Mean (mm) | Median (mm) | CoM motion (mm) | ICD lead tip motion (mm) |
|---|---|---|---|---|---|---|---|
| Patient 1 | RL | -1.1 | 1.4 | 0.2 | 0.2 | 0.2 | 0.7 |
| | AP | -3.7 | -1.2 | -2.5 | -2.6 | -2.5 | 2.7 |
| | SI | -3.0 | 0.5 | -0.4 | -0.2 | -0.4 | 0.1 |
| | 3D | 1.3 | 4.2 | 2.7 | 2.8 | 2.6 | 2.7 |
| Patient 2 CTV 1 | RL | -0.9 | 1.3 | 0.1 | 0.1 | 0.1 | 0.0 |
| | AP | -1.5 | 0.0 | -0.8 | -0.8 | -0.8 | 0.9 |
| | SI | 0.0 | 4.1 | 1.6 | 1.4 | 1.6 | 1.1 |
| | 3D | 0.6 | 4.3 | 1.9 | 1.7 | 1.8 | 1.4 |
| Patient 2 CTV 2 | RL | -1.1 | 0.7 | -0.2 | -0.2 | -0.2 | 0.0 |
| | AP | -1.7 | 0.1 | -0.6 | -0.6 | -0.6 | 0.9 |
| | SI | -1.7 | 0.7 | -0.4 | -0.3 | -0.4 | 1.1 |
| | 3D | 0.1 | 1.9 | 1.0 | 0.9 | 0.8 | 1.4 |
| Patient 3 | RL | -0.3 | 4.6 | 2.4 | 2.5 | 2.4 | 3.6 |
| | AP | -3.3 | 1.9 | -0.7 | -0.7 | -0.7 | 0.5 |
| | SI | -4.6 | 0.4 | -1.8 | -1.9 | 1.8 | -2.6 |
| | 3D | 1.4 | 6.0 | 3.4 | 3.4 | 3.1 | 4.4 |
| Patient 4 | RL | -2.8 | 0.3 | -1.5 | -1.6 | -1.5 | 5.5 |
| | AP | -4.9 | -1.4 | -2.9 | -2.6 | -2.9 | -2.7 |
| | SI | -3.7 | 1.1 | -1.2 | -1.1 | -1.2 | 3.3 |
| | 3D | 1.8 | 5.5 | 3.7 | 3.5 | 3.5 | 7.0 |
| Patient 5 | RL | 3.3 | 5.9 | 4.6 | 4.6 | 4.6 | 5.8 |
| | AP | -5.9 | -0.4 | -3.1 | -3.3 | -3.1 | 1.8 |
| | SI | -4.7 | 4.5 | 0.6 | 1.0 | 0.6 | 0.2 |
| | 3D | 4.0 | 8.2 | 6.0 | 6.1 | 5.5 | 6.1 |
| Patient 6 | RL | -4.1 | -0.8 | -2.8 | -2.9 | -2.8 | 3.0 |
| | AP | -5.3 | -1.2 | -3.2 | -3.1 | -3.2 | 1.2 |
| | SI | -1.5 | 1.4 | 0.1 | 0.2 | 0.1 | -4.1 |
| | 3D | 1.6 | 6.3 | 4.3 | 4.4 | 4.2 | 5.3 |
| Patient 7 | RL | -2.8 | 2.6 | 0.0 | 0.0 | 0.0 | 0.2 |
| | AP | -5.9 | 0.4 | -2.3 | -2.0 | -2.3 | 3.9 |
| | SI | -5.9 | 2.0 | -2.0 | -2.1 | -2.0 | -2.1 |
| | 3D | 1.0 | 8.3 | 3.5 | 3.3 | 3.1 | 4.4 |
| Patient 8 | RL | -2.5 | 3.8 | -0.6 | -0.9 | -0.6 | 0.8 |
| | AP | -3.6 | 0.9 | -2.0 | -2.2 | -2.0 | 0.0 |
| | SI | -1.2 | 4.7 | 1.0 | 0.7 | 1.0 | -1.6 |
| | 3D | 0.7 | 5.5 | 3.0 | 3.0 | 2.3 | 1.8 |
| Patient 9 CTV 1 | RL | 0.9 | 6.1 | 3.0 | 3.0 | 3.0 | 8.1 |
| | AP | -6.0 | -1.5 | -3.4 | -3.2 | -3.4 | 0.0 |
| | SI | -4.6 | 0.8 | -1.2 | -0.9 | -1.2 | 2.6 |
| | 3D | 2.1 | 8.5 | 4.8 | 5.0 | 4.7 | 8.5 |
| Patient 9 CTV 2 | RL | -1.6 | 7.1 | 2.6 | 2.5 | 2.6 | 8.1 |
| | AP | -7.6 | -0.4 | -3.2 | -2.8 | -3.2 | 0.0 |
| | SI | -7.7 | -1.1 | -4.2 | -3.9 | -4.2 | 2.6 |
| | 3D | 2.7 | 12.2 | 6.3 | 5.8 | 5.9 | 8.5 |
| Patient 10 | RL | -1.7 | 5.2 | 1.9 | 2.0 | 1.9 | 6.9 |
| | AP | -3.5 | 0.2 | -1.5 | -1.4 | -1.5 | 1.2 |
| | SI | -4.9 | 0.7 | -1.9 | -1.7 | -1.9 | -1.0 |
| | 3D | 1.5 | 7.1 | 3.5 | 3.2 | 3.0 | 7.0 |

moderate positive correlation in the RL direction (0.56), weak positive correlation in the AP direction (0.10), weak negative correlation in the SI direction (-0.20) and strong positive correlation in 3D (0.84). Statistically significant differences in motion between the ICD lead tip and CTV (CoM) were observed in the RL, AP and 3D directions, with p-values of 0.001, 0.000 and 0.005, respectively. However, no significant difference was found in the SI direction (p-value = 0.470). The Euclidean distances between ICD lead tip motion and CTV (CoM) motion in the RL, AP, SI and 3D directions were 13.0 mm, 12.1 mm, 10.5 mm and 7.4 mm, respectively. In the 3 cases with ICD lead tip motion > 7.0 mm, the motion difference to the CTV (> 2.0 mm) was greater than in cases with ICD lead tip motion < 7.0 mm.

The Euclidean distance between ICD lead tip motion and 17 LV segments motion in the RL, AP, SI and 3D directions are shown on the 17-segment bull's-eye maps in Figure 6.5. The Euclidean distances between the ICD lead tip motion and 17 LV segments motion were 12.0 ± 3.4 mm, 9.2 ± 2.9 mm, 8.2 ± 1.9 mm and 9.1 ± 2.6 mm in the RL, AP, SI and 3D directions, respectively. In 3D, the smallest Euclidean distance was observed in segment 3, while the largest occurred in segment 17.

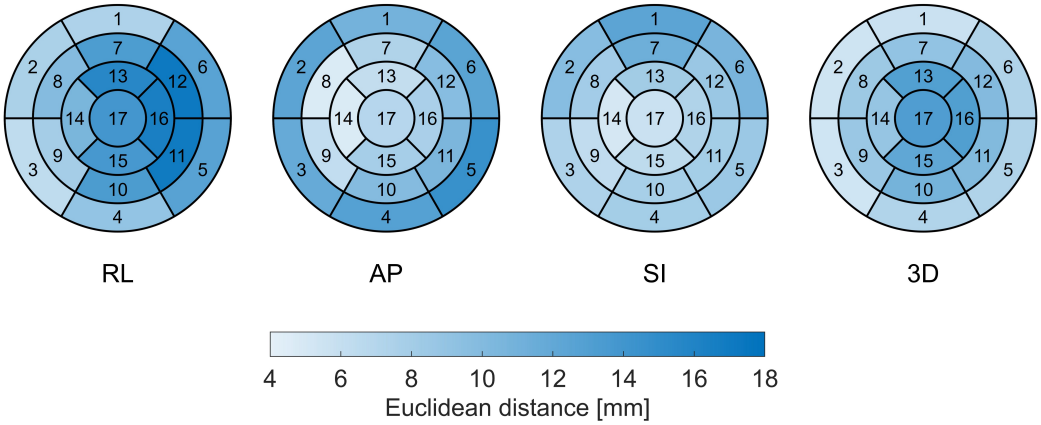


FIGURE 6.5: Euclidean distances between implantable cardioverter-defibrillator (ICD) lead tip motion and American Heart Association (AHA) 17 left ventricle segments motion in the right-left (RL), anterior-posterior (AP), superior-inferior (SI) and 3D directions, displayed on AHA 17-segment bull's-eye maps.

## 6.7 Discussion

In this chapter, a patient- and segment-specific cardiac motion estimation method based on ECG-gated contrast-enhanced breath-hold cardiac CT has been achieved as proof-of-concept, by using an intensity-based non-rigid automatic image registration method. In addition, the motion range of the ICD lead tip

was also calculated for evaluation of accordance with the cardiac CTV and AHA 17 LV segments motion. This analysis provides reference data on patient- and segment-specific cardiac motion for STAR treatment planning in VT patients.

It is demonstrated that the CTVs (CoM) moved 3.4 ± 1.4 mm, and 10 out of 12 CTVs exhibiting < 5 mm cardiac motion in 3D. Cardiac CTs were acquired during end-inspiratory breath-hold so that the results present an approximation to cardiac motion without respiratory motion. Similarly, Ouyang *et al.* [116] investigated the motion range of the centroids of the LV, RV, ascending aorta, ostia of the right coronary artery, left coronary artery and left anterior descending artery using breath-hold cardiac gated CT of 10 patients who underwent transcatheter aortic valve replacement, and reported that more than 90% of the measured displacements were < 5 mm. In another study conducted by Petzl *et al.* [118], vectorial motion data from the ablation catheter was used to calculate the heart rate and segment each trace to isolate the cardiac contribution to cardiorespiratory motion, and an average cardiac excursion of 1.62 ± 1.21 mm was reported. Li *et al.* [117] analyzed the geometric centroid of the substrate target of 12 patients with refractory arrhythmia treated by STAR, using 4D cardiac CT and 4D CT with a deformation vector field. In their study, the mean maximum displacement of the substrate target in 3D due to cardiac pulsation was 5.2 mm (range: 2.6-8.0 mm). There was a recent study that measured the displacement of transvenous right atrial appendage, RV ICD, coronary sinus lead tips and prosthetic cardiac devices across the cardiac cycle from breath-hold 4D cardiac CT in 31 patients who underwent catheter ablation procedure for atrial or ventricular arrhythmias [121]. In that study, there was considerable variation in cardiac contractile motion among the patients, ranging from 1 to 15 mm. Cardiac motion of the CTV (CoM) in this study generally fell within this range, except for a slightly smaller minimum value.

While the CoM motion of the CTV represents an averaged value, the motion of individual CTV points provides complementary cardiac motion information. The comparison of the cardiac motion of the CoM for individual CTVs with the mean value of the individual CTV points suggested that cardiac motion was relatively uniform and centralized across the CTV point cloud in these individual 10 patients, indicating coherent movement with no substantial deviations in different regions of a specific CTV. Therefore, CTV motion (CoM) can serve as an estimate of cardiac motion estimation, except when the CTV moves in a significant regional inhomogeneous manner.

In the radiosurgery platform CyberKnife (Accuray, Inc., Sunnyvale, California, USA), the tip of the ICD lead is used as a tracking marker for motion management during STAR for VT [1], [155], [156], [161]. In this analysis, the motion of the RV ICD lead tip was 4.9 ± 2.2 mm, which is smaller than the cardiac contractile motion observed in the study by Wu *et al.* [121] (8.6 ± 3.5 mm). For 7/10 patients, the motion difference between RV ICD lead tip (located near segment 14) and CTV in 3D was $\leq$ 2 mm. In these 7 cases, the ICD lead tracking technique appears to be sufficient as a reference for the cardiac motion of the CTV. It was observed that as the motion of the ICD lead tip increased, the difference in motion increased accordingly, making it less reliable to use ICD lead tracking as a reference for cardiac motion estimation. A lower value of the Euclidean distance between ICD lead tip motion and 17 LV segments motion indicates that the motion pattern of the specific segment is relatively more aligned with the ICD lead tip motion. In these 10 patients, the Euclidean distances were generally axisymmetric on the AHA 17-segment model bull's-eye maps (see Figure 6.5). Overall, they decreased from the apical segments to the mid-cavity and basal segments in the RL and 3D directions, while they increased from the apical segments to the mid-cavity and basal segments in the AP and SI directions. In those LV segments with lower Euclidean distances, ICD lead tracking seems to be an adequate surrogate for estimating cardiac motion during STAR. Segments 13 and 15-17 showed the highest Euclidean distances, suggesting their motion was least correlated with the ICD lead tip motion. For the 10 patients, segments 1-9 and 14 are more suitable for ICD lead tracking.

Overall, cardiac motion of the CTV and 17 LV segments showed asymmetry, similar to previously published studies [162]–[164]. It exhibited considerable individual variability in both the CTV and the 17 LV segments in 10 patients, which is consistent with the STOPSTORM.eu consortium review [26]. When adequate respiratory motion management strategies, such as gating, DIBH or tracking, are employed, the information on patient- and segment-specific cardiac motion is very helpful for creating an appropriate individualized cardiac ITV margin for STAR. Additionally, the proposed motion estimation method could help identify VT patients with larger cardiac motion who would particularly benefit from active motion management strategies [27], [28]. This can greatly enhance the accuracy of radiation delivery in STAR treatment for VT. Compared to previously published cardiac motion analysis methods, the method proposed in this study requires only contrast-enhanced breath-hold ECG-gated cardiac CT at end-diastolic and end-systolic phases, which are more readily available in clinical

practice and has potential for future clinical use. In addition, this cardiac motion estimation method has been integrated into the CARDIO-RT software as a module, and it holds potential for other medical image modalities such as MRI and ultrasound data.

As of the writing of this dissertation, to the best of the author's knowledge, no commercially available solutions or quality assurance tools currently exist for heart motion management in STAR for VT. Advancing technology in this area would help standardize and refine these procedures while enhancing patient safety. Moreover, since cardiac motion can significantly affect the accuracy of radiation delivery, its dosimetric impact is crucial and needs further investigation.

**Limitations**

This study has several limitations. The number of patients included in this study was relatively small with only 10 datasets as this study was aiming for proof-of-concept. A larger sample size of VT patients with a broader spectrum of patient characteristics (e.g., the location of CTV) would be beneficial for evaluating the performance of cardiac motion estimation methods and further investigate the accordance between ICD lead tip motion and CTV/17 LV segments motion. The contrast-enhanced breath-hold ECG-gated cardiac CT used in this study included only cardiac motion and did not account for respiratory motion. Including free-breathing 4D CT in the future would allow for a more comprehensive estimation of both cardiac and respiratory motion of the cardiac substructures, and the proposed method could be utilized in such cardiorespiratory motion studies. Additionally, the voxel-wise CT image registration in this study relies on precise CTV definition and LV myocardium contouring for accurate cardiac motion estimation. The use of an auto-contouring tool specifically tailored for STAR [165] could significantly improve motion estimation outcomes. Moreover, the patients in this study had VT and a lower left ventricular ejection fraction (LVEF), so the observed cardiac motion may not be applicable to patients with a higher LVEF.

## 6.8 Chapter Summary

In this chapter, an ECG-gated cardiac CT based patient- and segment-specific cardiac motion estimation method in STAR for VT was demonstrated to address research question Q4.

The intensity-based non-rigid automatic image registration method was employed to register the 3D ECG-gated contrast-enhanced breath-hold cardiac CT volumes at end-diastolic and end-systolic phases to acquire the 4D displacement field, which was then applied to the cardiac CTV and 17 LV segments obtained using the CARDIO-RT 17-segment model registration method for motion analysis. Meanwhile, the ICD lead tip was also manually segmented at both phases to analyze its motion and the accordance of its motion with the cardiac CTV/LV segment motion.

The estimated cardiac motion showed considerable individual variability in the CTV and 17 LV segments among 10 different patients. The results show that the cardiac CTVs (CoM) moved 3.4 ± 1.4 mm, and the motion of the ICD lead tips was 4.9 ± 2.2 mm in 3D. The maximum motion per patient was observed in basal (segments 1, 3, 5 and 6) and mid-cavity (segments 8, 9 and 10) regions of the LV. Acquiring information on patient- and segment-specific cardiac motion is highly recommended for creating an appropriate individualized cardiac ITV margin and for selecting motion management strategy in STAR. The proposed cardiac motion estimation method could enhance STAR accuracy and has potential for future clinical applications in STAR. The impact of cardiac motion on the dosimetry needs further investigation.

# Chapter 7

# Conclusion

In this chapter, a summary of all topics addressed in this dissertation is presented. Then, the research questions from section 1.1 are discussed, and future work is proposed.

## 7.1 Summary

In this dissertation, the software CARDIO-RT was developed to transfer the VT target structure, defined by the treatment team in the EAM system, to the radiation TPS using three practical methods: the AHA 17-segment model registration, 3D-3D registration and 2D-3D registration. The software was validated as a quality assurance tool using 5 real-world VT patient datasets within the RAVENTA trial. A cross-validation study comparing the 2D-3D registration method and the 3D-3D registration method from the 3D Slicer extension EAMapReader was conducted, demonstrating high agreement. Furthermore, an ECG-gated cardiac CT based patient- and segment-specific cardiac motion estimation method was proposed to provide reference data for the creation of a personalized cardiac ITV margin and the selection of VT patients who would particularly benefit from active motion management strategies in STAR.

In detail, Chapter 4 demonstrates the workflows of the three VT target registration methods. For the AHA 17-segment model registration, the LV myocardium structure is divided into 17 sections according to the AHA 17-segment model. LV segment(s) of interest can then be visualized on the treatment planning CT, enabling the clinicians to assess the targeted LV segment(s). The 3D-3D registration method currently supports RHYTHMIA HDx, CARTO 3 and EnSite EAM systems. It transfers the 3D VT ablation points exported from the EAM system to the 3D LV contours with respect to the treatment planning imaging data. The 2D-3D registration method is a versatile approach that supports any EAM system

and enables the transfer of the VT target region marked on the 2D EAM screenshots in standard anatomical views to the 3D VT contours with respect to the treatment planning imaging data. Additionally, the 2D-3D registration method has potential for applications in other radiotherapy treatments within the human body where the target is identifiable using 2D imaging data. These three proposed VT target registration methods are semi-automatic rather than fully automatic due to strict accuracy requirements in clinical applications. Automatic registration methods may not be sufficiently reliable, as the LV structures are derived from different modalities, which can introduce inaccuracies and data incompleteness, making them unsuitable for clinical use. In contrast, the proposed semi-automatic registration methods have demonstrated practical feasibility on real-world STAR datasets. They provide the necessary flexibility, allowing clinicians to refine the registration process based on their expertise and the specific characteristics of each STAR case, ensuring both accuracy and clinical applicability. In addition, the significance of aorta mapping in the EAM systems for the 2D-3D registration method was presented, and three additional functions were demonstrated: (1) visualization of the cardiac PTV and dose calculation as isodose lines for quality assurance purposes, (2) registration between cardiac CT and planning CT, and (3) generation of transmural VT target structure.

In Chapter 5, as a clinical validation, the CARDIO-RT software was successfully applied to 5 STAR cases for VT patients as a quality assurance tool, demonstrating the current diversity of EAM systems (RYTHMIA HDx, CARTO 3, and EnSite) and the range of EAM-treatment planning imaging registration methods used in the field of STAR. Particularly, the newly developed registration method in the CARDIO-RT software, based on the novel concept of 2D-3D registration, addresses the challenges and limitations of earlier 3D-3D EAM mesh data registration methods by eliminating reliance on proprietary vendor-specific data formats exported from different EAM systems. The successful transfer of the EAM to the planning CT using 2D-3D registration enabled a highly accurate definition of the previously identified VT substrates. Furthermore, the conformity between the CARDIO-RT 2D-3D registration and the 3D Slicer extension EAMapReader was analyzed through a multi-center cross-validation study. These two VT registration methods demonstrated good agreement with a DSC value of $0.84 \pm 0.04$. Both techniques are thus suitable for VT target transfer, quality assurance and analysis in STAR treatment. Semi-automated software solutions have the potential to minimize operator-dependent errors during cardiac CTV delineation in STAR treatment planning procedure, simplifying and harmonizing the cardiac

target volume definition process across clinical studies.

In Chapter 6, the need for acquiring information on cardiac motion for cardiac ITV margin creation and VT patient selection for active motion management strategies was addressed. An ECG-gated cardiac CT based patient- and segment-specific cardiac motion estimation using an intensity-based non-rigid automatic image registration method was proposed, and was performed on 10 real-world VT patient datasets to estimate the cardiac motion of the previously defined CTV as well as 17 LV segments. The accordance of the ICD lead tip motion with the CTV and 17 segments motion was also investigated.

## 7.2 Conclusion on the Research Questions

In this section, the research questions defined in section 1.1 are answered.

**Q1: What are the practical methods for registering a VT target structure from the EAM system to radiation TPS for STAR? Is there a versatile VT target registration method applicable to all EAM systems?**
In this work, a software including three practical semi-automatic registration methods, namely the AHA 17-segment model registration, 3D-3D registration and 2D-3D registration, was developed to transfer the VT target defined in the EAM system to the radiation treatment planning CT for STAR (see Chapter 4). For the AHA 17-segment model registration, the LV myocardium structure contoured from contrast-enhanced CT is divided into 17 segments according to the AHA 17-segment model. Therefore, once the cardiac electrophysiologist has defined the targeted AHA LV segment(s) of the VT region, the targeted LV segment(s) can be visualized on CT slices for assessment. The 3D-3D registration method reads the EAM raw data in vendor-specific formats and registers the 3D EAM points of the LV and aorta (optional) with the corresponding 3D CT contours to transfer the catheter ablation points to the treatment planning CT. This method currently supports three commonly used EAM systems in clinical practice: RHYTHMIA HDx, CARTO 3 and EnSite. The 2D-3D registration method enables the transfer of the VT target region, marked on the 2D EAM screenshots in standard anatomical views, to the 3D LV contours with respect to the treatment planning imaging data. Since different EAM system vendors use proprietary export data formats, and different versions of the same EAM system may have varying data structures in export files, specific scripts are required to read raw data from a given EAM

system version for the 3D-3D VT target registration. The proposed 2D-3D registration method is versatile and applicable to different EAM systems, regardless of version or potential future changes.

**Q2: Is it possible to employ the VT target registration methods in the quality assurance process for STAR?**
Yes, in section 5.2, the software including three practical VT target registration methods that is specifically dedicated to additional quality assurance of the target transfer process from EAM systems to radiation TPS, was validated for 5 patient cases within the multi-center multi-platform RAVENTA trial. The semi-automated EAM-treatment planning imaging data registration enables quality assurance of the manually transferred cardiac CTV structure, reducing clinician-dependent inconsistencies and enhancing the safety and robustness of the VT target registration. This approach facilitates standardized STAR treatment planning processes that are less dependent on the expertise of the treating center. Additionally, this software may furthermore be used to obtain a detailed statistical analysis of previously performed STAR treatments, allowing retrospective assessments of VT target transfer accuracy and dose-response analyses. Retrospective findings of incorrectly transferred VT target could potentially help explain VT recurrence.

**Q3: Is it possible to assess the accuracy of the VT target registration methods used for STAR in the absence of ground truth?**
The answer is yes. Currently, there is a lack of ground truth for the registered VT target structure in the treatment planning CT, as manual target transfer is prone to significant inter-observer variation and thus unsuitable as a ground truth. Therefore, a cross-validation study between two conceptually different in-house developed software solutions (the CARDIO-RT 2D-3D registration and the 3D-3D registration from the 3D Slicer extension EAMapReader) for target transfer quality assurance in STAR using clinical data was conducted in section 5.3. By comparing the registered cardiac CTVs' characteristics for overlap and similarity, these two methods showed high conformity with a DSC value of $0.84 \pm 0.04$. Therefore, both VT target registration methods can be used for VT target transfer, quality assurance and analysis for STAR.

**Q4: Is it possible to estimate the cardiac motion of the cardiac CTV and substructures based on ECG-gated contrast-enhanced breath-hold CT?**

The answer to this research question is yes. In Chapter 6, an intensity-based non-rigid automatic image registration was used to achieve a patient- and segment-specific cardiac motion estimation method for the cardiac CTV and substructures based on ECG-gated contrast-enhanced breath-hold CT. The estimated cardiac motion showed considerable individual variability in the CTV and 17 LV segments among 10 different patients. The results show that the cardiac CTVs (CoM) moved 3.4 ± 1.4 mm, and the motion of the ICD lead tips was 4.9 ± 2.2 mm in 3D. Therefore, acquiring information on patient- and segment-specific cardiac motion is highly recommended for creating an appropriate individualized cardiac ITV margin and for selecting motion management strategy in STAR. Additionally, this analysis provides reference data on patient- and segment-specific cardiac motion for STAR treatment planning in VT patients. The proposed cardiac motion estimation method could enhance STAR accuracy and has potential for future clinical applications in STAR.

## 7.3 Future Work

In the future, it will be beneficial to validate the proposed practical VT target registration methods on a larger number of VT patient datasets prospectively and retrospectively. This will enhance its robustness and resolve the potential bugs. For the proposed patient- and segment-specific cardiac motion estimation method, a larger, more diverse VT patient sample would better evaluate the performance of this method and would help further investigating the accordance between ICD lead tip motion and the CTV/17 segments motion. Additionally, the 2D-3D registration method has the potential for application in other radiotherapy treatments within the human body.

As a quality assurance tool, the conformity between the registered VT target structure and the isodose lines from the DICOM dose calculation file or the cardiac PTV structure can be quantified and visualized in the GUI of the CARDIO-RT software in the future.

Additionally, since currently there is no ground truth for the registered VT target, cross-validating the target registration methods in the CARDIO-RT software with other VT target registration solutions would help evaluate the effectiveness. Additionally, the accuracy of the proposed VT target registration methods can further be assessed on a dynamic cardiac phantom [142], where a ground truth for the transferred VT target on the synthetic LV structure can be defined.

Recently, assessing the impact of cardiac motion on radiation dosimetry in patients with refractory VT is an ongoing topic [21], [117], [166]. This area also requires further investigation to achieve a comprehensive understanding of motion management strategies for STAR.

# Appendix A

# Ethics Approval

The RAdiosurgery for VENtricular TAchycardia (RAVENTA) trial (NCT03867747) was approved by the German Radiation Protection Agency (Bundesamt für Strahlenschutz, reference number Z5-22463/2-2018-054) and by the leading independent ethics committee of the Christian-Albrechts-University of Kiel (reference number D555/18) as well as by the respective independent ethics committees of the participating centers. All treated patients gave their written informed consent for participation in the study and hence for publication of their anonymized data. The corresponding ethics approval documents for the RAVENTA trial are provided on the following pages.

**MEDIZINISCHE FAKULTÄT**
**DER CHRISTIAN-ALBRECHTS-UNIVERSITÄT ZU KIEL**

ETHIK-KOMMISSION

A.D. 1665

Universitäts-Kinderklinik · Schwanenweg 20 · 24105 Kiel

Dr. Oliver Blanck
UKSH Schleswig-Holstein, Campus Kiel
Klinik für Strahlentherapie
Arnold-Heller-Straße 3, Haus 50
24105 Kiel

Postadresse:
Arnold-Heller-Straße 3 / Haus 9
D-24105 Kiel

Telefon 04 31 / 500-14 191
Telefax 04 31 / 500-14 195
ethikkomm@email.uni-kiel.de

Datum: 04. Februar 2019

cc.: E-Mail: oliver.blanck@uksh.de; hendrik.bonnemeier@uksh.de

| | |
|---|---|
| **AZ.:** | **D 555/18** (bitte stets angeben) |
| **Studienplan:** | **Radiochirurgie zur Behandlung therapierefraktärer ventrikulärer Extrasystolen und Tachykardien (RAVENTA)**<br>Anschreiben v. 15.10.18; Basisformular für einen Ethikantrag vom 15.10.18; Studienprotokoll V1.0 v. 12.10.18; Patienteninformation und Einwilligungserklärung V1.0 v. 12.10.18 |
| **Antragsteller:** | **Dr. Oliver Blanck, Klinik für Strahlentherapie, UKSH Kiel** |
| **Studienleiter:** | **Prof. Dr. Hendrik Bonnemeier, Klinik für Innere Medizin III,**<br>**Prof. Dr. Jürgen Dunst, Klinik für Strahlentherapie**<br>**UKSH, Campus Kiel** |
| **In Kooperation:** | **Klinik für Innere Medizin III (Kardiologie/Angiologie)**<br>**Abteilung für Elektrophysiologie und Rhythmologie, UKSH Kiel** |
| **Antrag vom:** | **15. Oktober 2018 (Eingang: 24. Oktober 2018)** |
| **Überarbeitung:** | **21. Januar 2019 (Eingang: 28. Januar 2019)**<br>Anschreiben und Stellungnahme v. 21.01.19; Basisformular für einen Ethikantrag ohne Unterschriften; Studienprotokoll V1.2 v. 21.01.19 incl. Unterschriften; Patienteninformation und Einwilligungserklärung V1.2 v. 21.01.19; CRF V1.2 v. 21.01.19 |

Sehr geehrter Herr Dr. Blanck,

die Ethik-Kommission der Medizinischen Fakultät der Christian-Albrechts-Universität zu Kiel hat die zu dem obengenannten Antrag eingereichten Unterlagen gemäß § 15 Berufsordnung (BO) der Ärztekammer Schleswig-Holstein beraten. Die Studie unterliegt dem Medizinproduktegesetz (MPG § 23 b) und dem Strahlenschutzgesetz (StrlSchG). Nach Durchsicht der geänderten Unterlagen durch die Geschäftsstelle und durch mich als Vorsitzenden der Ethik-Kommission bestehen gegen die Durchführung der Studie nunmehr keine berufsethischen und berufsrechtlichen Bedenken.

Wir teilen wir Ihnen ferner folgende Stellungnahme gemäß § 36 (3) Strahlenschutzgesetz (StrlSchG) mit:

1. Das Forschungsvorhaben ist geeignet, nach dem Stand der Wissenschaft einem wissenschaftlichen Erkenntnisgewinn zu dienen.
2. Das Forschungsvorhaben, einschließlich der Anzahl der in das Forschungsvorhaben eingeschlossenen Personen, ist geeignet zur Beantwortung der wissenschaftlichen Fragestellung.

3. Das Risiko für die einzelne Person im Hinblick auf den potentiellen Nutzen für die Gesellschaft ist vertretbar.
4. Die schriftliche Information über das Forschungsvorhaben, die die in das Forschungsvorhaben eingeschlossene Person erhält, klärt ausreichend über Nutzen und Risiken auf und ermöglicht somit eine informierte Einwilligung.

**Die im Folgenden aufgeführten Hinweise müssen beachtet werden:**

1. Wir bitten um Nachreichung der Versicherungsbestätigung und der Allgemeinen Versicherungsbedingungen vor Studienbeginn per E-Mail.
2. Datenschutzrechtliche Aspekte von Forschungsvorhaben werden durch die Ethik-Kommission grundsätzlich nur kursorisch geprüft. Dieses Votum ersetzt mithin nicht die Konsultation des zuständigen Datenschutzbeauftragten.
3. Es wird darauf hingewiesen, dass künftige Änderungen der Studie der Ethik-Kommission anzuzeigen sind und gegebenenfalls eine erneute Beratung erforderlich machen.
4. Über alle unerwarteten schwerwiegenden unerwünschten Ereignisse (USADE), die während der Studie auftreten, **muss** die Kommission umgehend benachrichtigt werden. Ferner sind die jährlichen Sicherheitsberichte gemäß Protokoll vorzulegen.
5. Die ethische und rechtliche Verantwortung für die Durchführung dieser Studie verbleibt bei den Studienleitern.
6. Die Ethik-Kommission weist darauf hin, dass für eventuell in Zukunft weitere teilnehmende Zentren eine berufsrechtliche Beratung bei der jeweils für sie zuständigen Ethik-Kommission erforderlich ist.
7. Gemäß Deklaration von Helsinki **muss** die Studie vor Beginn der Rekrutierung in einer öffentlich zugänglichen Datenbank registriert werden. Wir empfehlen die Registrierung im Deutschen Register für Klinische Studien (www.drks.de).
8. Gemäß Deklaration von Helsinki **muss** der Ethik-Kommission nach Studienende ein Abschlussbericht vorgelegt werden, der eine Zusammenfassung der Ergebnisse und Schlussfolgerungen der Studie enthält.

Wir wünschen Ihnen für die Durchführung der Studie viel Erfolg.

Mit freundlichen Grüßen

Prof. Dr. med. H. M. Mehdorn
Vorsitzender der Ethik-Kommission

Dr. med. Christine Glinicke
Geschäftsführung der Ethik-Kommission

**Nachfolgend sind die Mitglieder der Ethik-Kommission aufgeführt, die diese Studie im Umlaufverfahren beurteilt und in der Sitzung am 18.12.2018 beraten haben:**

Dr. med Ruwen Böhm (Pharmakologie)
Dr. phil. Christoph Borzikowsky (Medizinische Informatik und Statistik)
Dr. rer. nat. Amke Caliebe (Medizinische Informatik und Statistik)
Dr. med. Rainer Günther (Innere Medizin I)
Prof. Dr. jur. Andreas Hoyer (Rechtswissenschaften)
Pfarrer Gereon Lemke (Krankenhausseelsorge)
PD Dr. med. Ulf Lützen (Strahlentherapie)
Prof. Dr. med. Maximilian Mehdorn (Neurochirurgie)
PD Dr. med. Hiltrud Muhle (Neuropädiatrie)
Prof. Dr. med. Martin Schrappe (Pädiatrie)
Dr. phil. Monika. Schwinge (Pröpstin i.R.)

**MEDIZINISCHE FAKULTÄT**
**DER CHRISTIAN-ALBRECHTS-UNIVERSITÄT ZU KIEL**

ETHIK-KOMMISSION

A.D. 1665

Universitäts-Kinderklinik · Schwanenweg 20 · 24105 Kiel

Postadresse:
Arnold-Heller-Straße 3 / Haus 9
D-24105 Kiel

Telefon 0431 / 500-14191
Telefax 0431 / 500-14195
ethikkomm@email.uni-kiel.de

Dr. Oliver Blanck
UKSH Schleswig-Holstein, Campus Kiel
Klinik für Strahlentherapie
Arnold-Heller-Straße 3, Haus 50
24105 Kiel

Datum:

09. Juli 2019

cc.: E-Mail: oliver.blanck@uksh.de
Fax: Prof. Dr. Hendrik Bonnemeier, 0431-500-22808

| | |
|---|---|
| **AZ.:** | **D 555/18** (bitte stets angeben) |
| **Studienplan:** | **Radiochirurgie zur Behandlung therapierefraktärer ventrikulärer Extrasystolen und Tachykardien (RAVENTA)** |
| **Antragsteller:** | **Dr. Oliver Blanck, Klinik für Strahlentherapie, UKSH Kiel** |
| **Studienleiter:** | **Prof. Dr. Hendrik Bonnemeier, Klinik für Innere Medizin III**<br>**Prof. Dr. Jürgen Dunst, Klinik für Strahlentherapie**<br>**UKSH, Campus Kiel** |
| **In Kooperation:** | **Klinik für Innere Medizin III (Kardiologie/Angiologie)**<br>**Abteilung für Elektrophysiologie und Rhythmologie, UKSH Kiel** |
| **Antrag vom:** | **20. Mai 2019 (Eingang: 28. Juni 2019)**<br>Anschreiben v. 20.05.19; Genehmigung des Bundesamtes für Strahlenschutz vom 18.04.19; Versicherungsbestätigung und Bedingungen vom 19-02-2019; Studienprotokoll V1.3.1 v. 02.05.19; Patienteninformation und Einwilligungserklärung V1.3 v. 02.05.19; Case Report Form V1.3.4 v. 02.05.2019 |

Sehr geehrter Herr Dr. Blanck, sehr geehrter Herr Prof. Bonnemeier,

wir bestätigen den Eingang und die Kenntnisnahme des Amendments zu oben genannter Studie.
Nach Durchsicht der Unterlagen durch die Geschäftsstelle und durch mich als Vorsitzenden der Ethik-Kommission bestehen gegen das Amendment und die Fortführung der Studie keine berufsethischen und berufsrechtlichen Bedenken.

Wir weisen darauf hin, dass datenschutzrechtliche Aspekte von Forschungsvorhaben durch die Ethik-Kommission grundsätzlich nur kursorisch geprüft werden. Diese Bewertung ersetzt nicht die Konsultation des zuständigen Datenschutzbeauftragten.

Wir wünschen Ihnen für die Durchführung der Studie weiterhin viel Erfolg.

Mit freundlichen kollegialen Grüßen

Prof. Dr. med. H. M. Mehdorn
Vorsitzender der Ethik-Kommission

Dr. med. Christine Glinicke
Geschäftsführung der Ethik-Kommission

# Appendix B

# Case Histories

The case histories [138] of the 5 datasets used in section 5.2 are shown below.

**Patient 1**
A 68-year-old male presented with a dilative cardiomyopathy (LVEF of 45-50%) secondary to myocarditis. Secondary prophylactic ICD implantation took place after cardiopulmonary resuscitation due to ventricular fibrillation in 2017. In 2020, the ICD was upgraded to the cardiac resynchronization system. Multiple anti-arrhythmic medication was administered in maximally tolerated doses without freedom from VT episodes (amiodarone, beta-blockers, mexiletine, chinidine, verapamil and lidocaine). A total of 7 prior endo- and epicardial catheter ablations had been performed. Due to AF, a pulmonary vein isolation was performed in 2019. The patient was presented in July 2020 with recurrent VT and ICD shocks. At the time of presentation, the patient took amiodaron 200 mg o.d. and metoprolol 95 mg b.i.d. Due to the multiple previous interventions, repeat catheter ablation was not deemed suitable so the patient was scheduled for STAR. The total dose was 25 Gy prescribed to the 83%-isodose. Treatment was delivered with a Varian TrueBeam STX linear accelerator using 6 dynamic conformal arcs. The patient tolerated the treatment well. During the first 4 weeks following the procedure, repeated episodes of AF occurred which subsided after temporarily increasing the dose of amiodarone to 200 mg b.i.d. Due to the negligible radiation dose to the left atrium (Dmax 7.2 Gy, Dmean 3.4 Gy), this event was not deemed treatment related. The amiodarone-dose was reduced to 200 mg o.d. The patient is free from VT since the procedure at a follow-up of 12 months. There was no treatment-related late toxicity. LVEF remained stable at 45%.

**Patient 2**
A 52-year-old female presented with a non-ischemic dilated cardiomyopathy and

moderately reduced LVEF of 45%. The patient had experienced a sustained VT five years ago and had been treated with antiarrhythmic medication (beta-blocker and amiodarone) and an ICD, which had to be explanted one year later due to intolerable pain. A re-implantation was refused by the patient. Since then, multiple (> 50) episodes of sustained VTs occurred, partly hemodynamically tolerated for up to 30 minutes and repeatedly terminated by external electrical cardioversion. Following repeated endocardial and epicardial EAM procedures, several ablation procedures were performed in the infero-basal as well as septal regions of the LV. All efforts remained without long term effect, finally, after several additional events with sustained VT the patient was evaluated for STAR. Treatment was performed on a Varian TrueBeam STX system with Varian Eclipse planning software based on 4D planning with an ITV concept. The primary treatment outcome was excellent with no new VT episodes within the first six months post-treatment. The patient did not experience any short-term toxicity, a thoracic CT 12 weeks following the procedure did not show any signs of pneumonitis. The left ventricular function as assessed by repeated echocardiography did not show any changes of ejection fraction.

**Patient 3**

A 66-year-old male patient diagnosed with ischemic cardiomyopathy and implanted with an ICD in 2008 presented with recurrent therapy-refractory monomorphic VT despite escalated antiarrhythmic therapy with beta blocker and amiodarone. The patient underwent a total of five endocardial catheter ablations since 2014 only with moderate mid-term success and recurrent ICD shocks. Due to progressive heart failure, the VT was hemodynamically unstable and was cardioverted promptly. After planning in DIBH, the patient was treated with an Elekta Versa HD linear accelerator with flattening filter free beams. A volumetric modulated arc therapy plan with 3 arcs was created in Monaco V. Image guidance was performed with DIBH-only cone beam CTs after each arc to minimize intrafraction drift. Table time was 65 minutes including free breathing phases and additional intra-fractional imaging. The patient tolerated the treatment well, no adverse effects were registered. Follow-up examinations showed no deterioration of the LVEF or regional wall motion abnormalities. No further VTs occurred after the treatment. At the time of writing, the patient is alive 9 months post-radiotherapy without new tachycardia episodes.

**Patient 4**

The patient (61-year-old, male) with non-ischemic dilated cardiomyopathy and heart failure with severely reduced ejection fraction was admitted for recurrent slow VT with appropriate ICD therapies. A total of 5 previous endocardial and epicardial RF catheter ablations for VT had been attempted, the last one in 03/2021. The patient was discharged on amiodarone and mexiletine but was emergently admitted in 11/2021 with decompensated heart failure due to sustained slow VT below the ICD detection rate at that time. Incidentally, Amiodarone-induced hyperthyroidism was diagnosed during that hospitalization and Amiodarone was changed to Sotalol. The patient was readmitted one month later with multiple ICD therapies for VT. Another ablation attempt was deemed futile, and antiarrhythmic drugs had been proved to be insufficient (with VT recurrence even while on amiodarone and mexiletine). Radiotherapy was planned on a respiration-gated 4D CT (Somatom, Siemens) after Vacuum-immobilization of the patient. Using a Versa HD linear accelerator (Elekta AB) with volumetric modulated arc therapy technology, 25 Gy was irradiated to cover 95% of the PTV. $D_{2\%}$ was 30.1 Gy). The patient developed nausea and vomiting on day 2 after radiation which could be managed with antiemetics and pantoprazole and which resolved completely by day 5. No other acute toxicity was observed.

**Patient 5**

A 60-year-old male patient with ischemic dilatative cardiomyopathy and a severely reduced left ventricular ejection fraction (LVEF, 15%) suffered from daily occurring recurrent incessant VTs with repeated partially effective antitachycardia pacing and appropriate ICD shocks from his two-chamber ICD. External triggers were excluded as a cause of these episodes. Despite optimized guideline-directed heart failure treatment, maximum-tolerated antiarrhythmic medication amiodarone (200 mg daily) and endocardial radiofrequency ablations (08/2019; 01/2020), life-threatening VT and electrical storm occurred onwards. Heart transplantation was not feasible due to severe comorbidities including a chronic kidney insufficiency (Kidney Disease: Improving Global Outcomes category G3b) and essential thrombocythemia.

The patient was treated on a Varian TrueBeam linear accelerator (Varian Medical Systems; Palo Alto, USA). The total duration of the whole procedure (cone beam CT imaging and beam delivery) was 30 minutes. An ITV + PTV concept was employed and during free breathing intrafraction the patient position was

monitored using real-time position management (Varian Medical Systems). Heart rate and oxygen saturation remained stable throughout the beam delivery. No interruption due to patient-related factors was necessary, in particular no VT occurred during the intervention. ICD function was normal and cardiac enzymes remained stable after STAR. Despite STAR, VT occurrence persisted with recurrent conversion attempts throughout the next weeks. Therefore, an additional invasive endocardial ablation was performed 3 weeks after STAR in LV segment 7 leading to a permanent cessation of the VTs. Post treatment, amiodarone medication was discontinued. During 18 months follow-up, no episodes of sustained VTs, further complications associated with the treatment, or acute side effects were reported or could be detected by ICD interrogations. The patient reported an augmented quality of life. LVEF determined by transthoracic echocardiography improved to 24% without pericardial effusion.

# Bibliography

[1] B. W. Loo, S. G. Soltys, L. Wang, A. Lo, B. P. Fahimian, A. Iagaru, *et al.*, "Stereotactic ablative radiotherapy for the treatment of refractory cardiac ventricular arrhythmia," *Circulation: Arrhythmia and Electrophysiology*, vol. 8, no. 3, pp. 748–750, 2015. DOI: 10.1161/CIRCEP.115.002765.

[2] P. S. Cuculich, M. R. Schill, R. Kashani, S. Mutic, A. Lang, D. Cooper, *et al.*, "Noninvasive cardiac radiation for ablation of ventricular tachycardia," *The New England Journal of Medicine*, vol. 377, no. 24, pp. 2325–2336, 2017. DOI: 10.1056/NEJMoa1613773.

[3] M. H. van der Ree, O. Blanck, J. Limpens, C. H. Lee, B. V. Balgobind, E. M. Dieleman, *et al.*, "Cardiac radioablation - A systematic review," *Heart Rhythm*, vol. 17, no. 8, pp. 1381–1392, 2020. DOI: 10.1016/j.hrthm.2020.03.013.

[4] D. Krug, A. Zaman, L. Eidinger, M. Grehn, J. Boda-Heggemann, B. Rudic, *et al.*, "Radiosurgery for ventricular tachycardia (RAVENTA): Interim analysis of a multicenter multiplatform feasibility trial," *Strahlentherapie und Onkologie*, vol. 199, pp. 621–630, 2023. DOI: 10.1007/s00066-023-02091-9.

[5] M. Grehn, S. Mandija, M. Miszczyk, D. Krug, B. Tomasik, K. E. Stickney, *et al.*, "Stereotactic arrhythmia radioablation (STAR): The Standardized Treatment and Outcome Platform for Stereotactic Therapy Of Re-entrant tachycardia by a Multidisciplinary consortium (STOPSTORM.eu) and review of current patterns of STAR practice in Europe," *EP Europace*, vol. 25, no. 4, pp. 1284–1295, 2023. DOI: 10.1093/europace/euac238.

[6] M. Miszczyk, W. F. Hoeksema, K. Kuna, S. Blamek, P. S. Cuculich, M. Grehn, *et al.*, "Stereotactic arrhythmia radioablation (STAR) - A systematic review and meta-analysis of prospective trials on behalf of the STOPSTORM.eu consortium," *Heart Rhythm*, vol. 22, no. 1, pp. 80–89, 2024. DOI: 10.1016/j.hrthm.2024.07.029.

[7] K. M. Menezes, H. Wang, M. Hada, and P. B. Saganti, "Radiation matters of the heart: A mini review," *Frontiers in Cardiovascular Medicine*, vol. 5, 2018, Art. no. 83. DOI: 10.3389/fcvm.2018.00083.

[8] B. Kovacs, H. I. Lehmann, M. Manninger, A. M. Saguner, P. Futyma, D. Duncker, *et al.*, "Stereotactic arrhythmia radioablation and its implications for modern cardiac electrophysiology: Results of an EHRA survey," *EP Europace*, vol. 26, no. 5, 2024, Art. no. euae110. DOI: 10.1093/europace/euae110.

[9] H. M. Haqqani and F. E. Marchlinski, "Electrophysiologic substrate underlying postinfarction ventricular tachycardia: Characterization and role in catheter ablation," *Heart Rhythm*, vol. 6, no. 8, S70–S76, 2009. DOI: 10.1016/j.hrthm.2009.04.023.

[10] M. E. Josephson and E. Anter, "Substrate mapping for ventricular tachycardia," *JACC: Clinical Electrophysiology*, vol. 1, no. 5, pp. 341–352, 2015. DOI: 10.1016/j.jacep.2015.09.001.

[11] K. Zeppenfeld, R. Rademaker, A. Al-Ahmad, C. Carbucicchio, C. De Chillou, M. Ebert, *et al.*, "Patient selection, ventricular tachycardia substrate delineation and data transfer for stereotactic arrhythmia radioablation. A clinical consensus statement of the European Heart Rhythm Association (EHRA) of the ESC and the Heart Rhythm Society (HRS)," *EP Europace*, 2024, Art. no. euae214. DOI: 10.1093/europace/euae214.

[12] C. Gianni, D. Rivera, J. D. Burkhardt, B. Pollard, E. Gardner, P. Maguire, *et al.*, "Stereotactic arrhythmia radioablation for refractory scar-related ventricular tachycardia," *Heart Rhythm*, vol. 17, no. 8, pp. 1241–1248, 2020. DOI: 10.1016/j.hrthm.2020.02.036.

[13] J. Wight, T. Bigham, A. Schwartz, A. T. Zahid, N. Bhatia, S. Kiani, *et al.*, "Long term follow-up of stereotactic body radiation therapy for refractory ventricular tachycardia in advanced heart failure patients," *Frontiers in Cardiovascular Medicine*, vol. 9, 2022, Art. no. 849113. DOI: 10.3389/fcvm.2022.849113.

[14] S. Ninni, T. Gallot-Lavallée, C. Klein, B. Longère, F. Brigadeau, C. Potelle, *et al.*, "Stereotactic radioablation for ventricular tachycardia in the setting of electrical storm," *Circulation: Arrhythmia and Electrophysiology*, vol. 15, no. 9, 2022, Art. no. e010955. DOI: 10.1161/CIRCEP.122.010955.

[15] J. Boda-Heggemann, O. Blanck, F. Mehrhof, F. Ernst, D. Buergy, J. Fleckenstein, *et al.*, "Interdisciplinary clinical target volume generation for cardiac radioablation: Multicenter benchmarking for the radiosurgery for ventricular tachycardia (RAVENTA) trial," *International Journal of Radiation Oncology, Biology, Physics*, vol. 110, no. 3, pp. 745–756, 2021. DOI: 10.1016/j.ijrobp.2021.01.028.

[16] M. H. van der Ree, P. S. Cuculich, M. van Herk, G. D. Hugo, J. C. Balt, M. Bates, *et al.*, "Interobserver variability in target definition for stereotactic arrhythmia radioablation," *Frontiers in Cardiovascular Medicine*, vol. 10, 2023, Art. no. 1267800. DOI: 10.3389/fcvm.2023.1267800.

[17] M. Chalkia, V. Kouloulias, D. Tousoulis, S. Deftereos, D. Tsiachris, D. Vrachatis, *et al.*, "Stereotactic arrhythmia radioablation as a novel treatment approach for cardiac arrhythmias: Facts and limitations," *Biomedicines*, vol. 9, no. 10, 2021, Art. no. 1461. DOI: 10.3390/biomedicines9101461.

[18] P. Peichl, M. Sramko, J. Cvek, and J. Kautzner, "A case report of successful elimination of recurrent ventricular tachycardia by repeated stereotactic radiotherapy: The importance of accurate target volume delineation," *European Heart Journal - Case Reports*, vol. 5, no. 2, 2021, Art. no. ytaa516. DOI: 10.1093/ehjcr/ytaa516.

[19] J. Haskova, K. Jedlickova, J. Cvek, L. Knybel, R. Neuwirth, and J. Kautzner, "Oesophagopericardial fistula as a late complication of stereotactic radiotherapy for recurrent ventricular tachycardia," *EP Europace*, vol. 24, no. 6, p. 969, 2022. DOI: 10.1093/europace/euab326.

[20] C. Wei, P. C. Qian, M. Boeck, J. S. Bredfeldt, R. Blankstein, U. B. Tedrow, *et al.*, "Cardiac stereotactic body radiation therapy for ventricular tachycardia: Current experience and technical gaps," *Journal of Cardiovascular Electrophysiology*, vol. 32, no. 11, pp. 2901–2914, 2021. DOI: 10.1111/jce.15259.

[21] J. Bellec, L. Rigal, A. Hervouin, R. Martins, M. Lederlin, N. Jaksic, *et al.*, "Cardiac radioablation for ventricular tachycardia: Which approach for incorporating cardiorespiratory motions into the planning target volume?" *Physica Medica*, vol. 95, pp. 16–24, 2022. DOI: 10.1016/j.ejmp.2022.01.004.

[22] P. Dvorak, L. Knybel, D. Dudas, P. Benyskova, and J. Cvek, "Stereotactic ablative radiotherapy of ventricular tachycardia using tracking: Optimized target definition workflow," *Frontiers in Cardiovascular Medicine*, vol. 9, 2022, Art. no. 870127. DOI: 10.3389/fcvm.2022.870127.

[23] S. Lydiard PGD, O. Blanck, G. Hugo, R. O'Brien, and P. Keall, "A review of cardiac radioablation (CR) for arrhythmias: Procedures, technology, and future opportunities," *International Journal of Radiation Oncology, Biology, Physics*, vol. 109, no. 3, pp. 783–800, 2021. DOI: 10.1016/j.ijrobp.2020.10.036.

[24] J. Boda-Heggemann, A. Jahnke, M. K. Chan, F. Ernst, A. L. Ghaderi, U. Attenberger, *et al.*, "In-vivo treatment accuracy analysis of active motion-compensated liver SBRT through registration of plan dose to post-therapeutic MRI-morphologic alterations," *Radiotherapy and Oncology*, vol. 134, pp. 158–165, 2019. DOI: 10.1016/j.radonc.2019.01.023.

[25] M. Cerqueira, N. Weissman, V. Dilsizian, A. Jacobs, S. Kaul, W. Laskey, *et al.*, "Standardized myocardial segmentation and nomenclature for tomographic imaging of the heart: A statement for healthcare professionals from the Cardiac Imaging Committee of the Council on Clinical Cardiology of the American Heart Association," *Circulation*, vol. 105, no. 4, pp. 539–542, 2002. DOI: 10.1161/hc0402.102975.

[26] R. R. Stevens, C. Hazelaar, M. F. Fast, S. Mandija, M. Grehn, J. Cvek, *et al.*, "Stereotactic arrhythmia radioablation (STAR): Assessment of cardiac and respiratory heart motion in ventricular tachycardia patients - A STOPSTORM.eu consortium review," *Radiotherapy and Oncology*, vol. 188, 2023, Art. no. 109844. DOI: 10.1016/j.radonc.2023.109844.

[27] O. Akdag, P. T. Borman, P. Woodhead, P. Uijtewaal, S. Mandija, B. Van Asselen, *et al.*, "First experimental exploration of real-time cardiorespiratory motion management for future stereotactic arrhythmia radioablation treatments on the MR-linac," *Physics in Medicine & Biology*, vol. 67, no. 6, 2022, Art. no. 065003. DOI: 10.1088/1361-6560/ac5717.

[28] O. Akdag, P. T. Borman, S. Mandija, P. L. Woodhead, P. Uijtewaal, B. W. Raaymakers, *et al.*, "Experimental demonstration of real-time cardiac physiology-based radiotherapy gating for improved cardiac radioablation on an MR-linac," *Medical Physics*, vol. 51, no. 4, pp. 2354–2366, 2024. DOI: 10.1002/mp.17024.

[29] O. Blanck, D. Buergy, M. Vens, L. Eidinger, A. Zaman, D. Krug, *et al.*, "Radiosurgery for ventricular tachycardia: Preclinical and clinical evidence and study design for a German multi-center multi-platform feasibility trial (RAVENTA)," *Clinical Research in Cardiology*, vol. 109, pp. 1319–1332, 2020. DOI: 10.1007/s00392-020-01650-9.

[30] E. Borzov, R. Efraim, M. Suleiman, R. Bar-Deroma, S. Billan, J. Xie, *et al.*, "Implementing stereotactic arrhythmia radioablation with STOP-STORM.eu consortium support: Intermediate results of a prospective Israeli single-institutional trial," *Strahlentherapie und Onkologie*, vol. 201, pp. 126–134, 2025. DOI: 10.1007/s00066-024-02300-z.

[31] S. M. Al-Khatib, W. G. Stevenson, M. J. Ackerman, W. J. Bryant, D. J. Callans, A. B. Curtis, *et al.*, "2017 AHA/ACC/HRS Guideline for management of patients with ventricular arrhythmias and the prevention of sudden cardiac death: A report of the American College of Cardiology/American Heart Association Task Force on Clinical Practice Guidelines and the Heart Rhythm Society," *Journal of the American College of Cardiology*, vol. 72, no. 14, e91–e220, 2018. DOI: 10.1016/j.jacc.2017.10.054.

[32] K. Shivkumar, "Catheter ablation of ventricular arrhythmias," *The New England Journal of Medicine*, vol. 380, no. 16, pp. 1555–1564, 2019. DOI: 10.1056/NEJMra1615244.

[33] W. G. Stevenson, "Ventricular scars and ventricular tachycardia," *Transactions of the American Clinical and Climatological Association*, vol. 120, pp. 403–412, 2009.

[34] J. K. Donahue, J. Chrispin, and O. A. Ajijola, "Mechanism of ventricular tachycardia occurring in chronic myocardial infarction scar," *Circulation Research*, vol. 134, no. 3, pp. 328–342, 2024. DOI: 10.1161/CIRCRESAHA.123.321553.

[35] W. S. Aronow, C. Ahn, A. D. Mercando, S. Epstein, and I. Kronzon, "Prevalence and association of ventricular tachycardia and complex ventricular arrhythmias with new coronary events in older men and women with and without cardiovascular disease," *The Journals of Gerontology: Series A*, vol. 57, no. 3, pp. M178–M180, 2002. DOI: 10.1093/gerona/57.3.m178.

[36] P. Santangeli, D. Muser, S. Maeda, A. Filtz, E. S. Zado, D. S. Frankel, *et al.*, "Comparative effectiveness of antiarrhythmic drugs and catheter ablation for the prevention of recurrent ventricular tachycardia in patients with

implantable cardioverter-defibrillators: A systematic review and meta-analysis of randomized controlled trials," *Heart Rhythm*, vol. 13, no. 7, pp. 1552–1559, 2016. DOI: 10.1016/j.hrthm.2016.03.004.

[37] D. S. Cannom and E. N. Prystowsky, "Management of ventricular arrhythmias: Detection, drugs, and devices," *JAMA*, vol. 281, no. 2, pp. 172–179, 1999. DOI: 10.1001/jama.281.2.172.

[38] R. Parkash, I. Nault, L. Rivard, L. Gula, V. Essebag, P. Nery, *et al.*, "Effect of baseline antiarrhythmic drug on outcomes with ablation in sschemic ventricular tachycardia: A VANISH substudy (ventricular tachycardia ablation versus escalated antiarrhythmic drug therapy in ischemic heart disease)," *Circulation: Arrhythmia and Electrophysiology*, vol. 11, no. 1, 2018, Art. no. e005663. DOI: 10.1161/CIRCEP.117.005663.

[39] J. W. Mason, "A comparison of seven antiarrhythmic drugs in patients with ventricular tachyarrhythmias," *The New England Journal of Medicine*, vol. 329, no. 7, pp. 452–458, 1993. DOI: 10.1056/NEJM199308123290702.

[40] E. Friedmann, S. A. Thomas, P. Inguito, C. W. Kao, M. Metcalf, F. J. Kelley, *et al.*, "Quality of life and psychological status of patients with implantable cardioverter defibrillators," *Journal of Interventional Cardiac Electrophysiology*, vol. 17, pp. 65–72, 2006. DOI: 10.1007/s10840-006-9053-1.

[41] S. R. Dukkipati, J. S. Koruth, S. Choudry, M. A. Miller, W. Whang, and V. Y. Reddy, "Catheter ablation of ventricular tachycardia in structural heart disease: Indications, strategies, and outcomes-part II," *Journal of the American College of Cardiology*, vol. 70, no. 23, pp. 2924–2941, 2017. DOI: 10.1016/j.jacc.2017.10.030.

[42] D. S. Frankel, S. E. Mountantonakis, M. R. Robinson, E. S. Zado, D. J. Callans, and F. E. Marchlinski, "Ventricular tachycardia ablation remains treatment of last resort in structural heart disease: Argument for earlier intervention," *Journal of Cardiovascular Electrophysiology*, vol. 22, no. 10, pp. 1123–1128, 2011. DOI: 10.1111/j.1540-8167.2011.02081.x.

[43] R. M. John, U. B. Tedrow, B. A. Koplan, C. M. Albert, L. M. Epstein, M. O. Sweeney, *et al.*, "Ventricular arrhythmias and sudden cardiac death," *The Lancet*, vol. 380, no. 9852, pp. 1520–1529, 2012. DOI: 10.1016/S0140-6736(12)61413-5.

[44] B. Dinov, A. Arya, L. Bertagnolli, V. Schirripa, K. Schoene, P. Sommer, *et al.*, "Early referral for ablation of scar-related ventricular tachycardia is associated with improved acute and long-term outcomes: Results from the Heart Center of Leipzig ventricular tachycardia registry," *Circulation: Arrhythmia and Electrophysiology*, vol. 7, no. 6, pp. 1144–1151, 2014. DOI: 10.1161/CIRCEP.114.001953.

[45] F. E. Marchlinski, C. I. Haffajee, J. F. Beshai, T.-M. L. Dickfeld, M. D. Gonzalez, H. H. Hsia, *et al.*, "Long-term success of irrigated radiofrequency catheter ablation of sustained ventricular tachycardia: Post-approval THERMOCOOL VT trial," *Journal of the American College of Cardiology*, vol. 67, no. 6, pp. 674–683, 2016. DOI: 10.1016/j.jacc.2015.11.041.

[46] G. S. Guandalini, J. J. Liang, and F. E. Marchlinski, "Ventricular tachycardia ablation: Past, present, and future perspectives," *JACC: Clinical Electrophysiology*, vol. 5, no. 12, pp. 1363–1383, 2019. DOI: 10.1016/j.jacep.2019.09.015.

[47] M. Tokuda, P. Kojodjojo, S. Tung, U. B. Tedrow, E. Nof, K. Inada, *et al.*, "Acute failure of catheter ablation for ventricular tachycardia due to structural heart disease: Causes and significance," *Journal of the American Heart Association*, vol. 2, no. 3, 2013, Art. no. e000072. DOI: 10.1161/JAHA.113.000072.

[48] M. Bohnen, W. G. Stevenson, U. B. Tedrow, G. F. Michaud, R. M. John, L. M. Epstein, *et al.*, "Incidence and predictors of major complications from contemporary catheter ablation to treat cardiac arrhythmias," *Heart Rhythm*, vol. 8, no. 11, pp. 1661–1666, 2011. DOI: 10.1016/j.hrthm.2011.05.017.

[49] P. Peichl, D. Wichterle, L. Pavlu, R. Cihak, B. Aldhoon, and J. Kautzner, "Complications of catheter ablation of ventricular tachycardia: A single-center experience," *Circulation: Arrhythmia and Electrophysiology*, vol. 7, no. 4, pp. 684–690, 2014. DOI: 10.1161/CIRCEP.114.001530.

[50] C. Palaniswamy, D. Kolte, P. Harikrishnan, S. Khera, W. S. Aronow, M. Mujib, *et al.*, "Catheter ablation of postinfarction ventricular tachycardia: Ten-year trends in utilization, in-hospital complications, and in-hospital mortality in the United States," *Heart Rhythm*, vol. 11, no. 11, pp. 2056–2063, 2014. DOI: 10.1016/j.hrthm.2014.07.012.

[51] J. Fernandez-Armenta, D. Soto-Iglesias, E. Silva, D. Penela, B. Jáuregui, M. Linhart, *et al.*, "Safety and outcomes of ventricular tachycardia substrate ablation during sinus rhythm: A prospective multicenter registry," *JACC: Clinical Electrophysiology*, vol. 6, no. 11, pp. 1435–1448, 2020. DOI: 10.1016/j.jacep.2020.07.028.

[52] M. F. Fast, S. Lydiard, J. Boda-Heggemann, S. Tanadini-Lang, L. P. Muren, C. H. Clark, *et al.*, "Precision requirements in stereotactic arrhythmia radioablation for ventricular tachycardia," *Physics and Imaging in Radiation Oncology*, vol. 28, 2023, Art. no. 100508. DOI: 10.1016/j.phro.2023.100508.

[53] P. Santangeli, D. S. Frankel, R. Tung, M. Vaseghi, W. H. Sauer, W. S. Tzou, *et al.*, "Early mortality after catheter ablation of ventricular tachycardia in patients with structural heart disease," *Journal of the American College of Cardiology*, vol. 69, no. 17, pp. 2105–2115, 2017. DOI: 10.1016/j.jacc.2017.02.044.

[54] P. Maury, B. Monteil, L. Marty, A. Duparc, P. Mondoly, and A. Rollin, "Three-dimensional mapping in the electrophysiological laboratory," *Archives of Cardiovascular Diseases*, vol. 111, no. 6-7, pp. 456–464, 2018. DOI: 10.1016/j.acvd.2018.03.013.

[55] L. Gepstein, G. Hayam, and S. A. Ben-Haim, "A novel method for nonfluoroscopic catheter-based electroanatomical mapping of the heart : In vitro and in vivo accuracy results," *Circulation*, vol. 95, no. 6, pp. 1611–1622, 1997. DOI: 10.1161/01.cir.95.6.1611.

[56] Y.-H. Kim, S.-A. Chen, S. Ernst, C. E. Guzman, S. Han, Z. Kalarus, *et al.*, "2019 APHRS expert consensus statement on three-dimensional mapping systems for tachycardia developed in collaboration with HRS, EHRA, and LAHRS," *Journal of Arrhythmia*, vol. 36, no. 2, pp. 215–270, 2020. DOI: 10.1002/joa3.12308.

[57] H. Nakagawa, A. Ikeda, T. Sharma, R. Lazzara, and W. M. Jackman, "Rapid high resolution electroanatomical mapping," *Circulation: Arrhythmia and Electrophysiology*, vol. 5, no. 2, pp. 417–424, 2012. DOI: 10.1161/CIRCEP.111.968602.

[58] E. Anter, C. M. Tschabrunn, F. M. Contreras-Valdes, J. Li, and M. E. Josephson, "Pulmonary vein isolation using the Rhythmia mapping system: Verification of intracardiac signals using the Orion mini-basket catheter,"

*Heart Rhythm*, vol. 12, no. 9, pp. 1927–1934, 2015. DOI: 10.1016/j.hrthm.2015.05.019.

[59] E. Anter, T. H. McElderry, F. M. Contreras-Valdes, J. Li, P. Tung, E. Leshem, *et al.*, "Evaluation of a novel high-resolution mapping technology for ablation of recurrent scar-related atrial tachycardias," *Heart Rhythm*, vol. 13, no. 10, pp. 2048–2055, 2016. DOI: 10.1016/j.hrthm.2016.05.029.

[60] S. Rolf, G. Hindricks, P. Sommer, S. Richter, A. Arya, A. Bollmann, *et al.*, "Electroanatomical mapping of atrial fibrillation: Review of the current techniques and advances," *Journal of Atrial Fibrillation*, vol. 7, no. 4, 2014, Art. no. 1140. DOI: 10.4022/jafib.1140.

[61] S. M. Narayan and R. M. John, "Advanced electroanatomic mapping: Current and emerging approaches," *Current Treatment Options in Cardiovascular Medicine*, vol. 26, pp. 69–91, 2024. DOI: 10.1007/s11936-024-01034-6.

[62] L. Leksell, "The stereotaxic method and radiosurgery of the brain," *Acta Chirurgica Scandinavica*, vol. 102, no. 4, pp. 316–319, 1951.

[63] B. K. Chang and R. D. Timmerman, "Stereotactic body radiation therapy: A comprehensive review," *American journal of clinical oncology*, vol. 30, no. 6, pp. 637–644, 2007. DOI: 10.1097/COC.0b013e3180ca7cb1.

[64] R. D. Timmerman, R. Paulus, H. I. Pass, E. M. Gore, M. J. Edelman, J. Galvin, *et al.*, "Stereotactic body radiation therapy for operable early-stage lung cancer: Findings from the NRG oncology RTOG 0618 trial," *JAMA Oncology*, vol. 4, no. 9, pp. 1263–1266, 2018. DOI: 10.1001/jamaoncol.2018.1251.

[65] E. Gkika, D. Bettinger, L. Krafft, M. Schultheiss, H. P. Neeff, L. Maruschke, *et al.*, "The role of albumin-bilirubin grade and inflammation-based index in patients with hepatocellular carcinoma treated with stereotactic body radiotherapy," *Strahlentherapie und Onkologie*, vol. 194, pp. 403–413, 2018. DOI: 10.1007/s00066-017-1256-0.

[66] A. Widmark, A. Gunnlaugsson, L. Beckman, C. Thellenberg-Karlsson, M. Hoyer, M. Lagerlund, *et al.*, "Ultra-hypofractionated versus conventionally fractionated radiotherapy for prostate cancer: 5-year outcomes of the HYPO-RT-PC randomised, non-inferiority, phase 3 trial," *The Lancet*, vol. 394, no. 10196, pp. 385–395, 2019. DOI: 10.1016/S0140-6736(19)31131-6.

[67] J. Rieber, J. Streblow, L. Uhlmann, *et al.*, "Stereotactic body radiotherapy (SBRT) for lung metastases - A pooled analysis of the German working group "stereotactic radiotherapy"," *Lung Cancer*, vol. 97, pp. 51–58, 2016. DOI: 10.1016/j.lungcan.2016.04.012.

[68] N. Andratschke, H. Alheid, M. Allgäuer, G. Becker, O. Blanck, J. Boda-Heggemann, *et al.*, "The SBRT database initiative of the German society for radiation oncology (DEGRO): Patterns of care and outcome analysis of stereotactic body radiotherapy (SBRT) for liver oligometastases in 474 patients with 623 metastases," *BMC cancer*, vol. 18, 2018, Art. no. 283. DOI: 10.1186/s12885-018-4191-2.

[69] D. Palma, R. Olson, S. Harrow, S. Gaede, A. Louie, C. Haasbeek, *et al.*, "Stereotactic ablative radiotherapy for the comprehensive treatment of oligometastatic cancers: Long-term results of the SABR-COMET phase II randomized trial," *Journal of Clinical Oncology*, vol. 38, no. 25, pp. 2830–2838, 2020. DOI: 10.1200/JCO.20.00818.

[70] M. Pankratov, F. Benetti, and J. Vivian, *Method for non-invasive heart treatment*, US Patent 6,889,695, May 2005.

[71] A. Sharma, D. Wong, G. Weidlich, T. Fogarty, A. Jack, T. Sumanaweera, *et al.*, "Noninvasive stereotactic radiosurgery (CyberHeart) for creation of ablation lesions in the atrium," *Heart Rhythm*, vol. 7, no. 6, pp. 802–810, 2010. DOI: 10.1016/j.hrthm.2010.02.010.

[72] P. Maguire, E. Gardner, A. B. Jack, P. Zei, A. Al-Ahmad, L. Fajardo, *et al.*, "Cardiac radiosurgery (CyberHeart™) for treatment of arrhythmia: Physiologic and histopathologic correlation in the porcine model," *Cureus*, vol. 3, no. 8, 2011, Art. no. e32. DOI: 10.7759/CUREUS.32.

[73] E. Monroy, J. Azpiri, C. De La Peña, C. Cardona, M. Hinojosa, R. Zamarripa, *et al.*, "Late gadolinium enhancement cardiac magnetic resonance imaging post-robotic radiosurgical pulmonary vein isolation (RRPVI): First case in the world," *Cureus*, vol. 8, no. 8, 2016, Art. no. e738. DOI: 10.7759/cureus.738.

[74] R. Jumeau, M. Ozsahin, J. Schwitter, O. Elicin, T. Reichlin, L. Roten, *et al.*, "Stereotactic radiotherapy for the management of refractory ventricular tachycardia: Promise and future directions," *Frontiers in Cardiovascular Medicine*, vol. 7, 2020, Art. no. 108. DOI: 10.3389/fcvm.2020.00108.

[75] J. Whitaker, R. H. Mak, and P. C. Zei, "Non-invasive ablation of arrhythmias with stereotactic ablative radiotherapy," *Trends in Cardiovascular Medicine*, vol. 32, no. 5, pp. 287–296, 2022. DOI: 10.1016/j.tcm.2021.04.008.

[76] R. Neuwirth, J. Cvek, L. Knybel, O. Jiravsky, L. Molenda, M. Kodaj, *et al.*, "Stereotactic radiosurgery for ablation of ventricular tachycardia," *EP Europace*, vol. 21, no. 7, pp. 1088–1095, 2019. DOI: 10.1093/europace/euz133.

[77] C. G. Robinson, P. P. Samson, K. M. Moore, G. D. Hugo, N. Knutson, S. Mutic, *et al.*, "Phase I/II trial of electrophysiology-guided noninvasive cardiac radioablation for ventricular tachycardia," *Circulation*, vol. 139, no. 3, pp. 313–321, 2019. DOI: 10.1161/CIRCULATIONAHA.118.038261.

[78] J. Lee, M. Bates, E. Shepherd, S. Riley, M. Henshaw, P. Metherall, *et al.*, "Cardiac stereotactic ablative radiotherapy for control of refractory ventricular tachycardia: Initial UK multicentre experience," *Open Heart*, vol. 8, no. 2, 2021, Art. no. e001770. DOI: 10.1136/openhrt-2021-001770.

[79] D. M. Zhang, R. Navara, T. Yin, J. Szymanski, U. Goldsztejn, C. Kenkel, *et al.*, "Cardiac radiotherapy induces electrical conduction reprogramming in the absence of transmural fibrosis," *Nature Communications*, vol. 12, 2021, Art. no. 5558. DOI: 10.1038/s41467-021-25730-0.

[80] S. Hohmann, H. A. Hillmann, J. Müller-Leisse, J. Eiringhaus, C. Zormpas, R. Merten, *et al.*, "Stereotactic radioablation for ventricular tachycardia," *Herzschrittmachertherapie + Elektrophysiologie*, vol. 33, pp. 49–54, 2022. DOI: 10.1007/s00399-021-00830-y.

[81] M. Ghita-Pettigrew, K. S. Edgar, R. Kuburas, K. H. Brown, G. M. Walls, C. Facchi, *et al.*, "Dose-dependent changes in cardiac function, strain and remodelling in a preclinical model of heart base irradiation," *Radiotherapy and Oncology*, vol. 193, 2024, Art. no. 110113. DOI: 10.1016/j.radonc.2024.110113.

[82] L. Wang, B. Fahimian, S. G. Soltys, P. Zei, A. Lo, E. A. Gardner, *et al.*, "Stereotactic arrhythmia radioablation (STAR) of ventricular tachycardia: A treatment planning study," *Cureus*, vol. 8, no. 7, 2016, Art. no. e694. DOI: 10.7759/cureus.694.

[83] S. Cozzi, N. Bottoni, A. Botti, V. Trojani, E. Alì, S. Finocchi Ghersi, *et al.*, "The use of cardiac stereotactic radiation therapy (SBRT) to manage ventricular tachycardia: A case report, review of the literature and technical notes," *Journal of Personalized Medicine*, vol. 12, no. 11, 2022, Art. no. 1783. DOI: 10.3390/jpm12111783.

[84] F. Guarracini, M. Tritto, A. Di Monaco, M. V. Mariani, A. Gasperetti, P. Compagnucci, *et al.*, "Stereotactic arrhythmia radioablation treatment of ventricular tachycardia: Current technology and evolving indications," *Journal of Cardiovascular Development and Disease*, vol. 10, no. 4, 2023, Art. no. 172. DOI: 10.3390/jcdd10040172.

[85] C. H. Siklody, E. Pruvot, P. Pascale, R. Kinj, R. Jumeau, M. Le Bloa, *et al.*, "Refractory ventricular tachycardia treated by a second session of stereotactic arrhythmia radioablation," *Clinical and Translational Radiation Oncology*, vol. 37, pp. 89–93, 2022. DOI: 10.1016/j.ctro.2022.07.005.

[86] J. Brownstein, M. Afzal, T. Okabe, T. T. Harfi, M. S. Tong, E. Thomas, *et al.*, "Method and atlas to enable targeting for cardiac radioablation employing the American Heart Association segmented model," *International Journal of Radiation Oncology, Biology, Physics*, vol. 111, no. 1, pp. 178–185, 2021. DOI: 10.1016/j.ijrobp.2021.03.051.

[87] M. H. van der Ree, J. Visser, R. N. Planken, E. M. Dieleman, S. M. Boekholdt, B. V. Balgobind, *et al.*, "Standardizing the cardiac radioablation targeting workflow: Enabling semi-automated angulation and segmentation of the heart according to the American Heart Association segmented model," *Advances in Radiation Oncology*, vol. 7, no. 4, 2022, Art. no. 100928. DOI: 10.1016/j.adro.2022.100928.

[88] E. Morris, R. Chin, T. Wu, C. Smith, S. Nejad-Davarani, and M. Cao, "AS-SET: Auto-Segmentation of the Seventeen SEgments for ventricular tachycardia ablation in radiation therapy," *Cancers*, vol. 15, no. 16, 2023, Art. no. 4062. DOI: 10.3390/cancers15164062.

[89] Y. S. Kaya, J. Stoks, C. Hazelaar, W. van Elmpt, S. Gommers, P. G. A. Volders, *et al.*, "3D-targeted, electrocardiographic imaging-aided stereotactic radioablation for ventricular tachycardia storm: A case report," *European Heart Journal - Case Reports*, vol. 8, no. 10, 2024, Art. no. ytae541. DOI: 10.1093/ehjcr/ytae541.

[90] S. Hohmann, C. Henkenberens, C. Zormpas, H. Christiansen, J. Bauersachs, D. Duncker, *et al.*, "A novel open-source software-based high-precision workflow for target definition in cardiac radioablation," *Journal of Cardiovascular Electrophysiology*, vol. 31, no. 10, pp. 2689–2695, 2020. DOI: 10.1111/jce.14660.

[91] A. Fedorov, R. Beichel, J. Kalpathy-Cramer, J. Finet, J.-C. Fillion-Robin, S. Pujol, *et al.*, "3D Slicer as an image computing platform for the quantitative imaging network," *Magnetic Resonance Imaging*, vol. 30, no. 9, pp. 1323–1341, 2012. DOI: 10.1016/j.mri.2012.05.001.

[92] C. Pinter, A. Lasso, A. Wang, D. Jaffray, and G. Fichtinger, "SlicerRT: Radiation therapy research toolkit for 3D Slicer," *Medical Physics*, vol. 39, no. 10, pp. 6332–6338, 2012. DOI: 10.1118/1.4754659.

[93] C. L. Brett, J. A. Cook, A. A. Aboud, R. Karim, E. T. Shinohara, and W. G. Stevenson, "Novel workflow for conversion of catheter-based electroanatomic mapping to dicom imaging for noninvasive radioablation of ventricular tachycardia," *Practical Radiation Oncology*, vol. 11, no. 1, pp. 84–88, 2021. DOI: 10.1016/j.prro.2020.04.006.

[94] H. Wang, C. R. Barbhaiya, Y. Yuan, D. Barbee, T. Chen, L. Axel, *et al.*, "A tool to integrate electrophysiological mapping for cardiac radioablation of ventricular tachycardia," *Advances in Radiation Oncology*, vol. 8, no. 6, 2023, Art. no. 101272. DOI: 10.1016/j.adro.2023.101272.

[95] S. Oh, E. H. Liu, M. G. Trombetta, G. C. Shaw, A. J. Thosani, R. W. Biederman, *et al.*, "A target definition based on electroanatomic maps for stereotactic arrhythmia radioablation," *Physica Medica*, vol. 115, 2023, Art. no. 103160. DOI: 10.1016/j.ejmp.2023.103160.

[96] L. Rigal, K. Benali, V. Barré, M. Bougault, J. Bellec, R. D. Crevoisier, *et al.*, "Multimodal fusion workflow for target delineation in cardiac radioablation of ventricular tachycardia," *Medical Physics*, vol. 51, no. 1, pp. 292–305, 2024. DOI: 10.1002/mp.16613.

[97] J. Hecko, L. Knybel, M. Rybar, M. Penhaker, O. Jiravský, R. Neuwirth, *et al.*, "Optimized target delineation procedure for the radiosurgery treatment of ventricular tachycardia: Observer-independent accuracy," *Reports of Practical Oncology and Radiotherapy*, vol. 29, no. 3, pp. 280–289, 2024. DOI: 10.5603/rpor.100387.

[98] S. L. Konermann, I. J. Gerard, M. L. Bernier, T. Hijal, G. Stroian, N. Kopek, *et al.*, "The conversion of electroanatomic maps for compatibility with treatment planning systems in cardiac radioablation target volume definition," *Medical Physics*, vol. 52, no. 2, pp. 1172–1181, 2025. DOI: 10.1002/mp.17531.

[99] A. Santos-Ortega, N. Rivas-Gándara, G. Pascual-González, A. Seoane, R. Granado, and V. Reyes, "Multimodality imaging fusion to guide stereotactic radioablation for refractory complex ventricular tachycardia," *HeartRhythm Case Reports*, vol. 8, no. 12, pp. 836–839, 2022. DOI: 10.1016/j.hrcr.2022.09.008.

[100] D. Krug, O. Blanck, T. Demming, M. Dottermusch, K. Koch, M. Hirt, *et al.*, "Stereotactic body radiotherapy for ventricular tachycardia (cardiac radiosurgery): First-in-patient treatment in Germany," *Strahlentherapie und Onkologie*, vol. 196, pp. 23–30, 2020. DOI: 10.1007/s00066-019-01530-w.

[101] M. Mayinger, B. Kovacs, S. Tanadini-Lang, S. Ehrbar, L. Wilke, M. Chamberlain, *et al.*, "First magnetic resonance imaging-guided cardiac radioablation of sustained ventricular tachycardia," *Radiotherapy and Oncology*, vol. 152, pp. 203–207, 2020. DOI: 10.1016/j.radonc.2020.01.008.

[102] E. M. Cronin, F. M. Bogun, P. Maury, P. Peichl, M. Chen, N. Namboodiri, *et al.*, "2019 HRS/EHRA/APHRS/LAHRS expert consensus statement on catheter ablation of ventricular arrhythmias: Executive summary," *EP Europace*, vol. 22, no. 3, pp. 450–495, 2020. DOI: 10.1093/europace/euz332.

[103] C. Wei, P. Qian, U. Tedrow, R. Mak, and P. C. Zei, "Non-invasive stereotactic radioablation: A new option for the treatment of ventricular arrhythmias," *Arrhythmia & Electrophysiology Review*, vol. 8, no. 4, pp. 285–293, 2019. DOI: 10.15420/aer.2019.04.

[104] C. Carbucicchio, D. Andreini, G. Piperno, V. Catto, E. Conte, F. Cattani, *et al.*, "Stereotactic radioablation for the treatment of ventricular tachycardia: Preliminary data and insights from the STRA-MI-VT phase Ib/II study," *Journal of Interventional Cardiac Electrophysiology*, vol. 62, pp. 427–439, 2021. DOI: 10.1007/s10840-021-01060-5.

[105] G. Molon, N. Giaj-Levra, A. Costa, S. Bonapace, F. Cuccia, A. Marinelli, *et al.*, "Stereotactic ablative radiotherapy in patients with refractory ventricular tachyarrhythmia," *European Heart Journal Supplements*, vol. 24, no. Supplement C, pp. C248–C253, 2022. DOI: 10.1093/eurheartj/suac016.

[106] W. I. Chang, H. H. Jo, M.-J. Cha, J. H. Chang, C. H. Choi, H. J. Kim, *et al.*, "Short-term and long-term effects of noninvasive cardiac radioablation for ventricular tachycardia: A single-center case series," *Heart Rhythm O2*, vol. 4, no. 2, pp. 119–126, 2023. DOI: 10.1016/j.hroo.2022.11.006.

[107] M. Miszczyk, M. Sajdok, J. Bednarek, T. Latusek, W. Wojakowski, B. Tomasik, *et al.*, "Stereotactic management of arrhythmia - Radiosurgery in treatment of ventricular tachycardia (SMART-VT). Results of a prospective safety trial," *Radiotherapy and Oncology*, vol. 188, 2023, Art. no. 109857. DOI: 10.1016/j.radonc.2023.109857.

[108] M. H. van der Ree, E. M. T. Dieleman, J. Visser, R. N. Planken, S. M. Boekholdt, R. H. A. de Bruin-Bon, *et al.*, "Non-invasive stereotactic arrhythmia radiotherapy for ventricular tachycardia: Results of the prospective STARNL-1 trial," *EP Europace*, vol. 25, no. 3, pp. 1015–1024, 2023. DOI: 10.1093/europace/euad020.

[109] M. Amino, S. Kabuki, E. Kunieda, J. Hashimoto, A. Sugawara, T. Sakai, *et al.*, "Interim report of a Japanese phase II trial for cardiac stereotactic body radiotherapy in refractory ventricular tachycardia - Focus on target determination," *Circulation Reports*, vol. 5, no. 3, pp. 69–79, 2023. DOI: 10.1253/circrep.CR-23-0003.

[110] P. C. Qian, K. Quadros, M. Aguilar, C. Wei, M. Boeck, J. Bredfeldt, *et al.*, "Substrate modification using stereotactic radioablation to treat refractory ventricular tachycardia in patients with ischemic cardiomyopathy," *JACC: Clinical Electrophysiology*, vol. 8, no. 1, pp. 49–58, 2022. DOI: 10.1016/j.jacep.2021.06.016.

[111] F. Englert, F. Bahlke, N. Erhard, H. Krafft, M.-A. Popa, E. Risse, *et al.*, "VT ablation based on CT imaging substrate visualization: Results from a large cohort of ischemic and non-ischemic cardiomyopathy patients," *Clinical Research in Cardiology*, vol. 113, pp. 1478–1484, 2024. DOI: 10.1007/s00392-023-02321-1.

[112] S. K. Das, T. Ryan, V. Panettieri, J. Hawson, T. Lim, N. Hardcastle, *et al.*, "Stereotactic arrhythmia radioablation (STAR) for refractory ventricular tachycardia – The initial Australian experience," *Heart Rhythm*, 2025. DOI: 10.1016/j.hrthm.2025.02.005.

[113] S. Abdel-Kafi, M. Sramko, S. Omara, M. de Riva, J. Cvek, P. Peichl, *et al.*, "Accuracy of electroanatomical mapping-guided cardiac radiotherapy for

ventricular tachycardia: Pitfalls and solutions," *EP Europace*, vol. 23, no. 12, pp. 1989–1997, 2021. DOI: 10.1093/europace/euab195.

[114] M. Kawamura, M. Shimojo, F. Tatsugami, K. Hirata, S. Fujita, D. Ueda, *et al.*, "Stereotactic arrhythmia radioablation for ventricular tachycardia: A review of clinical trials and emerging roles of imaging," *Journal of Radiation Research*, vol. 66, no. 1, pp. 1–9, 2025. DOI: 10.1093/jrr/rrae090.

[115] C. Q. Reis and J. L. Robar, "Evaluation of the feasibility of cardiac gating for SBRT of ventricular tachycardia based on real-time ECG signal acquisition," *Journal of Applied Clinical Medical Physics*, vol. 24, no. 2, 2023, Art. no. e13814. DOI: 10.1002/acm2.13814.

[116] Z. Ouyang, P. Schoenhagen, O. Wazni, P. Tchou, W. I. Saliba, J. H. Suh, *et al.*, "Analysis of cardiac motion without respiratory motion for cardiac stereotactic body radiation therapy," *Journal of Applied Clinical Medical Physics*, vol. 21, no. 10, pp. 48–55, 2020. DOI: 10.1002/acm2.13002.

[117] G. Li, G. Wang, W. Wei, Z. Li, Q. Xiao, H. He, *et al.*, "Cardiorespiratory motion characteristics and their dosimetric impact on cardiac stereotactic body radiotherapy," *Medical Physics*, vol. 51, no. 11, pp. 8551–8567, 2024. DOI: 10.1002/mp.17284.

[118] A. Petzl, K. Benali, N. Mbolamena, K. Dyrda, L. Rivard, S. Seidl, *et al.*, "Patient-specific quantification of cardiorespiratory motion for cardiac stereotactic radioablation treatment planning," *Heart Rhythm O2*, vol. 5, no. 4, pp. 234–242, 2024. DOI: 10.1016/j.hroo.2024.03.006.

[119] J. Poon, R. B. Thompson, M. W. Deyell, D. Schellenberg, H. Clark, S. Reinsberg, *et al.*, "Analysis of left ventricle regional myocardial motion for cardiac radioablation: Left ventricular motion analysis," *Journal of Applied Clinical Medical Physics*, vol. 25, no. 5, 2024, Art. no. e14333. DOI: 10.1002/acm2.14333.

[120] J. Poon, R. B. Thompson, M. W. Deyell, D. Schellenberg, K. Kohli, and S. Thomas, "Left ventricle segment-specific motion assessment for cardiac-gated radiosurgery," *Biomedical Physics & Engineering Express*, vol. 10, no. 2, 2024, Art. no. 025040. DOI: 10.1088/2057-1976/ad29a4.

[121] B. Wu, T. Atwood, A. J. Mundt, J. Karunamuni, P. Stark, A. Hsiao, *et al.*, "Characterizing cardiac contractile motion for noninvasive radioablation of ventricular tachycardia," *Heart Rhythm O2*, vol. 5, no. 2, pp. 131–136, 2024. DOI: 10.1016/j.hroo.2023.12.006.

[122] The MathWorks Inc., *MATLAB version: 24.2 (R2024b)*, Natick, Massachusetts, United States, 2024. [Online]. Available: https://www.mathworks.com.

[123] S. Hohmann, J. Xie, M. Grehn, N. Karfoul, F. Mehrhof, R. Merten, *et al.*, "Reproducible target transfer from electroanatomic mapping to radiotherapy planning systems for cardiac radioablation - Cross-validation for the RAVENTA trial," *EP Europace*, vol. 25, no. Supplement 1, pp. i491–i492, 2023. DOI: 10.1093/europace/euad122.303.

[124] L. Kaestner, J. Boda-Heggemann, H. Fanslau, J. Xie, A. Schweikard, F. A. Giordano, *et al.*, "Electroanatomical mapping after cardiac radioablation for treatment of incessant electrical storm: A case report from the RAVENTA trial," *Strahlentherapie und Onkologie*, vol. 199, pp. 1018–1024, 2023. DOI: 10.1007/s00066-023-02136-z.

[125] L. Kaestner, J. Xie, H. Fanslau, K. Siebenlist, J. Fleckenstein, M. Eckl, *et al.*, "Bestrahlungsplanung für kardiale stereotaktische Radioablation (STAR) bei Patienten mit subkutanen implantierbaren Cardioverter Defibrillatoren (S-ICD)," *Strahlentherapie und Onkologie*, vol. 200, S158, 2024. DOI: 10.1007/s00066-024-02233-7.

[126] F. Mehrhof, J. Hüttemeister, R. Tanacli, M. Bock, M. Bögner, F. Schoenrath, *et al.*, "Cardiac radiotherapy transiently alters left ventricular electrical properties and induces cardiomyocyte-specific ventricular substrate changes in heart failure," *EP Europace*, vol. 26, no. 1, 2024, Art. no. euae005. DOI: 10.1093/europace/euae005.

[127] S. Hohmann, J. Xie, M. Eckl, M. Grehn, N. Karfoul, C. Janorschke, *et al.*, "Semi-automated reproducible target transfer for STAR – Cross-validation within the RAVENTA trial," *Radiotherapy and Oncology*, vol. 194, S2879–S2880, 2024. DOI: 10.1016/S0167-8140(24)00976-9.

[128] S. Hohmann, J. Xie, M. Grehn, N. Karfoul, C. Janorschke, F. Mehrhof, *et al.*, "Zielübertragung vom elektroanatomischen mapping auf das planungs-ct für die kardiale stereotaktische strahlentherapie - kreuzvalidierung zweier software-ansätze für die raventa-studie," *Strahlentherapie und Onkologie*, vol. 199, no. Supplement 1, S119, 2024. DOI: 10.1007/s00066-023-02083-9.

[129] J. Xie, B. Rudic, A. Zaman, M. Kuru, X. Lu, C. Janorschke, *et al.*, "A novel cardiac motion estimation method for stereotactic arrhythmia radioablation (STAR) based on ECG-gated cardiac 4D CT," *Strahlentherapie und Onkologie*, vol. 200, no. Supplement 1, S8–S9, 2024. DOI: 10.1007/s00066-024-02233-7.

[130] J. Xie, B. Rudic, A. Zaman, M. Kuru, X. Lu, C. Janorschke, *et al.*, "A patient-specific cardiac motion estimation method for stereotactic arrhythmia radioablation (STAR) based on ECG-gated cardiac 4D CT," *Physica Medica*, vol. 125, S305–S306, 2024. DOI: 10.1016/j.ejmp.2024.103899.

[131] S. Hohmann, J. Xie, M. Eckl, M. Grehn, N. Karfoul, C. Janorschke, *et al.*, "Semi-automated reproducible target transfer for cardiac radioablation – A multi-center cross-validation study within the RAVENTA trial," *Radiotherapy and Oncology*, vol. 200, 2024, Art. no. 110499. DOI: 10.1016/j.radonc.2024.110499.

[132] J. Xie, A. S. Bicu, M. Grehn, M. Kuru, A. Zaman, X. Lu, *et al.*, "Electrocardiogram-gated cardiac computed tomography-based patient- and segment-specific cardiac motion estimation method in stereotactic arrhythmia radioablation for ventricular tachycardia," *Physics and Imaging in Radiation Oncology*, vol. 33, 2025, Art. no. 100700. DOI: 10.1016/j.phro.2025.100700.

[133] P. Besl and N. D. McKay, "A method for registration of 3-D shapes," *IEEE Transactions on Pattern Analysis and Machine Intelligence*, vol. 14, no. 2, pp. 239–256, 1992. DOI: 10.1109/34.121791.

[134] M. Orini, A. Graham, M. Dhinoja, R. Hunter, R. J. Schilling, A. W. Chow, *et al.*, "Early results on the utilisation of ECG-imaging during catheter ablation procedures for prediction of sites of earliest activation during re-entrant ventricular tachycardia," in *2018 Computing in Cardiology Conference (CinC)*, IEEE, vol. 45, 2018, pp. 1–4. DOI: 10.22489/CinC.2018.283.

[135] G. Cheniti, S. Puyo, C. A. Martin, A. Frontera, K. Vlachos, M. Takigawa, *et al.*, "Noninvasive mapping and electrocardiographic imaging in atrial and ventricular arrhythmias (CardioInsight)," *Cardiac Electrophysiology Clinics*, vol. 11, no. 3, pp. 459–471, 2019. DOI: 10.1016/j.ccep.2019.05.004.

[136] A. J. Graham, M. Orini, E. Zacur, G. Dhillon, H. Daw, N. T. Srinivasan, *et al.*, "Evaluation of ECG imaging to map hemodynamically stable and

unstable ventricular arrhythmias," *Circulation: Arrhythmia and Electrophysiology*, vol. 13, no. 2, 2020, Art. no. e007377. DOI: 10.1161/CIRCEP.119.007377.

[137] A. J. Graham, M. Orini, E. Zacur, G. Dhillon, D. Jones, S. Prabhu, *et al.*, "Assessing noninvasive delineation of low-voltage zones using ECG imaging in patients with structural heart disease," *JACC: Clinical Electrophysiology*, vol. 8, no. 4, pp. 426–436, 2022. DOI: 10.1016/j.jacep.2021.11.011.

[138] M. Mayinger, J. Boda-Heggemann, F. Mehrhof, D. Krug, S. Hohmann, J. Xie, *et al.*, "Quality assurance process within the radiosurgery for ventricular tachycardia (RAVENTA) trial for the fusion of electroanatomical mapping and radiotherapy planning imaging data in cardiac radioablation," *Physics and Imaging in Radiation Oncology*, vol. 25, 2023, Art. no. 100406. DOI: 10.1016/j.phro.2022.12.003.

[139] M. Takigawa, J. Duchateau, F. Sacher, R. Martin, K. Vlachos, T. Kitamura, *et al.*, "Are wall thickness channels defined by computed tomography predictive of isthmuses of postinfarction ventricular tachycardia?" *Heart Rhythm*, vol. 16, no. 11, pp. 1661–1668, 2019. DOI: 10.1016/j.hrthm.2019.06.012.

[140] A. Esposito, A. Palmisano, S. Antunes, G. Maccabelli, C. Colantoni, P. M. V. Rancoita, *et al.*, "Cardiac CT with delayed enhancement in the characterization of ventricular tachycardia structural substrate: Relationship between CT-segmented scar and electro-anatomic mapping," *JACC: Cardiovascular Imaging*, vol. 9, no. 7, pp. 822–832, 2016. DOI: 10.1016/j.jcmg.2015.10.024.

[141] T. R. Maher, B. L. Freedman, A. H. Locke, M. Tracey, J. W. Waks, D. Litmanovich, *et al.*, "Correlation between functional substrate mapping and cardiac computed tomography–derived wall thinning for ventricular tachycardia ablation," *Clinical Electrophysiology*, vol. 9, no. 9, pp. 1878–1889, 2023. DOI: 10.1016/j.jacep.2023.05.018.

[142] M. Grehn, D. Krug, A. Zaman, E. Lyan, and O. Blanck, "Customized dynamic cardiac phantom for end-to-end-testing of stereotactic arrhythmia radioablation (STAR) treatments," *Physica Medica*, vol. 125, no. Supplement 1, S178, 2024. DOI: 10.1016/j.ejmp.2024.103696.

[143] K. W. Gregg, C. Ruff, G. Koenig, K. I. Penev, A. Shepard, G. Kreissler, *et al.*, "Development and first implementation of a novel multi-modality cardiac

motion and dosimetry phantom for radiotherapy applications," *Medical Physics*, vol. 51, no. 10, pp. 7479–7491, 2024. DOI: 10.1002/mp.17315.

[144] D. Krug, O. Blanck, N. Andratschke, M. Guckenberger, R. Jumeau, F. Mehrhof, *et al.*, "Recommendations regarding cardiac stereotactic body radiotherapy for treatment refractory ventricular tachycardia," *Heart Rhythm*, vol. 18, no. 12, pp. 2137–2145, 2021. DOI: 10.1016/j.hrthm.2021.08.004.

[145] G. Ho, T. F. Atwood, A. R. Bruggeman, K. L. Moore, E. McVeigh, C. T. Villongco, *et al.*, "Computational ECG mapping and respiratory gating to optimize stereotactic ablative radiotherapy workflow for refractory ventricular tachycardia," *Heart Rhythm O2*, vol. 2, no. 5, pp. 511–520, 2021. DOI: 10.1016/j.hroo.2021.09.001.

[146] M. Guckenberger, W. W. Baus, O. Blanck, S. E. Combs, J. Debus, R. Engenhart-Cabillic, *et al.*, "Definition and quality requirements for stereotactic radiotherapy: Consensus statement from the DEGRO/DGMP Working Group Stereotactic Radiotherapy and Radiosurgery," *Strahlentherapie und Onkologie*, vol. 196, pp. 417–420, 2020. DOI: 10.1007/s00066-020-01603-1.

[147] D. Schmitt, O. Blanck, T. Gauer, M. K. Fix, T. B. Brunner, J. Fleckenstein, *et al.*, "Technological quality requirements for stereotactic radiotherapy: Expert review group consensus from the DGMP Working Group for Physics and Technology in Stereotactic Radiotherapy," *Strahlentherapie und Onkologie*, vol. 196, pp. 421–443, 2020. DOI: 10.1007/s00066-020-01583-2.

[148] B. Kovacs, M. Mayinger, M. Schindler, J. Steffel, N. Andratschke, and A. M. Saguner, "Stereotactic radioablation of ventricular arrhythmias in patients with structural heart disease – A systematic review," *Radiotherapy and Oncology*, vol. 162, pp. 132–139, 2021. DOI: 10.1016/j.radonc.2021.06.036.

[149] M. Eckl, L. Hoppen, G. R. Sarria, J. Boda-Heggemann, A. Simeonova-Chergou, V. Steil, *et al.*, "Evaluation of a cycle-generative adversarial network-based cone-beam ct to synthetic ct conversion algorithm for adaptive radiation therapy," *Physica Medica*, vol. 80, pp. 308–316, 2020. DOI: 10.1016/j.ejmp.2020.11.007.

[150] P. C. Zei and S. Soltys, "Ablative radiotherapy as a noninvasive alternative to catheter ablation for cardiac arrhythmias," *Current Cardiology Reports*, vol. 19, 2017, Art. no. 79. DOI: 10.1007/s11886-017-0886-2.

[151] A. J. Sharp, R. Mak, and P. C. Zei, "Noninvasive cardiac radioablation for ventricular arrhythmias," *Current Cardiovascular Risk Reports*, vol. 13, 2019, Art. no. 1. DOI: 10.1007/s12170-019-0596-y.

[152] S. Ahmad, "Cardiac stereotactic ablative radiotherapy - a multidisciplinary approach," *Clinical Oncology*, vol. 35, no. 7, pp. 421–425, 2023. DOI: 10.1016/j.clon.2023.04.006.

[153] R. Lenarczyk, K. Zeppenfeld, J. Tfelt-Hansen, F. R. Heinzel, T. Deneke, E. Ene, *et al.*, "Management of patients with an electrical storm or clustered ventricular arrhythmias: A clinical consensus statement of the European Heart Rhythm Association of the ESC-endorsed by the Asia-Pacific Heart Rhythm Society, Heart Rhythm Society, and Latin-American Heart Rhythm Society," *EP Europace*, vol. 26, no. 4, 2024, Art. no. euae049. DOI: 10.1093/europace/euae049.

[154] K. Zeppenfeld, J. Tfelt-Hansen, M. de Riva, B. G. Winkel, E. R. Behr, N. A. Blom, *et al.*, "2022 ESC Guidelines for the management of patients with ventricular arrhythmias and the prevention of sudden cardiac death: Developed by the task force for the management of patients with ventricular arrhythmias and the prevention of sudden cardiac death of the European Society of Cardiology (ESC) Endorsed by the Association for European Paediatric and Congenital Cardiology (AEPC)," *European Heart Journal*, vol. 43, no. 40, pp. 3997–4126, 2022. DOI: 10.1093/eurheartj/ehac262.

[155] J. Cvek, R. Neuwirth, L. Knybel, L. Molenda, B. Otahal, J. Pindor, *et al.*, "Cardiac radiosurgery for malignant ventricular tachycardia," *Cureus*, vol. 6, no. 7, 2014, Art. no. e190. DOI: 10.7759/cureus.190.

[156] R. Jumeau, M. Ozsahin, J. Schwitter, V. Vallet, F. Duclos, M. Zeverino, *et al.*, "Rescue procedure for an electrical storm using robotic non-invasive cardiac radio-ablation," *Radiotherapy and Oncology*, vol. 128, no. 2, pp. 189–191, 2018. DOI: 10.1016/j.radonc.2018.04.025.

[157] E. P. Scholz, K. Seidensaal, P. Naumann, F. André, H. A. Katus, and J. Debus, "Risen from the dead: Cardiac stereotactic ablative radiotherapy as last rescue in a patient with refractory ventricular fibrillation storm,"

*HeartRhythm Case Reports*, vol. 5, no. 6, pp. 329–332, 2019. DOI: 10.1016/j.hrcr.2019.03.004.

[158] J. Wasserthal, H.-C. Breit, M. T. Meyer, M. Pradella, D. Hinck, A. W. Sauter, *et al.*, "TotalSegmentator: Robust segmentation of 104 anatomic structures in CT images," *Radiology: Artificial Intelligence*, vol. 5, no. 5, 2023, Art. no. e230024. DOI: 10.48550/arXiv.2208.05868.

[159] F. Isensee, P. F. Jaeger, S. A. Kohl, J. Petersen, and K. H. Maier-Hein, "nnU-Net: A self-configuring method for deep learning-based biomedical image segmentation," *Nature Methods*, vol. 18, pp. 203–211, 2021. DOI: 10.1038/s41592-020-01008-z.

[160] The MathWorks Inc., *Image Processing Toolbox version: 11.5 (R2022a)*, Natick, Massachusetts, United States, 2022. [Online]. Available: https://www.mathworks.com.

[161] C. Piccolo, S. Vigorito, E. Rondi, G. Piperno, A. Ferrari, M. Pepa, *et al.*, "Phantom study of stereotactic radioablation for ventricular tachycardia (STRA-MI-VT) using Cyberknife Synchrony Respiratory Tracking System with a single fiducial marker," *Physica Medica*, vol. 100, pp. 135–141, 2022. DOI: 10.1016/j.ejmp.2022.06.019.

[162] W. Tan, L. Xu, X. Wang, D. Qiu, G. Han, and D. Hu, "Estimation of the displacement of cardiac substructures and the motion of the coronary arteries using electrocardiographic gating," *OncoTargets and Therapy*, vol. 6, pp. 1325–1332, 2013. DOI: 10.2147/OTT.S52101.

[163] M. Levis, V. De Luca, C. Fiandra, S. Veglia, A. Fava, M. Gatti, *et al.*, "Plan optimization for mediastinal radiotherapy: Estimation of coronary arteries motion with ECG-gated cardiac imaging and creation of compensatory expansion margins," *Radiotherapy and Oncology*, vol. 127, no. 3, pp. 481–486, 2018. DOI: 10.1016/j.radonc.2018.04.014.

[164] P. van Haaren, F. Claassen-Janssen, I. van de Sande, L. Boersma, M. van der Sangen, and C. Hurkmans, "Heart position variability during voluntary moderate deep inspiration breath-hold radiotherapy for breast cancer determined by repeat cbct scans," *Physica Medica*, vol. 40, pp. 88–94, 2017. DOI: 10.1016/j.ejmp.2017.07.014.

[165] L. H. van der Pol, O. Blanck, M. Grehn, T. Blazek, L. Knybel, B. V. Balgobind, *et al.*, "Auto-contouring of cardiac substructures for stereotactic arrhythmia radioablation (STAR): A STOPSTORM.eu consortium study,"

*Radiotherapy and Oncology*, vol. 202, 2025, Art. no. 110610. DOI: 10.1016/j.radonc.2024.110610.

[166] J. Harms, E. Schreibmann, N. S. Mccall, M. S. Lloyd, K. A. Higgins, and R. Castillo, "Cardiac motion and its dosimetric impact during radioablation for refractory ventricular tachycardia," *Journal of Applied Clinical Medical Physics*, vol. 24, 2023, Art. no. e13925. DOI: 10.1002/acm2.13925.

# List of Figures

2.1 RHYTHMIA HDx electroanatomical mapping system. *Image provided courtesy of Boston Scientific. ©2025 Boston Scientific Corporation or its affiliates. All rights reserved.* . . . . . 9
2.2 Commonly used radiotherapy systems in clinical practice. Left: Varian TrueBeam. *Image courtesy of Varian Medical Systems, Inc. All rights reserved.*; right: Cyberknife M6. *Images used with permission from Accuray Incorporated. All rights reserved.* . . . . . 11
2.3 Definitions of cardiac volumes in stereotactic arrhythmia radioablation. See main text for details. Abbreviations: CTV = clinical target volume; ITV = internal target volume; PTV = planning target volume. . . . . 11

3.1 American Heart Association (AHA) 17 myocardial segments with recommended nomenclature for the left ventricle tomographic imaging displayed on a bull's-eye map (circumferential polar plot). The AHA guidelines highlight the significant variability in the coronary artery blood supply to different myocardial segments. With the recognition of the anatomic variability the individual segments may be assigned to specific coronary artery territories: left anterior descending (LAD, cyan), right coronary artery (RCA, yellow) and left circumflex (LCX, magenta). . . . . 15

4.1 CARDIO-RT American Heart Association (AHA) 17-segment model registration. See main text for details. Abbreviations: LV = left ventricle; VT = ventricular tachycardia; CT = computed tomography; DICOM = Digital Imaging and Communications in Medicine; PTV = planning target volume; RTSS = radiotherapy structure set; PCA = principal component analysis. . . . . 25
4.2 Original and rasterized left ventricle (LV) point clouds. . . . . 26

4.3 Representative case for the American Heart Association 17-segment model registration with the spheres of apex (red), mitral valve center (green) and aortic valve center (blue) as registration references. The left ventricle (LV) segments are shown in different colors, and the basket of the 17-segment model is shown as black concentric circles and radial lines. (A) The LV myocardium structure before the 17-segment model registration. (B) The LV myocardium structure after the 17-segment model registration. . . . . 29
4.4 Representative case: Visualization of the registered left ventricle segment 13 (red) on the cardiac computed tomography (CT) (A) and planning CT (B) in the CARDIO-RT software. . . . . 31
4.5 Representative case: Visualization of the registered American Heart Association left ventricle 17 segments (in different colors) and aorta (pink). . . . . 32
4.6 3D-3D registration workflow. See main text for details. Abbreviations: EAM= electroanatomical mapping; LV = left ventricle; VT = ventricular tachycardia; CT = computed tomography; DICOM = Digital Imaging and Communications in Medicine; PTV = planning target volume; RTSS = radiotherapy structure set; ICP = iterative closest point; ROI = region of interest. . . . . 34
4.7 Orientation of the coordinate system for the 3D-3D registration and three planes for translation and rotation. $x$-axis: right-left direction; $y$-axis: anterior-posterior direction; $z$-axis: inferior-posterior direction. Abbreviations: SUP = superior; LL = left lateral; AP = anterior-posterior. . . . . 36
4.8 Representative case of the 3D-3D registration. Blue: left ventricle (LV) and aorta electroanatomical mapping (EAM) points; green: ventricular tachycardia catheter ablation points; red: computed tomography (CT) LV contours; black: CT aorta contours. (A) Position of the EAM point cloud and CT contours before registration. (B) Position of the EAM point cloud and CT contours after registration. 37
4.9 (A-C) The 3D-3D registered ventricular tachycardia (VT) target points (red) within the left ventricle (LV) blood pool, shown in axial, sagittal and coronal views of the cardiac computed tomography (CT). (D-F) The 3D-3D registered VT target points projected onto the LV point cloud (red), shown in axial, sagittal and coronal views of the cardiac CT. . . . . 39

4.10 Electroanatomical mapping left ventricle and aorta points (blue) and a set of sparse ventricular tachycardia catheter ablation points (green). . . . . 40
4.11 Representative case of 3D-3D registration for the feature border fill. (A) Computed tomography (CT) left ventricle (LV) points (black) in the front section and registered VT catheter ablation points (green). (B) Visualization of the polygonal region of interest (ROI, red). (C) Defined VT target points (red) within the polygonal ROI. (E) Visualization of the aorta and defined VT target points (red) on the LV structure in the 3D view. . . . . 42
4.12 Representative 3D-3D registered ventricular tachycardia target points (red) on the cardiac computed tomography (CT) (A) and planning CT (B) visualized in the CARDIO-RT software. . . . . 44
4.13 Representative electroanatomical mapping (EAM) screenshots in standard anatomical views captured from the CARTO 3 system. The left ventricle and aorta structures are mapped, with two ventricular tachycardia target regions marked in the CARTO 3 system as yellow shapes. AP = anterior-posterior; PA = posterior-anterior; RL = right lateral; LL = left lateral; SUP = superior; INF = inferior; RAO = right anterior oblique; LAO = left anterior oblique. . . . . 46
4.14 Representative fluoroscopic screenshots captured from the CARTO 3 system. (A) Standard anterior-posterior (AP) view. (B) Non-standard left anterior oblique (LAO) view (49°). The endocardial left ventricle is shown in cyan, while the catheter ablation points are represented as pink spheres. This STAR case was performed in Erlangen, Germany, and only 2D CARTO 3 fluoroscopic images from the standard AP view and the non-standard LAO view (49°) were available. . . . . 47
4.15 Computed tomography contours of the endocardial left ventricle (pink) and coronary arteries (red). . . . . 47
4.16 2D-3D registration workflow. See main text for details. Abbreviations: EAM = electroanatomical mapping; VT = ventricular tachycardia; CT = computed tomography; DICOM = Digital Imaging and Communications in Medicine; LV = left ventricle; PTV = planning target volume; RTSS = radiotherapy structure set; ROI = region of interest. . . . . 49

4.17 Representative case of the rotation function for the 2D-3D registration. The ventricular tachycardia target region is marked as a light blue shape on the electroanatomical mapping screenshot from the right anterior oblique (RAO, 30°) view. Red: left ventricle (LV) point cloud; blue: aorta point cloud. (A) The LV and aorta point clouds before overlay. (B) The overlaid LV and aorta point clouds with translation and scale only. (C) The LV and aorta point clouds with additional rotation about the $y$-axis. . . . . 52

4.18 Orientation of the standard anatomical views and rotation directions about the $x$-, $y$- and $z$-axes (A) and a representative case for the 2D-3D registration method. (B) The position of left ventricle (LV) (red) and aorta (blue) point clouds before registration. (C) The position of LV and aorta point clouds after registration. (D) Generation of a polygonal region of interest (ROI, red) by defining some points (red) along the marked ventricular tachycardia (VT) target region (black) on the electroanatomical mapping screenshot in the anterior-posterior view. (E) Visualization of the aorta and LV structures in the 3D view. (F) Selected LV points (red) within the polygonal ROI as the VT target points. (G) Visualization of the aorta and selected LV points (red) on LV structure and structures in the 3D view. Abbreviations: AP = anterior-posterior; PA = posterior-anterior; SUP = superior; INF = inferior; CRA = cranial; CAU = caudal; RL = right lateral; LL = left lateral; RAO = right anterior oblique; LAO = left anterior oblique. . . . . 53

4.19 Representative 2D-3D registered ventricular tachycardia target points (red) on the cardiac computed tomography (CT) (A) and planning CT (B) visualized in the CARDIO-RT software. . . . . 55

4.20 Representative case of the visualization of the planning target volume (blue) and 2D-3D registered ventricular tachycardia target points (red) in coronal (A), 3D (B), axial (C) and sagittal (D) views. 58

4.21 Representative case of the dose calculation visualization with the 2D-3D registered ventricular tachycardia target points (red) on the cardiac computed tomography slices in axial view. . . . . 59

4.22 Representative case of the rigid registration between the cardiac computed tomography (CT) and planning CT. Green: left ventricle (LV); pink: aorta. (A) Visualization of the LV and aorta structures in coronal view of the cardiac CT before registration. (B) Visualization of the LV and aorta structures in coronal view of the registered cardiac CT. (C) Visualization of the LV and aorta structures in the 3D view. (D) Visualization of the LV and aorta structures in axial view of the registered cardiac CT. (E) Visualization of the LV and aorta structures in sagittal view of the registered cardiac CT. . . . . 60

4.23 Representative case of the generation of transmural ventricular tachycardia (VT) target points (blue) based on the 2D-3D registered VT target points (red) and a left ventricle myocardium thickness of 10 mm, approximated from the corresponding cardiac computed tomography. . . . . 62

5.1 Workflow of ventricular tachycardia (VT) target identification, manual clinical target volume (CTV) delineation, CARDIO-RT electroanatomical mapping (EAM)-treatment planning imaging data registration and verification during quality assurance process. 73

5.2 Case 1. (A) Electroanatomical mapping (EAM) data with the marked ventricular tachycardia (VT) target region (red) in anterior-posterior view from RHYTHMIA HDx system. (B) Computed tomography (CT) contours (red: left ventricle, LV; black: aorta) and EAM points (blue: LV and aorta; green: catheter ablation points) before 3D-3D registration. (C) CT contours and EAM points after 3D-3D registration. (D) 3D view of the LV, aorta and 3D-3D registered target points (red). (E-G) Axial, sagittal and coronal views of the cardiac CT with the 3D-3D registered VT target points. (H-J) Axial, sagittal and coronal views of the cardiac CT with the final cardiac clinical target volume (CTV, red). (K) 3D view of the CTV (red) and cardiac substructures (light green: aorta; green: LV; yellow: right ventricle; rose: right atrium; orange: left atrium). . . . . 76

5.3 Case 2. (A, B, E) Electroanatomical mapping data with the ventricular tachycardia (VT) target region (red) in anterior-posterior and left lateral views from EnSite NavX system. (C) Pre-stereotactic arrhythmia radioablation contrast-enhanced cardiac computed tomography (CT) in systolic phase. Red arrow: septal-apical hypoattenuation indicating fibrosis/scarring. (D) 3.0 Tesla cardiac magnetic resonance imaging, transaxial navigated 3D fast low angle shot magnetic resonance imaging sequence with inversion recovery showing pronounced late gadolinium enhancement indicating cardiac fibrosis/scarring. (F-H) Axial, sagittal and coronal views of the cardiac CT with 2D-3D registered VT target (green). (I) 3D view of the left ventricle point cloud and the 2D-3D registered VT target points (red). (J-L) Axial, sagittal and coronal views of the planning CT with the final cardiac clinical target volume (red). . . . 77

5.4 Case 3. (A, E) Electroanatomical mapping (EAM) data with the ventricular tachycardia target region (red) in inferior and posterior-anterior views from CARTO 3 system. (B-D) Axial, sagittal and coronal views of the cardiac computed tomography (CT) with manually transferred clinical target volume (CTV, magenta). (F-H) Axial, sagittal and coronal views of the cardiac CT with the 2D-3D registered CTV (red). (I) 3D view of the registered CTV. (J-L) Axial, sagittal and coronal views of the cardiac CT with the final CTV (red). 78

5.5 Case 4. (A-C) Electroanatomical mapping data with the marked ventricular tachycardia (VT) region (yellow) in superior (SUP), inferior (INF) and left lateral (LL) views from CARTO 3 system. (D, E) SUP and INF views during the 2D-3D registration with the defined VT target points (red). (F) A 3D rendering (LL view) of the resulting clinical target volume (CTV, green) shown in the context of the cardiac chambers and great vessels, as segmented from the cardiac computed tomography (CT). (G-I) Axial, sagittal and coronal views of the cardiac CT with the final CTV (red). . . . . 80

5.6 Manually defined clinical target volume (CTV, green) and the 2D-3D registered CTV (yellow) for case 4, shown on the cardiac computed tomography in axial, sagittal and coronal views. . . . . 81

5.7 Case 5. (A, E) Electroanatomical mapping (EAM) data with the marked ventricular tachycardia (VT) target region (yellow) in superior and anterior-posterior views from CARTO 3 system. (B) 3D view of the left ventricle (LV) point cloud and the 2D-3D registered VT target points (red). (C) Computed tomography (CT) contours (red: LV; black: aorta) and EAM data (blue: LV; green: ablation points) before the 3D-3D registration. (D) CT contours and EAM data after the 3D-3D registration. (F-H) Axial, sagittal and coronal CT slices with marked (red) region by 2D-3D match; (I) 3D structures from the planning CT with final clinical target volume (CTV, red), LV (green), right ventricle (yellow) and aorta (light green). (J-L) Axial, sagittal and coronal CT slices with the final treated CTV (red, without assistance of the CARDIO-RT software). . . . . 82

5.8 Study design and analysis workflow. See main text for details. Abbreviations: EAM = electroanatomical mapping; VT = ventricular tachycardia; CT = computed tomography; CTV = clinical target volume. . . . . 86

5.9 Representative case of 3D-3D registration followed by target creation using 3D Slicer software and the EAMapReader extension. (A) Contouring of relevant cardiac structures. Magenta: left ventricle (LV) cavity; light blue: aorta; brown: LV myocardium. (B) 3D representation of the segmentation and geometry of the electroanatomical mapping (EAM, yellow). (C, D) 3D rendering (C) and short-axis reformation (D) of the EAM data (LV and aorta) after rigid registration with the segmentation. (E) Side-by-side view of the imported EAM in 3D Slicer (left) and the corresponding screenshot from the CARTO 3 EAM system (right). The white shape in the EAM screenshot (right) is the predefined ventricular tachycardia target. Note the corresponding contouring in progress (red) on the imported model (left). (F, G) Final transmural cardiac clinical target volume (green). While (A-G) demonstrate a case using the CARTO 3 EAM system, other EAM systems lead to similar results. (H) Corresponding step to panel (E) in a case using RHYTHMIA HDx system. (I) Corresponding step to panel (E) in a case using EnSite NavX system. . . . . 90

5.10 Representative case of 2D-3D registration followed by target creation using CARDIO-RT and 3D Slicer softwares. (A) CARTO 3 electroanatomical mapping (EAM) screenshot and the computed tomography (CT) point clouds of left ventricle (LV) blood pool (red) and aorta (blue) used as additional registration reference before registration. The EAM screenshot and CT-based point clouds are both visualized from superior view, and the white shape in the EAM screenshot is the predefined ventricular tachycardia (VT) target. (B) Registered EAM screenshot and CT contours. (C) Target points on the LV blood pool defined by delineated polygon along the intended target. (D) Registered VT target (red) on the cardiac CT slices and 3D view of the LV, aorta and VT target. (E) Transmural cardiac clinical target volume (green) according to the 2D-3D output. . . . . 91
5.11 Axial, sagittal and coronal views of cardiac computed tomography with a representative transferred transmural cardiac clinical target volume (CTV). (A-C) CTV transferred by EAMapReader 3D-3D registration (green). (D-F) CTV transferred by CARDIO-RT 2D-3D registration (red). (G-I) Overlay both CTV structures. . . . . 93
5.12 (A) Electroanatomical mapping screenshot with marked ventricular tachycardia target region (white shape). (B) 3D view of the cardiac CTV transferred by 3D-3D registration (green). (C) 3D view of the cardiac clinical target volume (CTV) transferred by CARDIO-RT 2D-3D registration (red). (D) Overlay of both CTV structures. Magenta: left ventricular blood pool; blue: aorta; orange: coronary arteries. . . . . 94
5.13 Absolute rotation angles about the three axes. . . . . 96

6.1 Diagram of cardiac motion estimation workflow. Processes and data in light blue boxes relate to the cardiac motion of the clinical target volume (CTV) and American Heart Association (AHA) 17 left ventricle (LV) segments, while those in orange relate to implantable cardioverter-defibrillator (ICD) lead tip motion. Abbreviations: CT = computed tomography; ITV = internal target volume. 106
6.2 Motion vectors representing the deformation of a clinical target volume (CTV) point cloud on the left ventricle (LV) at the end-diastolic phase. . . . . 107

6.3 Cardiac motion of the center of mass (CoM) for individual clinical target volumes (CTVs, bar chart) and individual CTV points (box chart) in the right-left (RL), anterior-posterior (AP), superior-inferior (SI) and 3D directions. Each patient had one CTV, with the exception of patients 2 and 9 with two CTVs. Mean values are shown as dots in the box chart. For the cardiac motion of individual CTV points, the mean and median values are similar and comparable. . . . . 110

6.4 Cardiac motion of the center of mass for the American Heart Association 17 segments of the left ventricle in 3D on 17-segment bull's-eye maps with the locations of the clinical target volumes (CTVs, orange borders) and implantable cardioverter-defibrillator lead tips (red dots) for each patient. Each patient had one CTV, with the exception of patients 2 and 9 with two CTVs. CTVs are numbered in ascending order from inferior to superior in the manuscript. . . . . 111

6.5 Euclidean distances between implantable cardioverter-defibrillator (ICD) lead tip motion and American Heart Association (AHA) 17 left ventricle segments motion in the right-left (RL), anterior-posterior (AP), superior-inferior (SI) and 3D directions, displayed on AHA 17-segment bull's-eye maps. . . . . 113

# List of Tables

4.1 Inter- and intra-observer variabilities for the 2D-3D registration method, comparing electroanatomical mapping data with and without the aorta structure. Abbreviations: DSC = Dice-Sørensen coefficient; CoM = center of mass; SD = standard deviation. . . . . 57

5.1 Patient characteristics. Abbreviations: LVEF = left ventricular ejection fraction; VT = ventricular tachycardia; ICD = implantable cardioverter-defibrillator; STAR = stereotactic arrhythmia radioablation; EAM = electroanatomical mapping; LV = left ventricle; CTV = clinical target volume. . . . . 72

5.2 EAM-treatment planning imaging data transfer in the 5 patient cases. Abbreviations: LV = left ventricle. *Based on the American Heart Association 17-segment model. . . . . 75

5.3 Structure analysis for cases 3 and 4. Abbreviations: CTV = clinical target volume; DSC = Dice-Sørensen coefficient; HD = Hausdorff distance. . . . . 79

5.4 Patient characteristics. Abbreviations: EAM = electroanatomical mapping; LV = left ventricle; RV = right ventricle. *Based on the American Heart Association 17-segment model. . . . . 88

5.5 Structure analysis results. Abbreviations: HD = Hausdorff distance; DSC = Dice-Sørensen coefficient; 3D CoM = three-dimensional center of mass; CTV = clinical target volume; RV = right ventricle; SD = standard deviation. °Cases with no additional map of the aorta/RV. *Mean difference of generated volumes -0.37 $cm^3$, 95 % confidence interval [-1.66 $cm^3$; 0.93 $cm^3$], p-value = 0.5366. ** Mean difference of generated surfaces -2.14 $cm^2$, 95 % confidence interval [-5.48 $cm^2$; 1.20 $cm^2$], p-value = 0.181. . . . . 95

6.1 Patient characteristics. Abbreviations: BMI = body mass index; LVEF = left ventricular ejection fraction; CTV = clinical target volume; LV = left ventricle; CT = computed tomography. * Based on the American Heart Association 17-segment model. . . . . 103
6.2 Cardiac motion of the clinical target volume (CTV) points and the center of mass (CoM) for each patient. Positive values indicate motion in the left, posterior, and superior directions, while negative values indicate motion in the right, anterior, and inferior directions. Abbreviations: RL = right-left; AP = anterior-posterior; SI = superior-inferior. . . . . 112

# Acknowledgements

This dissertation would not have been possible without the support of many people. First and foremost, I would like to express my deepest appreciation to my supervisor, Prof. Dr.-Ing. Achim Schweikard, for granting me this project and introducing me to the fascinating field of stereotactic arrhythmia radioablation. His guidance and conceptual insights have been invaluable throughout my research journey. I would also like to express my gratitude to Prof. Dr. med. Dirk Rades for serving as my second supervisor and for helping me enhance the quality of this work. Additionally, I am thankful to Prof. Dr. rer. nat. habil. Floris Ernst for his support throughout my doctoral journey.

Words cannot express my gratitude to my colleague, Ralf Bruder, for his continuous support, insightful discussions and invaluable suggestions. His expertise and willingness to engage with my questions and ideas were instrumental in accomplishing this work..

Many thanks to my current and former colleagues at the Institute of Robotics and Cognitive Systems for creating an inspiring working environment and for their helping hands. In particular, I am grateful to Marius Krusen, Dr. rer. nat. Honghu Xue, Christian Janorschke, Xinyu Lu, Dr. rer. nat. Daniel Wulff and Dr. rer. nat. Niclas Erben for their thorough support. Special thanks go to Cornelia Rieckhoff for her kind support on administrative challenges during my doctoral journey and for her help in proofreading.

My appreciation also goes to all collaborators for their invaluable advice and support on this work, especially Priv.-Doz. Dr. rer. hum. biol. Oliver Blanck, Priv.-Doz. Dr. med. Dr. rer. nat. Judit Boda-Heggemann, Priv.-Doz. Dr. med. Stephan Hohmann, Dr. med. Lena Kästner, Priv.-Doz. Dr. med. Michael Mayinger, Dr. med. Alicia S. Bicu, Melanie Grehn, Dr. Egor Borzov, , Priv.-Doz. Dr. med. Felix Mehrhof, Prof. Dr. med. Roland R. Tilz, Dr. sc. nat. Stefanie Ehrbar, Priv.-Doz. Dr. med. Boris Rudic, Dr. Marcin Miszczyk, Dr. Tomasz Jadczyk, Dr. med. Boldizsár Kovács, Dr. rer. biol. hum. Tobias Brandt and Prof. Dr. Coen Hurkmans.

I am blessed to have my friends and family. To my friends, thank you for

your kindness, encouragement and help. Mama and Baba, thank you for your unconditional support from the very beginning. To my partner, Mengwen, your love and support all the way from high school, through the highs and lows, have been my pillar of strength. Thank you for sharing both the happiness and challenges of raising our little one, Mingxiao.

This dissertation was supported by a scholarship from the Center for Doctoral Studies Lübeck (CDSL) of the University of Lübeck and by the European Union's Horizon 2020 research and innovation programme STOPSTORM under grant agreement No. 945119.